SIMULATION AND ASSESSMENT OF HIGHLY ALTERED HYDROLOGIC SYSTEM RESPONSES TO ANTHROPOGENIC AND NATURAL STRESSORS AT THE WATERSHED SCALE

BY

ALEJANDRA BOTERO ACOSTA

DISSERTATION

Submitted in partial fulfillment of the requirements
for the degree of Doctor of Philosophy in Agricultural and Biological Engineering
with a concentration in Computational Science and Engineering
in the Graduate College of the
University of Illinois at Urbana-Champaign, 2018

Urbana, Illinois

Doctoral Committee:

Assistant Professor Maria Librada Chu, Chair
Professor Emeritus J. Wayland Eheart
Professor George F. Czapar
Professor Richard A. Cooke
Professor Yuanhui Zhang

ABSTRACT

Environmental stressors account for human activities and natural processes that provoke modification of an ecosystem and its behavior. These stressors are chemical, physical, or biological in nature and can have short- and long-term impacts on the ecosystem (EPA, 2017b). Watershed Management Practices (WMPs) are strategies intended to mitigate the impacts of environmental stressors at the watershed scale (Drake and Hogan, 2013). Examples of WMPs are riparian buffers, reduced tillage practice, filter strips, cover crops and crop rotation. Hence, WMPs may be viewed as anthropogenic stressors strategically implemented to reduce the impacts of farming activities on the ecosystem. The implementation of these practices requires the identification of the most vulnerable locations or areas suitable for WMP implementation across the watershed to focus efforts and resources in the most efficient way. The objective of this research is to assess the impacts of anthropogenic and natural stressors over the systemic responses of the ecosystem at the watershed scale. The effects of these stressors over the surface and groundwater resources, erosion processes, and non-point source pollution were studied through the physically based distributed watershed model MIKE-SHE coupled to the hydrodynamic model MIKE11. Other modeling tools (e.g., MaxEnt, MUSLE) also were used to achieve the proposed goal. The implementation of modeling tools for scenario-based analysis in lieu of actual field experimentation made it possible to assess the impacts of future climate and land use changes over the watershed responses. Although, the conceptualization of the physical processes representing the WMPs is challenging, the ability to create feasible land use scenarios under future climate projections is a powerful tool to assess the possible impacts of proposed environmental endeavors.

ACKNOWLEDGMENTS

I would like to express my great appreciation to Professor Maria L. Chu and Professor Jorge A. Guzman for their guidance and encouragement in the realization of this research and for contributing immensely in my personal and academic growth. To the members of my committee: Professor J. Wayland Eheart, Professor George F. Czapar, Professor Richard A. Cooke and Professor Yuanhui Zhang, my special thanks for their relevant inputs and feedback to improve the outcome of this research. I would like to extent my gratitude and love to my family: Magaly Acosta, Augusto Henry Botero, Andrea and Adriana Botero, for their continuous guidance and unconditional support. To my beloved John, thank you for always believing in me and giving me courage when I most needed it. Finally, I would like to thank the ABE squad: Sav, Juan, Nidhi and Alex, for being an essential part of this amazing experience.

Also, I want to recognize the Danish Hydraulic Institute (DHI) for providing the educational licenses of MIKE SHE and MIKE 11, and the US Department of Agriculture (USDA) National Institute of Food and Agriculture (NIFA) who provided funds for this research (project ILLU-741-380).

TABLE OF CONTENTS

GENERAL INTRODUCTION

Intensive and extensive agricultural practices intended to ensure food security have had great impacts on soil and water resources, affecting the distribution and movement of water and solutes through the watershed. Surface and groundwater extractions for irrigation purposes, vegetation removal for crop establishment, tillage practices, and fertilizer and pesticide applications, are some of the most common examples of environmental stressors for agricultural purposes and are all related to crop production. In addition, expected climate changes and population growth are expected to exacerbate these impacts, thereby jeopardizing the sustainability of future food production.

Environmental scientists are tasked to assess the responses of the ecosystem to human activities in order to use natural resources rationally as well as to enhance ecosystem resilience to climate change by the implementation of conservation practices. It is therefore widely recognized that a more comprehensive approach in understanding the impacts of environmental stressors, and how these stressors propagate through the ecological system, are central topics in the debate over sustainability. Employment of watershed models has largely facilitated this task. Scenario-based modeling allows simulating watershed responses considering temporal and spatial variations, and enables the study of WMPs under alternative future climate projections. It is expected that the same WMP scenario will behave differently under modified climate conditions especially because rainfall and temperature are the main drivers of all watershed processes.

Models are simplified representations of reality based on the universal physic principles or empirical laws (Giere, 2004). They can be classified as physical, scale, analogue and mathematical, and are abstract objects that represent a specific phenomenon or system. Implementation of models in hydrology has helped overcome obstacles for environmental researchers. For example, a calibrated model can provide hydrologic information at locations where no stream gauges are installed, as well as data for periods of time with no measurements. Additionally, it has enabled the simulation of non-existent scenarios such as future climate or new land use implementation. Models have become an important tool for decision-making and without them we are unable to make inferences into the future where measurements are not possible. Hydrologic models have gone from lumped conceptual models to physically based

distributed models capable of representing the behavior of the system in time and space. This evolution has been accompanied by a broader knowledge of physical processes brought about the improvement in computational capabilities and availability of field measurements (Islam, 2011).

To simulate the complex reality, combinations of models are required to integrate different processes to simulate the real world as a system. Modeling tools are implemented in the present study to simulate the effects of anthropogenic and natural stressors over the soil and water resources at the watershed scale. Three general objectives are proposed, each of which is developed in one chapter, as listed below:

- Chapter 1: The first objective is to integrate the watershed model, MIKE-SHE, with the habitat suitability model MaxEnt, to determine the probability of presence (POP) of erosion along the riparian zone. Environmental variables such as soil type, land use, Stream Power Index (SPI), lateral flow, discharge, and amount of overland water are used to identify vulnerable zones to erosion along streambanks and riparian zones for current and future climate conditions. Erosion and deposition of sediments in waterways are natural fluvial processes. However, extreme flooding and human disturbances can hasten the degradation of rivers' bed and banks, leading to major environmental problems. Implementation of conservation practices at a watershed scale to restore the riparian zones and mitigate future degradation require the identification of vulnerable areas.
- Chapter 2: The second objective of this study is to apply a physically-based watershed model to simulate the hydrologic response of an intensively managed watershed to anthropogenic stressors applied across the domain (e.g.: crop rotation, wetlands, riparian buffers, effect of tile drainage) and natural stressors (future climate projections). Water fluxes regulate the chemical, biological, and physical processes of the watershed. A major example of this is nonpoint source pollution caused by overland runoff and tile drainage flows, considered the most important current cause of water quality impairment in the United States (Arabi et. al., 2007). The understanding of how surface and groundwater resources behave in response to natural and anthropogenic stressors facilitates the work of managerial agents and stakeholders for insuring the preservation of the ecosystems and the services they provide to support human life.

- Chapter 3: The third objective is to apply a physically-based model to simulate the transport of nonpoint source pollutants in a highly altered watershed under selected WMPs (wetland, riparian buffers, crop rotation, cover crops, reduced till) and projected climate conditions. Soil losses caused by extreme rainfall-runoff events deteriorate farmland productivity, while washed-off fertilizers transported from croplands are deposited in streams, impairing water quality and aquatic habitats (Yan et al., 2015). These problems are further aggravated in highly altered watersheds where cropland and urban areas are the main land use types. Watershed Management Practices (WMPs) are implemented to address these issues. Nonetheless, the effectiveness of these practices and the corresponding watershed response rely on spatial and temporal connections that are hardly identified at a watershed scale. Hydrologic linkages across a watershed may produce distributed and delayed responses that are not easily detected in the field.

CHAPTER 1. RIPARIAN EROSION VULNERABILITY [1]

1.1. INTRODUCTION

Riparian zones are among the most productive and valuable natural resources in the world because they support numerous ecological services, such as high plant species diversity and wildlife habitat (Bentrup, 1998). However, they are also one of the most vulnerable, due to their proximity to water bodies that have the capacity to influence their physical, chemical, and biological characteristics. Although erosion and deposition are natural fluvial processes that shape the riparian zones, anthropogenic effects can lead to unnatural exacerbation of these processes, leading to major environmental problems. For example, tile drainage of agricultural areas and paving and roofing of urban areas increase the flashiness of basin hydrographs, leading to riparian soil erosion and streambank instability and failure. Chu-Agor et al., 2008a, 2008b; Chu-Agor et al., 2009; Daly et al., 2015 all note such effects, and Fox et al., 2016 report increased sediment load to streams from such failures. In fact, Wilson et al. (2008), using naturally occurring radionuclide traces, found that streambank erosion contributes about 48% of the suspended sediments in streams of the watershed in the present study area (described below). Shields (1995) reports that 480,000 km of eroded streambank in the U.S. produce approximately 450 million of tons of sediment per year. Increased sediment load to streams can result in water quality impairment that can cause human health problems and that also threatens the integrity of the aquatic ecosystem. Lost and degraded riparian zones also translate into destruction of wildlife habitat and consequently the wildlife that inhabits them. Riparian vegetation buffers decrease the impact of nonpoint source pollution by capturing nutrients and sediments from the overland flow (Bentrup, 1998) and reducing the vulnerability of banks to erosion. Conversion of riparian forests into grazing areas or row-crops fields can reduce or eliminate these ecosystem services and accelerate riparian and streambank degradation. Water quality issues and reductions in ecosystem services are some of the many reasons why streambank and riparian erosion are of major concern to environmental scientists, managers, and policy-makers. However, the spatial and temporal variability of the factors and mechanisms (e.g., precipitation, streamflow,

[1] Chapter 1 is a reprint of the article: Botero-Acosta, A., Chu, M.L., Guzman, J.A., Starks, P.J., Moriasi, D.N. 2017. Riparian erosion vulnerability model based on environmental features. Journal of Environmental Management 203: 592-602, which has been published in final form at http://dx.doi.org/10.1016/j.jenvman.2017.02.045 and the copyright is owned by Journal of Environmental Management.

elevation, land cover) that affect the erosion process make prevention and mitigation efforts challenging.

The last several decades have seen the implementation of riparian conservation practices to restore the riparian zones and mitigate future degradation of vulnerable areas. A large number of research efforts have focused on understanding streambank and riparian erosion processes and how to mitigate their effects (Bernhardt and Palmer, 2007; Correll 2005; Henderson, 1986; Purvis and Fox, 2016; Simon et al., 2011; Zaimes, 2004). However, before any conservation measures can be implemented, it is necessary first to identify the areas that are vulnerable to erosion, particularly as it may be exacerbated by climate variability and extremes. Predicting riparian and streambank erosion at the watershed scale is challenging because it requires constant monitoring of soil, hydrologic, and climate variables. Such monitoring can cost more than the conservation measures themselves.

Erosion at the watershed scale has been addressed from different perspectives. For instance, Fox and Papanicolaou (2007) used naturally-occurring nitrogen and carbon isotopes as tracers to identify temporal and spatial variability of erosion processes in a 0.71 km^2 sub watershed. This method required considerable field work and post processing of samples in order to establish rill/inter-rill and floodplain erosion, which limits the suitability of the method to very small watersheds. Distributed models have also been applied to simulate hydrologic event erosion. For example, KINEROS2 (Smith et al., 1990) and EUROSEM (Morgan et al., 1998) numerically solved the sediment mass balance equation using rainfall as input and avoiding the averaging effects of lumped models like USLE and RUSLE (Smith, et al.1995). Again, these models are suited for small watersheds and the erosion is evaluated per specific rainfall event only. On the other hand, Purvis and Fox (2016) estimated the eroded area along the riparian zone by analyzing aerial images of Delaware County, Oklahoma for 2003, 2008, 2010, and 2013 where streambanks were manually delineated from aerial photographs using polylines. The effects of stream power, riparian vegetation, and meandering on riparian erosion were studied. The two latter are environmental variables visually detected in the aerial images, while the former was computed from the monitored discharge during the study period. At the watershed scale, erosion vulnerability is commonly assessed using geospatial analysis of satellite images (e.g., Purvis and Fox, 2016; Chatterjee et al., 2014) instead of numerical models and environmental data. Studies that identify areas vulnerable to riparian erosion at the watershed scale based on the simulation

of physical processes are still very limited due to the rigors and expense involved in such endeavors. There is, therefore, a critical need to develop a modeling framework to identify and predict areas vulnerable to erosion along the riparian zones that combines simulations of physical processes and landscape level tools such as watershed scale environmental data. By being able to identify the most probable vulnerable areas for stream and riparian sediment mobilization, conservation and managerial practices can be focused on areas that need the most attention and resources.

The methodology applied in this chapter was: (1) integrate the hydrologic watershed model, MIKE-SHE, the river model, MIKE-11 (to simulate water movement across the watershed) with the habitat suitability model, MaxEnt, to determine the probability of presence (POP) of erosion along the riparian zone, and (2) determine vulnerable areas for erosion along the riparian zone at the watershed scale. The modeling framework was applied to the Fort Cobb Reservoir Experimental Watershed (FCREW) located in southcentral Oklahoma.

1.2. METHODS

1.2.1. STUDY AREA

The Fort Cobb Reservoir Experimental Watershed (FCREW) is a sub-watershed of the Washita River Basin located in south central Oklahoma, USA. It drains an area of approximately 800 km^2 to the Fort Cobb Reservoir. The land use in FCREW is predominantly agriculture with approximately 60% of its area used for crop cultivation (USGS, 2016b). The USDA-ARS Grazinglands Research Laboratory (GRL) in El Reno, OK, established the FCREW for participation in the Watershed Assessment Studies (WAS) portion of USDA-NRCS' Conservation Effects Assessment Project (CEAP) (Mausbach and Dedrick, 2004; Steiner et al., 2008). The CEAP WAS was designed to conduct hydrologic investigations for the improvement of watershed models to better assess the impact of conservation practices at the watershed scale. For this reason, FCREW is equipped with a network of climate and hydrologic monitoring stations (Figure 1) with long-term datasets that can support environmental assessment studies. The watershed has 18 rainfall stations, three observation wells, and three stream gauge stations with daily measurements.

The study area has a sub-humid climate with a bi-modal rainfall distribution (May-June and September-October) which produces a mean annual rainfall of approximately 800 mm (Starks et

al., 2014). FCREW climate is also characterized by wet and dry multiannual periods (Garbrecht and Schneider, 2008) which determine the overland flow and the sediment transport behavior in the watershed. Riparian areas have been affected by livestock grazing expansion, causing active degradation and bank failure in most of the channels in the FCREW (Simon and Klimetz, 2008). Crop production and management has changed in time with some farms implementing newer conservation practices and minimum tillage (Moriasi et al., 2014; Storm et al., 2006). However, the FCREW still experiences water quality problems, specifically transport of sediment and elevated phosphorus concentration, due to intensive agricultural activities and cropland erosion (Oklahoma Conservation Commission, 2009). Despite the fact that approximately 50% of the total suspended sediment load was estimated to come from the streambanks (Wilson et al., 2008), studies identifying vulnerable erosion areas along the riparian zone of FCREW are nonexistent. Erosion related studies conducted in the watershed are mostly focused on quantifying the total suspended sediment load produced in its waterways (e.g., Garbrecht and Starks, 2009; Wilson et al., 2008; Simon and Klimetz, 2008).

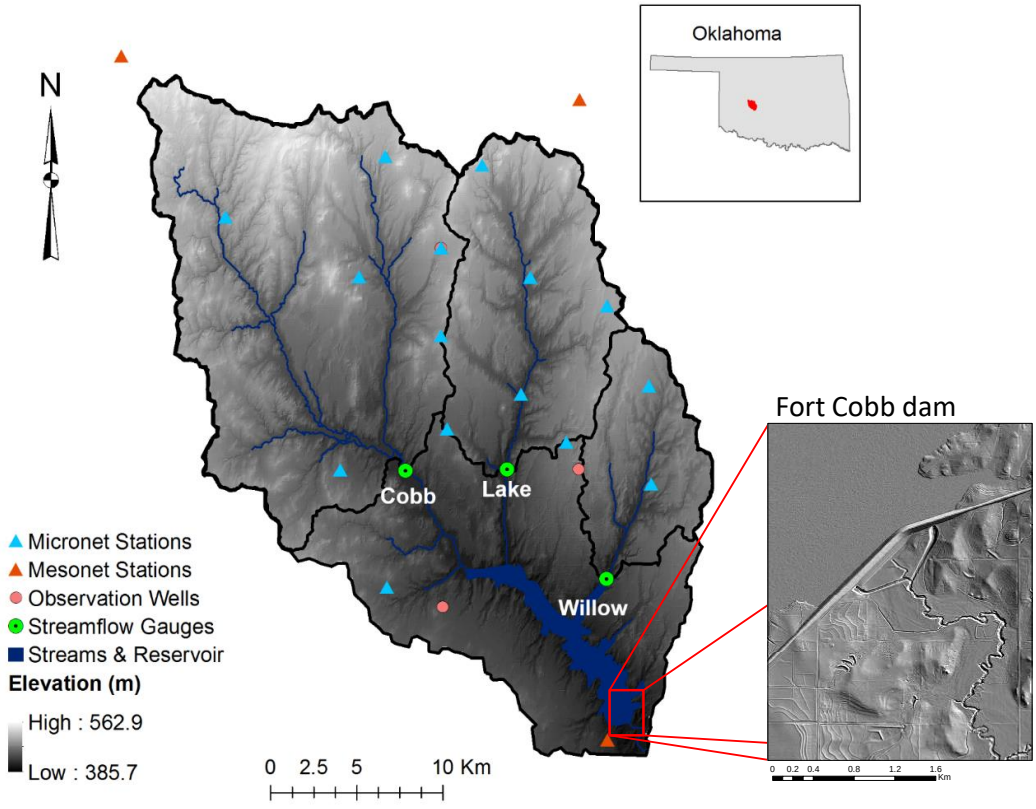

Figure. 1. The Fort Cobb Reservoir Experimental Watershed (FCREW) with its three sub-watersheds: Cobb, Lake, and Willow (Botero-Acosta et al., 2017)

The method developed in this research was composed of two main parts: the simulation of the hydrologic processes using the models, MIKE-SHE and MIKE 11, and the estimation of erosion POP using MaxEnt (Figure 2). The MIKE-SHE and MIKE 11 models were used to simulate the historic and projected hydrologic variables (discharge, lateral inflow and overland flow) in FCREW that were then used as environmental layers in MaxEnt. The hydrologic variables were used along with environmental maps and features (soil, land use, stream power index) to determine the probability of observing different levels of erosion in the riparian and streambank zones based on erosion location samples (Figure 2).

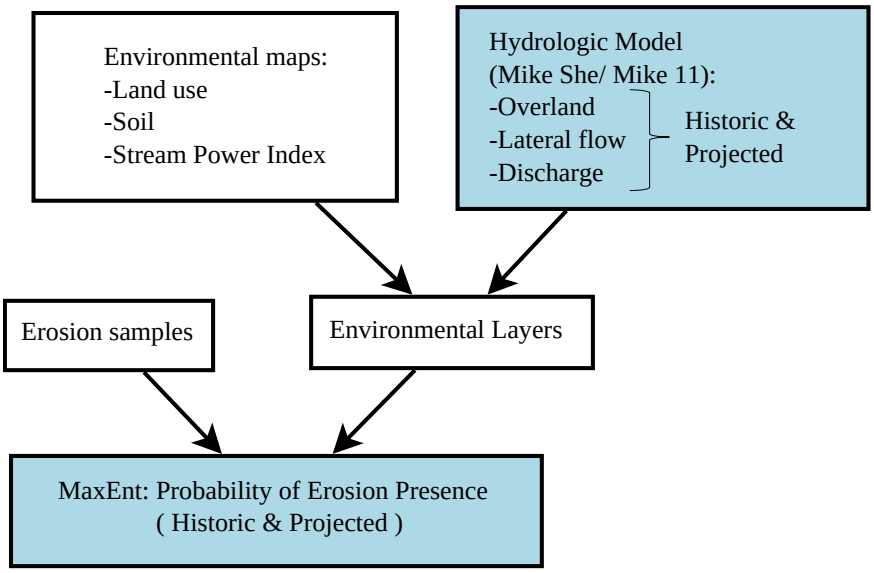

Figure 2. Overview of the methodology used to estimate the erosion POP in the riparian zone and streambank of FCREW (Botero-Acosta et al., 2017)

1.2.2. HYDROLOGIC MODEL

One of the most important factors affecting riparian erosion is water movement across the watershed. The surface-groundwater integrated model MIKE-SHE was used to simulate the daily stream discharge, lateral inflow, and overland flow depths between 2009 and 2012. As a physically-based and distributed model, MIKE-SHE simulates the processes in the hydrologic cycle considering their temporal and spatial variations across the watershed. MIKE-SHE was coupled with the MIKE 11 model to simulate watershed-river exchanges and streamflow. Inputs to MIKE SHE consist of climate, land cover information, soil properties, and hydrogeologic data, which can vary in space and/or time. Inputs to MIKE 11 consist of the river network, boundary conditions, and hydrodynamic parameters. Outputs from MIKE-SHE are time series of

maps of water movements on the surface, the unsaturated zone, and groundwater, while outputs from MIKE 11 are time series of streamflow at different points along the river.

1.2.2.1. Input Data and Model Setup

MIKE-SHE requires a model extent grid which defines the study domain. Climate data, as station-based time series inputs, include precipitation, reference evaporation, and air temperature. Daily precipitation data were obtained from the Micronet and Mesonet network for the simulation period (Guzman et al., 2014), while daily air temperature data were acquired from the Mesonet network. Daily reference evaporation estimates were computed using the modified Makkink equation (de Bruin and Lablans, 1998).

A 2006 land use map (USGS, 2016b) was used to establish the spatial distribution of vegetation, impervious surfaces, and the Manning roughness coefficient for the surface, *M*. The vegetation maps contained grid codes of the different types of vegetation cover in the watershed. For each vegetation type, the time series of the vegetation development stages, leaf-area-index (LAI), root depth, and crop coefficient were specified for the whole period of simulation. The impervious surface map defines the fraction of overland flow that is allowed to infiltrate and how much should be 'drained away'.

The overland flow in the watershed was simulated as a shallow free surface flow using the 2D conservation mass (Eq. 1) and momentum equations (Eq. 2) (St. Venant Equation) solved by the finite difference method. In order to reduce the numerical complexity of the dynamic St. Venant equation, the momentum losses caused by local and convective acceleration and inflows perpendicular to the main flow were neglected. The Manning's roughness coefficient, *M*, was required in order to estimate the friction slope in the direction of flow.

$$\frac{\partial h}{\partial t} + \frac{\partial}{\partial x}(uh) + \frac{\partial}{\partial y}(vh) = p \qquad \text{Eq. 1}$$

$$S_{fx} = S_{Ox} - \frac{\partial h}{\partial x} - \frac{u}{g}\frac{\partial u}{\partial x} - \frac{1}{g}\frac{\partial u}{\partial t} - \frac{qu}{gh}$$

$$S_{fy} = S_{Oy} - \frac{\partial h}{\partial y} - \frac{v}{g}\frac{\partial v}{\partial y} - \frac{1}{g}\frac{\partial v}{\partial t} - \frac{qv}{gh} \qquad \text{Eq. 2}$$

Where *h* is the flow depth above the ground surface, *u* and *v* are the velocities in *x* and *y* directions, *p* is the net input into OL flow, S_f is the friction slopes in both directions and S_O is the ground slope.

The unsaturated zone was simulated using a 2-layer water balance method that discretizes the zone into upper and lower layers representing average conditions. This method calculates the

actual evapotranspiration and the amount of water that recharges the aquifer using the vegetation and soil data by changing layer thicknesses according to the root depth and water table. The STATSGO soil map and database (SSS-NRCS, 2012) were used to characterize the spatial distribution of the different soil types in the watershed. For each soil type, the water content at saturation, field capacity, wilting point, and saturated hydraulic conductivity were estimated based on field measurements compiled from the Soil Characterization Database (NCSS, 2012).

Groundwater flow was simulated by a 3D Boussinesq equation solved by finite difference. To physically simulate groundwater flow, data of the aquifer extent and its properties were required. Maps of vertical and horizontal hydraulic conductivities, specific yield, and specific storage were obtained from hydrogeologic data of the Rush Springs aquifer (Becker, 1998; Guzman et al., 2015; Penderson, 1999). The Rush Springs aquifer is the second most highly developed aquifer in Oklahoma and is used predominantly for irrigation. It is mainly composed of the Rush Springs Formation, consisting of highly cross-bedded sandstone with some interbedded dolomite and gypsum (USGS 2016c). The Rush Springs aquifer is underlain by the Marlow Formation capped and confined at its western portion by the Cloud Chief Formation (OWRB, 2012). A map of the potential head was also added as an initial condition. To supply the water requirements for crop irrigation in the FCREW, farmers extensively used groundwater extracted from the Rush Springs aquifer. Data from 369 extraction wells between 2005 and 2012 from Guzman et al. (2015) were included in the model.

MIKE 11 was linked to MIKE-SHE to simulate the interaction between the river, the aquifer, and the surface. The linkage comprises the flow exchanged between the river and the aquifer, which can be to or from the river, and the distribution of the drained water from the surface either by overland flow or lateral inflow. River flow was simulated in MIKE 11 by kinematic routing. MIKE SHE is a mainly physically-based model with most of its parameters measurable from the field. However, some simplifications and empirical processes required the adjustment of some parameters. A comparison between simulated and observed discharge at the three streamflow gauges (Figure 1) was made with the aim of evaluating the performance of the integrated model in simulating streamflow. Three metrics were used to measure the performance of the model in simulating the streamflow: (a) Nash-Sutcliff (NS), which evaluated the agreement between the measured and simulated hydrographs, (b) Pearson's correlation

coefficient (r) to evaluate the correlation between the measured and simulated streamflow, and (c) the cumulative flow error to evaluate the error in the water balance.

1.2.3. MAXIMUM ENTROPY MODEL (MAXENT)

The MaxEnt model (Phillips et al., 2006) has been largely applied in environmental niche modeling to predict the spatial distribution of birds, corals, wildcats, ants, nematodes, bats, butterflies, forests, and many others (Elith et al., 2011; Merow et al., 2013). Recently, Heumann et al. (2013) applied MaxEnt to create a land suitability model to study the relationship between natural, built, and social environments with three major crops' spatial distributions. Similarly, Linhoss and Underwood (2015) created a land-cover suitability model for salt pannes (shallow depressions that contain water with very high salt concentration) along the gulf coast of Mississippi using sea level rise, land cover, elevation, and topographic depressions as environmental features.

The MaxEnt model is based on the principle of maximum entropy of a probability density function and predicts the best spatial distribution of a particular species based on sampled presence locations and selected environmental features that are continuous throughout the domain. To do so, the model contrasts the statistical moments of the environmental features at the predicted spatial distributions with those at the observed locations, selecting the ones that are most similar (Merow et al., 2013). The logistic output of MaxEnt corresponds to the probability of the species presence for each cell that preserves the mean and variance of the environmental features at observed locations. The MaxEnt algorithm approximates the probability distribution of a given species, π, over a set of X locations across a given landscape, subject to constraints derived from environmental variables. The entropy of the approximate probability distribution is defined as

$$H(\hat{\pi}) = -\sum_{x \in X} \hat{\pi}(x) \ln \hat{\pi}(x) \qquad \text{Eq. 3}$$

where π is the true distribution of a species over a set of X locations (e.g., set of pixels) across a given landscape and $\hat{\pi}$ is the approximate probability distribution that respects a set of environmental constraints. The environmental constraints or "features" can be estimated as the sample mean of the environmental features at the occurrence locations.

$$\sum_{x \in X} f_j(x)\pi(x) = \frac{1}{m}\sum_{i=1}^{m} f_j(x_i) \quad \text{Eq. 4}$$

where f_j represents the valued functions of the *j* environmental features over *X*. The aim is to find the probability distribution, $\hat{\pi}$, with maximum entropy under the constraint of each environmental feature (Phillips et al., 2006).

Inputs in MaxEnt consist of the presence locations of each independent species (i.e., longitude and latitude), maps of environmental features, and model parameters. MaxEnt performs one training and one test of its algorithm for each species. The sampled presence locations are randomly split into two sub-samples, one set is used as training locations for the model and the second as testing locations. This process is analogous to a calibration and validation process. The receiver operating curve (ROC) of the model and the area under this curve (AUC) are then applied to estimate the prediction power of the model. The ROC plots the true-positives (sensitivity) against false-positives and the area under this curve expresses how well the model fits the presence data. An AUC of 0.5 means that the model behavior is no different than a random prediction while values closer to 1 represent better model performances (Linhoss and Underwood., 2015). MaxEnt determines the most important environmental variable that affects the POP using the jackknife test. This test identifies the environmental variable which provides the highest gain of information when it is the only one used, while at the same time decreasing the gain the most when absent.

1.2.3.1. Erosion presence locations

To identify erosion-vulnerable areas along the riparian zone, the MaxEnt model was developed for FCREW were erosion presence locations were used instead of species presence location. The erosion presence locations were estimated across the watershed as the difference in elevation between two LiDAR datasets, one collected in 2009 (from NRCS personal communication) and the other in 2011 (USGS, 2016a). To prepare the erosion map for FCREW, each LiDAR file was re-sampled to a 3-m grid and the probable changes in elevation were computed by subtracting the two LiDAR readings. A thorough screening of the differences in elevation between the two LiDAR data sets was also performed to eliminate the noise derived from LiDAR sensor accuracy, post data acquisition processing, and man-made elevation changes. The elevation of the road on the crest of the dam in the Fort Cobb Reservoir (Figure 1)

was used as a benchmark to quantify the noise between the two DEMs derived from the LiDAR flights. The noise was estimated based on the mean differences in elevation at the top of the dam. The mean difference in elevation between the two DEMs at the crest of the dam, found to be equal to 1 cm, was then subtracted from the erosion map.

Since the processes controlling the erosion in the streambank differs from the rest of the riparian zone, two erosion maps were prepared: one for the streambank and another for the remainder of the riparian zone. To create the maps, 91 cross sections of the river network were extracted from the 2009 LiDAR data, from which the base of the streambank was digitally identified. The mode of the streambank width across the watershed was estimated from these 91 cross sections to be 150 m and was used to establish a value of the streambank buffer. The streambank map was constructed by buffering the base of the streambank 150 m outward and the riparian map was generated by creating a second 150-meter buffer around the streambank (Figure 3).

Areas hypothesized to be vulnerable to elevation changes, were digitally classified in four categories: low (0.5 - 0.7 m), medium (0.7 - 1 m), high (1 - 1.7 m) and very high (1.7 - 5.9 m). The difference in elevation lower than 0.5 m was not included since preliminary runs of the MaxEnt model identified that erosion samples below this threshold were randomly located (AUC $\approx$ 0.5) along the study domain. An inspection of these erosion samples along with the land use map established that their location was predominantly in crops (41.9 % for riparian and 22.3 % for streambank) and herbaceous (51.6 % for riparian and 67.5 % for streambank) land use categories. The locations (i.e., x- and y- coordinates) of the four erosion categories (low, medium, high, and very high) within the streambank and riparian buffers were used as erosion presence locations

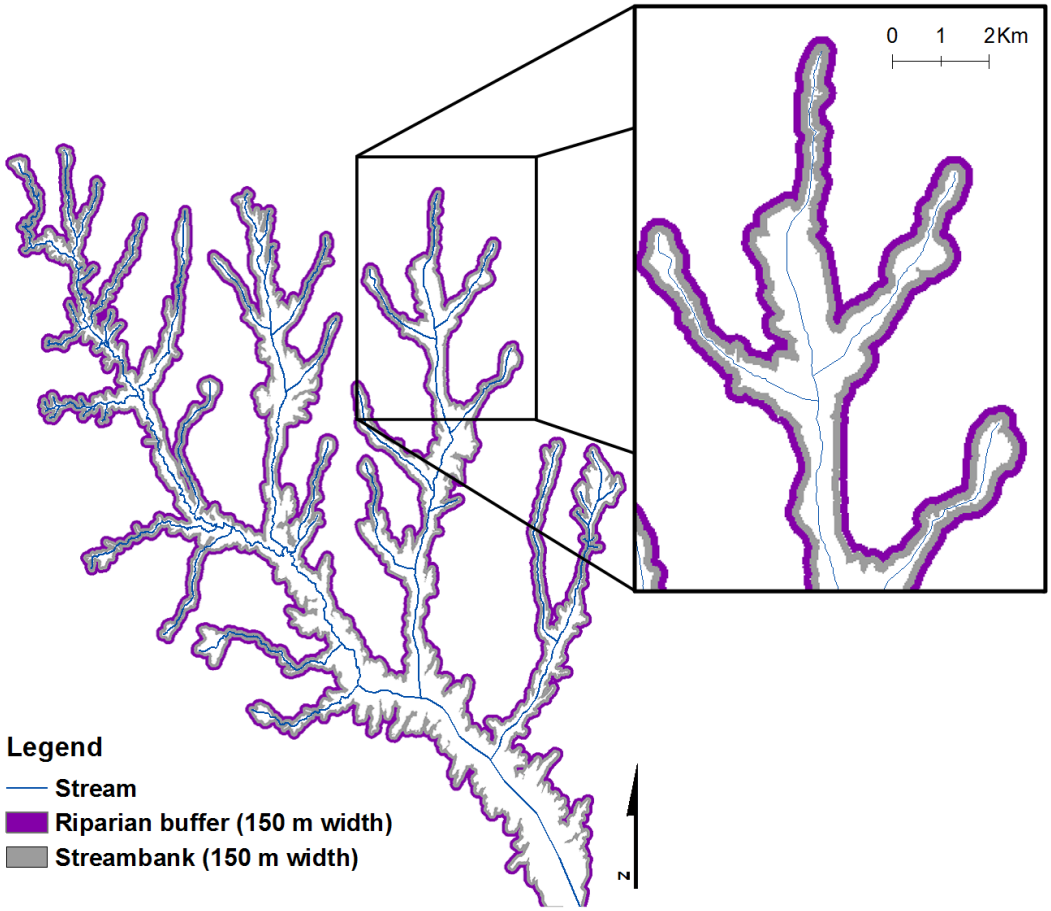

Figure.3. Buffers used to define the riparian zone and the streambank (Botero-Acosta et al., 2017)

1.2.3.2. Environmental features

Uncorrelated environmental features were used to constrain the erosion presence predictions in MaxEnt. The environmental features selected to constrain the prediction of presences of erosion in FCREW were stream discharge, lateral inflow, overland flow depth, Stream Power Index (SPI), soil type, and land use. The SPI is a secondary topographic index applied in digital terrain analysis that can be computed from DEM data. It estimates the erosive power of the water movement as a function of the specific cell area, which is the area of the cells draining to that particular cell, and the local slope (Moore et al., 1991; Jacoby et al., 2011; Wilson and Gallant, 2000; Minnesota Department of Agriculture, 2010, Conoscenti et al., 2008). The SPI was computed as follows:

$$SPI = Ln(Ac * S) \qquad \text{Eq. 5}$$

where *Ac* is the specific catchment area of each cell and *S* is the local slope. Since erosion was assumed to have occurred between 2009 and 2012 (period between the two subtracted LiDARs), the hydrologic variables simulated using the MIKE models between 2009 and 2012 were converted to a grid format as a function of the minimum distance of the cell from the stream. The maximum daily discharge and lateral inflow from MIKE 11 were transformed from network format to a 30-m-square-cell grid comprising the streambank and riparian buffers. The daily overland flow depth maps from MIKE SHE were summed for the entire period of simulation and the data for both buffers were extracted (i.e., riparian or streambank). The categorical environmental layers, soil and land cover, were also extracted for the respective buffers (i.e. streambank or riparian) of the analyzed area. The soil map used was based on the SSURGO database (SSS-NRCS, 2016) while the land cover used was from 2011 (USGS, 2016b).

1.2.4. CLIMATE CHANGE EFFECTS

To evaluate the impacts of climate change on erosion vulnerability, the MIKE models were used to simulate changes in the hydrologic environmental layers (stream discharge, lateral inflow, and overland flow depth) under projected climate scenarios. These projected environmental layers were then used in Maxent to determine the probability of erosion presences under projected climate change. The projection was arbitrarily chosen to start in 2040 with a four-year duration (2040-2043) similar to the duration of the baseline model (2009-2012).

The Coupled Model Intercomparison Project (CMIP5) (CMIP5, 2016) is an international program that gathers and compares general climate models from research institutes around the world. General climate models are gridded based models that use atmospheric physics to simulate climate. Downscaled climate data from one of the models included in the CMIP5 were used as inputs in the MIKE model to simulate the projected hydrologic environmental layers for the period of 2040 to 2043. Daily precipitation and average temperature for the Max-Planck-Institute Earth System Model (MPI-ESM), with the Representative Concentration Pathway 8.5 (RCP8.5) was used. Each RCP corresponds to a change in the balance of incoming and outgoing radiation from the atmosphere due to changes in its composition. The RCP8.5 is characterized by scenarios leading to high greenhouse gas concentration levels, with an increasing trend over time (RCP Database, 2008). The combined effects of MPI-ESM and RCP8.5 lead to a critical climate

projection with estimated long-term global warming of 4.4 °C for the year 2100 in contrast to 1.5 °C for the RCP2.6 (Giorgetta et al., 2013).

1.2.5. EROSION VULNERABILITY

The erosion vulnerability of FCREW was evaluated by creating the vulnerability maps of the domain and constructing the erosion suitability curves of these maps. The vulnerability maps showed the probability of presences, as computed in MaxEnt, of all the erosion categories across the riparian zone and streambank of FCREW for the period 2009-2012 and 2040-2043. The erosion suitability curves were created by computing a unitless erosion suitability index as a function of the components of the different environmental layers (e.g. land use categories of the land use map). It shows how erosion preference varies with the different components of the environmental layers. The erosion suitability index was computed similar to that in Conklin et al. (1996) as follows:

$$P_{ij} = \frac{U_{ij}}{A_i} \qquad \text{Eq. 6}$$

where P_{ij} is the normalized suitability index of a component i of the environmental layer X (X_i) for a particular erosion category j, U_{ij} is the relative frequency of X_i for the erosion category j, and A_i is the relative frequency of X_i in all erosion categories.

1.3. RESULTS AND DISCUSSION

1.3.1. MIKE MODELS:

MIKE-SHE's measured physical parameters were tested (Figure 4) using a preliminary run for the period 2005-2009, for which measured streamflow at the three stream gauges (Figure 1) were available. Simulated and measured daily streamflow were compared at three locations (Cobb, Lake, and Willow). Simulated streamflow for stations Willow and Lake Creeks showed a good agreement with measured data, with NS of 0.89 and 0.73, respectively and *r* of 0.89 and 0.88, respectively (Figures 4b and 4c). Although the NS for one of the gauges (Cobb Creek) was 0.48 (Figure 4a) its cumulative error (0.25%) and r value (0.71) showed a good correspondence between simulated and measured discharges.

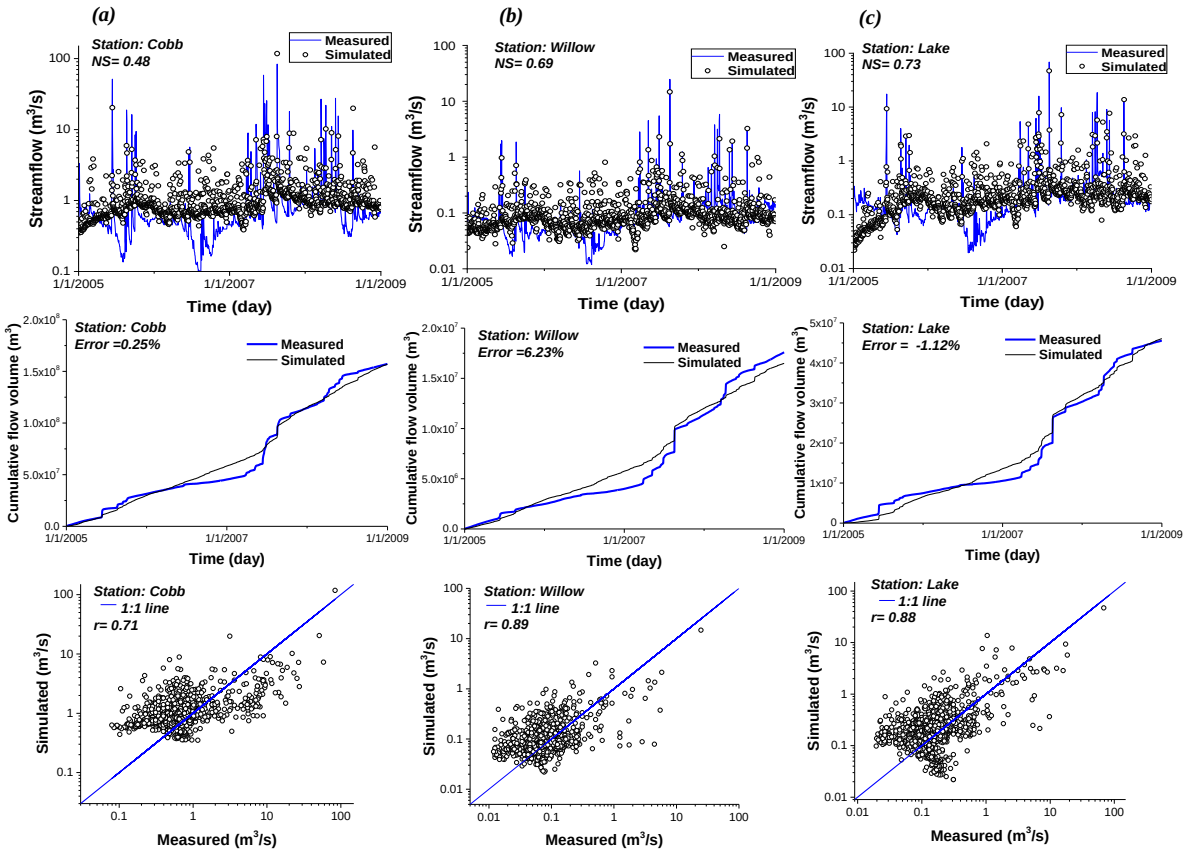

Figure 4. Model performance metrics for the three streamflow gauges: (a) Cobb, (b) Willow, and (c) Lake (Botero-Acosta et al., 2017).

In general, the projected climate for the 2040-2043 period was drier compared to the historic conditions which resulted in lower streamflow. These results are consistent with the findings of Garbrecht et al. (2014) when they analyzed the climate records in FCREW. They have observed a monotonic warming trend of 0.34°C per decade that started in the late 1970s. The simulated mean and maximum daily discharges for the 2009-2012 period were 8.6 m^3/s and 60 m^3/s, respectively. In contrast, the simulated mean and maximum discharges for the 2040-2043 period were only 6.35 m^3/s and 52.4 m^3/s, respectively. For the lateral inflow, the mean and maximum values were 0.92 m^3/s, and 8.21 m^3/s for 2009-2012, and 0.67 m^3/s and 4.3 m^3/s, respectively, for 2040-2043.

1.3.2. MAXENT

MaxEnt was set-up for the FCREW for both the riparian and streambank zones. For each zone, the model performed one training (calibration) and one test (validation) of its algorithm for

each erosion category resulting in eight models. MaxEnt computed the (POP) of all the erosion categories for each cell of the gridded domain. Results for high (1 - 1.7 m) and very high (1.7 - 5.9 m) erosion categories are presented in Figure 5. These categories are considered the most critical and are expected to require the most attention for conservation purposes. Results revealed that approximately 80% of the riparian zone has a probability of up to 30% to experience "high" erosion (1 - 1.7 m) and up to 20% for "very high" erosion (1.7 – 5.9 m). Similarly, 80% of the streambank has a probability of up to 30% to experience both "high" and "very high" erosion.

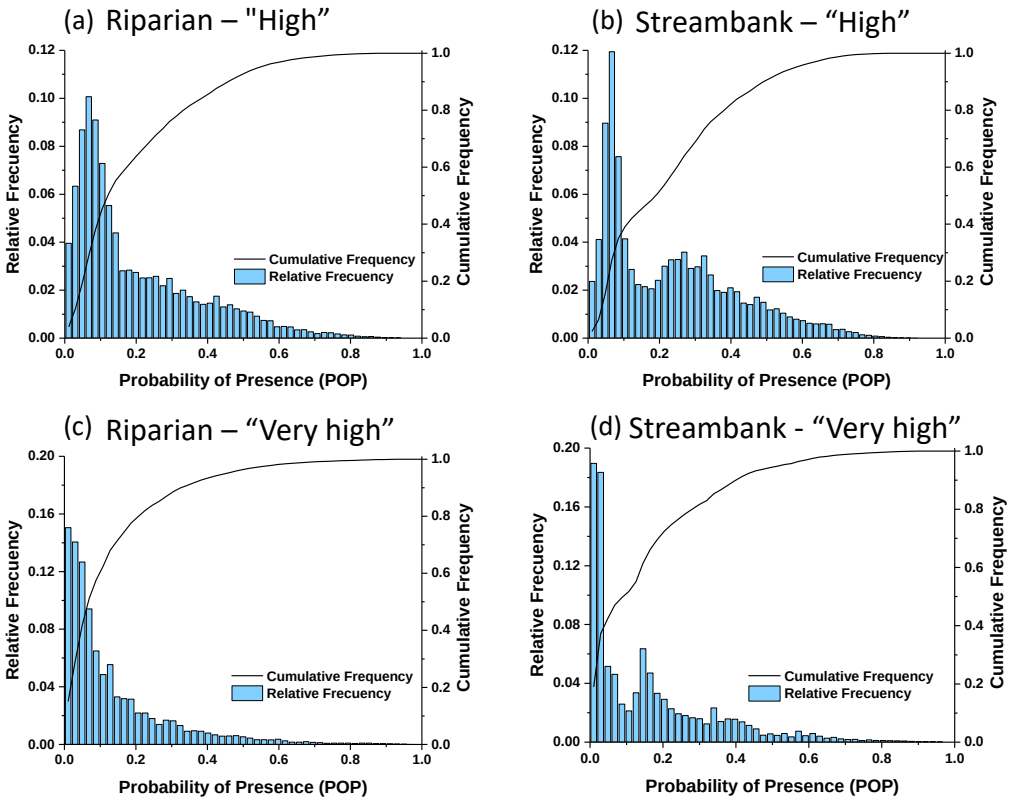

Figure 5. Histograms and Cumulative Distribution Function (CDF) of the erosion POP for the "high" erosion (a, b) and the "very high" erosion (c, d) categories in the riparian buffer and the streambank (Botero-Acosta et al., 2017).

The AUC of the riparian zone training models ranged from 0.71 to 0.90 indicating good model performance, particularly for "high" and very "high erosion" erosion categories (Table 1) under the climate conditions used in this study. Results of the jackknife test indicated that in general, the land use and soil layers provided the most useful information in predicting the presences of erosion in the riparian zone (Table 1). For the "low" category, the land use provided more than 50% of the information while for the "very high" category, soil was the most

dominant source of information (47.10%). The stream power index (SPI) contributed 9.2 to 16.80% of the information while discharge contributed 2.5 to 8.20%. The results for the streambank are parallel to that of the riparian zone (Table 1). The AUC for the "very high" erosion category was 0.89 for the training and 0.86 for the test. The jackknife test showed that the land use (37.2% contribution) provided the highest amount of information in estimating the probability to experience "very high" erosion in the streambanks, this was followed by the soil type with a 28.2% contribution.

Table 1. MaxEnt results for erosion categories in the riparian buffer and the streambank.

Erosion Category	AUC		Environmental Layer Contribution (%)					
	Training	Testing	Land Use	Soil	SPI	Discharge	Lateral Flow	Overland Flow
RIPARIAN								
Low: 0.5 - 0.7 m	0.71	0.71	57.80	29.90	9.20	2.50	0.00	0.50
Medium: 0.7 - 1.0 m	0.78	0.78	49.20	33.90	13.50	2.40	0.40	0.60
High: 1.0 - 1.7 m	0.85	0.83	44.00	32.10	16.80	5.30	1.30	0.40
Very High: 1.7 - 5.9 m	0.90	0.87	28.70	47.10	12.70	8.20	2.90	0.50
STREAMBANK								
Low: 0.5 - 0.7 m	0.64	0.63	56.20	28.70	6.40	5.10	1.90	1.60
Medium: 0.7 - 1.0 m	0.73	0.72	46.20	35.10	6.10	8.50	1.90	2.10
High: 1.0 - 1.7 m	0.81	0.81	41.40	32.80	10.40	10.90	3.50	1.00
Very High: 1.7 - 5.9 m	0.89	0.86	37.20	28.20	15.10	10.10	9.10	0.20

Based on the POP computed by MaxEnt, vulnerability maps were created that showed the locations of all the erosion categories with POP higher than 80% across the riparian zone and streambank of FCREW for the period 2009-2012 (Figure 6). The areas with the highest POP (0.8-1.0) for the "high" and "very high" erosion categories were found mostly in the upper reaches of the Cobb and Lake Creek sub-watersheds. However, more vulnerable areas were identified in the streambank than in the riparian zone. In particular, tributaries of the Cobb Creek were found to be more vulnerable to "very high" erosion (Figure 6c, 6d). These results are consistent with the findings of Storm et al. (2003), who simulated sediment yield from roads and upland areas in the FCEW using the Erosion Prediction Project model and the Soil and Water Assessment Tool (SWAT) model. Their results indicated higher erosion in the northern half of the basin which were visually validated in the field. Additionally, Steiner et al. (2008) stated that soils at the north and south-central zones of FCREW correspond to highly erosive fine sandy loams and loamy soils.

Future values of POP due to projected climate were simulated using the new hydrologic variables from the MIKE models. Results revealed that despite the decrease in the simulated flow in 2040-2043, the vulnerable areas did not change significantly. This is expected, since the land use and soil type, which are the main predictors of erosion presences, remained constant.

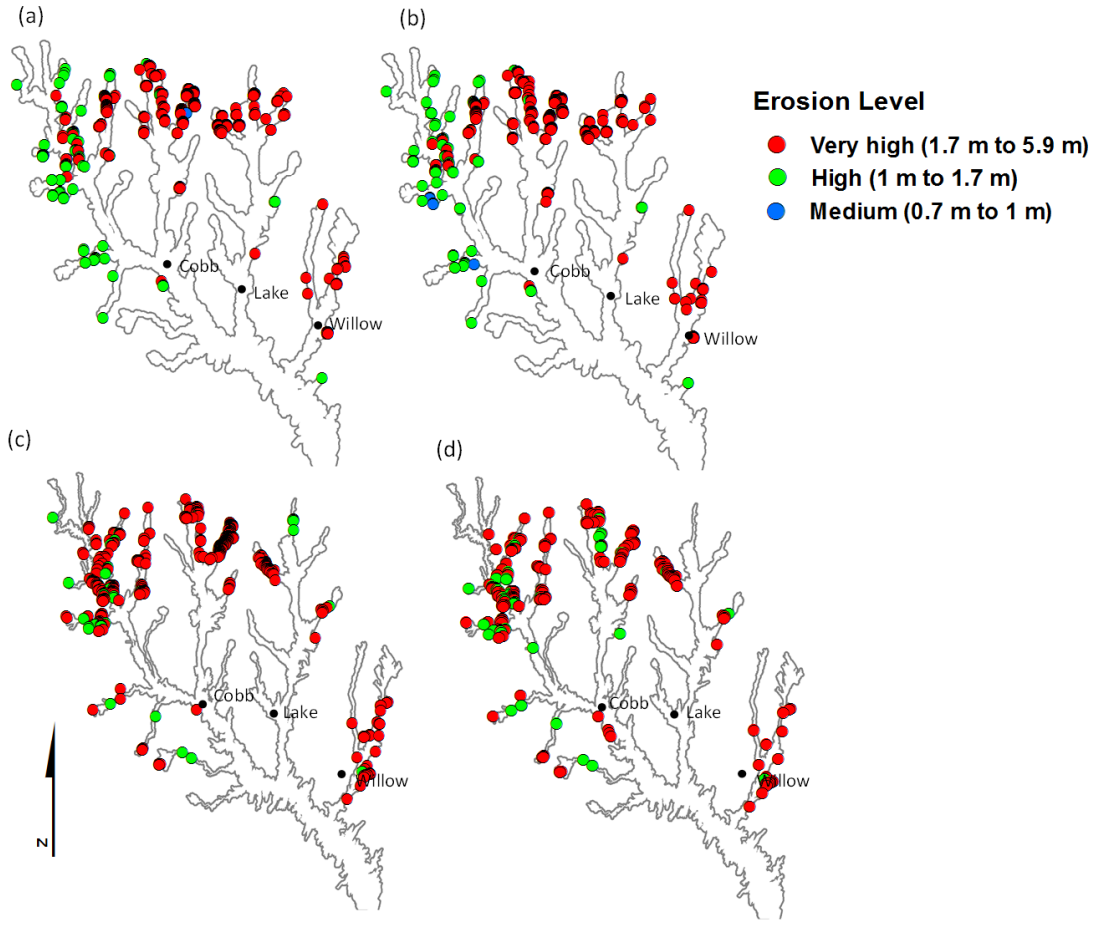

Figure 6. Probable location of vulnerable areas for medium, high, and very high erosion categories. Black dots represent Cobb, Lake and Willow stream gauges. Results shown are locations with probability of presence (POP) higher than 0.8 in the riparian zone for (a) 2009 and (b) 2040 scenarios, and the streambank for (c) 2009 and (d) 2040 (Botero-Acosta et al., 2017).

The erosion suitability curves were created for the very high erosion category of the vulnerability maps in Figure 6. A frequency distribution for each environmental layer was constructed based on the identified location of the very high erosion category (red dots in Figure 6). For the land cover map for instance, the number of cells of each land cover category with POP equal to or greater than 0.8 were determined. The erosion suitability index was then computed using Equation 4. For the streambank zone, the most important environmental layer

contributing to the erosion vulnerability was the land use. Within the land use, the highest suitability index in the very high erosion category was observed in the forest and herbaceous covers (Figure 7a). The forest (deciduous and evergreen) covers only approximately 5% of the streambank zone. Its inclusion as one of the land cover categories manifesting the highest suitability index can be due to the error in the erosion samples. Two LiDAR data sets collected over forested areas at different seasons can result in one scanning the canopy and the other the ground and hence posting a difference that is not due to land elevation changes. The soil types that manifested the highest erosion suitability index belonged to hydrologic soil groups B, C, and D all of them having predominantly silt or sand composition. Erosion suitability seemed to increase with the SPI, discharge, and lateral flow which agrees with the fact that large accumulation of water and high slope are more likely to experience "very high" erosion.

The suitability index curves for the riparian zone (Figure 7b) showed that "very high" erosion seemed to prefer the evergreen forest land use category. This result can be due to errors during LiDAR scans similar to that in the streambank. The soils that showed high suitability for erosion predominantly belonged to hydrologic soil groups B and C (Table 2) with high sand and silt content. Unlike the streambank, riparian erosion seemed to prefer lower SPI while the influences of discharge and lateral flow showed inconclusive trends.

The results of this study are in agreement with related studies and those conducted in the FCREW. Land use and soil are two of the most important environmental features that predict vulnerability to erosion, followed by SPI and discharge. Land use has long been established as affecting surface runoff and consequently surface erosion (e.g., Garcia-Ruiz, 2010; Martinez-Casasnovas and Sanchez-Bosch, 2000; van Oost et al., 2000; Walling, 1999). Similarly, results from Wynn and Mostaghini (2006) suggested that soil bulk density and texture are highly significant parameters when assessing erodibility and critical shear stresses. The soils found to be most prone to erosion in both the streambank and the riparian zones of FCREW belong to hydrologic groups B and C with relatively low bulk densities and high percentages of sand and/or silt. The SPI, as a function of the local slope, was also found to be an important predictor of erosion vulnerability. Steep slopes are a common factor in areas exhibiting major soil losses (Renard et al., 1991). Areas identified as prone to erosion are located at the upstream part of the watershed where slope is generally higher.

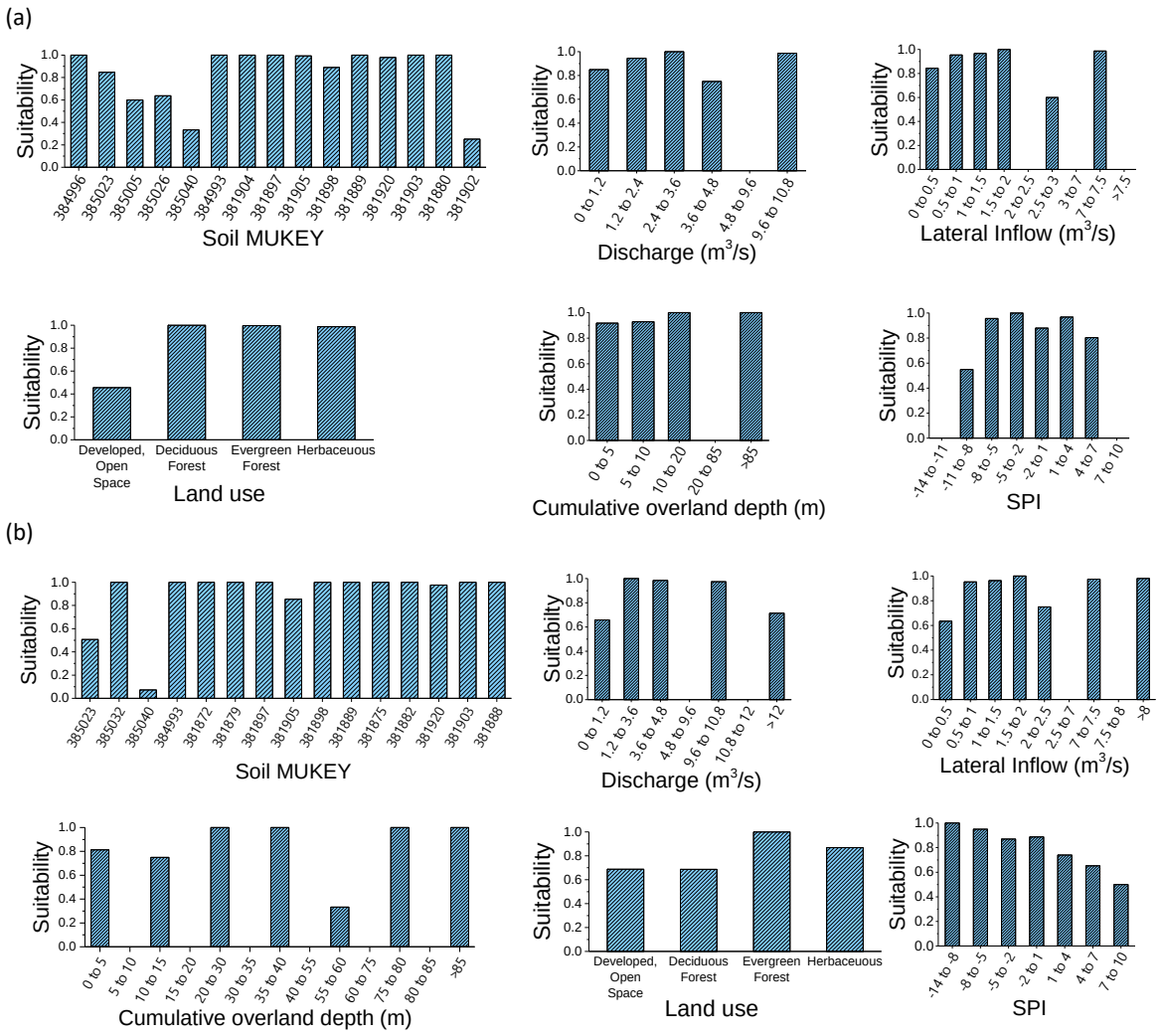

Figure 7. Suitability index curves for (a) streambank and (b) riparian zone (Botero-Acosta et al., 2017)

Within the context of the modeling scenarios, it was observed that the land cover and soils environmental layers played a more important role in erosion vulnerability than did water fluxes. Nonetheless, these results are not conclusive enough to suggest that hydrologic variables are not important determinants of erosion. In this study, the hydrologic variables were represented by the cumulative maximum discharge gridded across the domain as a function of the cell's distance from the stream. However, the ability of flowing water to mobilize particles is best described by its velocity. Flow velocity and its variability, which directly affects critical shear stress responsible for initiating particle movement, was not considered as environmental layer due to lack of river cross section data to support a full hydrodynamic model in MIKE 11. Moreover, the

process of converting the dynamic processes (e.g., overland flow, lateral flow, and discharge) into environmental layers requires some degree of averaging or cumulating. For example, in this study, overland flow was summed up for four years corresponding to the interval of the LiDAR scans. The smoothing process reduced the spatial variability of the processes against the erosion samples. As a result, the background information provided by the dynamic processes for different erosion sample points does not vary considerably, thereby reducing its importance.

Climate change did not have significant effects on the projected erosion vulnerability in FCREW. A study conducted by Garbrecht and Starks (2009) revealed that the effects of climate change and hydrologic regimes over sediment yield on the FCREW was negligible for the study period of 1940-1957. Since there is an existing warming trend in FCREW (Grabrecht et al., 2014), this condition is expected to continue. However, it is important to note that changes in precipitation regimes due to climate change in that period most likely did not manifest any significant change from the historic mean. Trenberth (2011) concluded that climate change impacts will be noticeable in increases in extremes shifting the precipitation regimes between wet and drought on a yearly basis. Soil erosion and its associated transport phenomena is strongly associated with the variability in rainfall. Since the environmental layers used in this study are snapshots of specific conditions (e.g., maximum streamflow), the direct effects of rainfall variability were not considered.

Table 2. Hydrologic groups for the soils found in the streambank and riparian zone.

MUKEY	Hydrologic Group	MUKEY	Hydrologic Group
384996	D	385032	B
384993	B	381872	B
381904	B	381879	C
381897	C	381898	C
381889	B	381875	B
381903	B	381882	A
381880	C	381888	B

Predicting erosion at the watershed scale is challenging, due to the large spatial and temporal variability of soil erosion phenomena and the uncertainty associated with input variables and model parameters used to predict these processes. Erosion and sediment transport processes are highly dependent on the probabilistic nature of the hydrologic regime in the watershed, the

physical characteristics of the watershed, and the stochastic structure of its soil properties (Aksoy and Kavvas, 2005). This complexity cannot be solved by constructing even more complete, and therefore more complex, models (Jetten et al., 2003). This was also supported by Merritt et al. (2003) who reviewed erosion and sediment transport models that are commonly used to estimate transport processes at the watershed scale. They recommended the development of distributed models that have relatively low complexity and plausible physical basis to address the growing requirements of watershed managers and stakeholders for tools that can effectively and efficiently capture spatial aspects of soil erosion. Indeed, there is a practical need, not relying on physically-based watershed models, to estimate soil erosion on watershed scales so that mitigation strategies can be planned in a comprehensive manner (Fox and Papanicolaou, 2008). The method developed in this study addresses this need. The use of a probabilistic approach (e.g. MaxEnt) in combination with a hydrologic model (e.g., MIKE-SHE or a comparable conceptual model) served to identify potential areas that are vulnerable to erosion by also accounting for the uncertainties derived from historic watershed responses. This approach is expected to provide a simple but comprehensive tool to environmental stakeholders to improve estimates of future watershed responses, and thus mitigation plans, while obviating the data requirements of physically-based erosion models.

1.4. CONCLUSION

This study developed a modeling framework that can be used to identify areas along riparian zones that are vulnerable to erosion, using readily available environmental data. MIKE SHE and MIKE 11 were integrated and used to create hydrologic maps of water movement along the streambanks and riparian zones that were used with land cover, soil, and stream power index as environmental layers in MaxEnt. MaxEnt simulated the probability of presences (POP) of different erosion categories along the streambank and the riparian zone separately. Erosion vulnerability maps were created for both the historic and future scenarios to quantify the possible impacts of climate change on the erosion regimes in FCREW.

In general, erosion presences were found to have similar behavior in both the riparian and streambank zones for which 80% of the area has up to 30% of probability to experience erosion greater than 1 m. The most vulnerable areas for erosion were found to be located at the upper riparian zone of the Cobb and Lake sub-watersheds. The main waterways of these sub-

watersheds were also found to be prone to streambank erosion. The projected climate change was found to have minimal effects on the probability of erosion presence in both zones. This is expected, since the impact of climate change was to reduce rainfall in the FCREW and, hence, to produce lower streamflow. Furthermore, the results from MaxEnt revealed that land use and soil type are the most important predictors of riparian erosion across the FCREW, followed by stream power index and streamflow. Since land use and soil remained constant when simulating the impacts of projected climate, these results were expected.

Although the results of our study were consistent with the results of other studies assessing erosion regimes in the Fort Cobb watershed, several pitfalls and limitations were illustrated by our methods, especially in converting the dynamic processes into environmental layers. Unlike environmental layers based on static environmental features (e.g. elevation, land cover, soil), dynamic processes changes in time, requiring some averaging or cumulating before they can be used as environmental layers. The smoothing process, however, can reduce both the temporal and spatial variability of these processes across the domain, hence reducing the importance of the background information that they provide. The conversion of dynamic processes into environmental layer maps to be input in the MaxEnt model, has to be given considerable attention to address this limitation.

Overall, this study presents a cost-efficient approach, relative to an on-ground-survey, to assess erosion vulnerability at the watershed scale that can be useful to conservationists. The framework developed in this study demonstrates the versatility of the method to incorporate changing scenarios such as climate, land use, or land management practices, in predicting their contributions to erosion vulnerability. By being able to identify areas most prone to erosion, conservation and restoration efforts can be focused on these sites for more efficient use of resources. Moreover, identification of environmental variables that can provide the most information in predicting erosion can be used as a basis for research prioritization. A comprehensive assessment of these variables will ensure reliable prediction of erosion.

CHAPTER 2: IMPACTS OF ENVIRONMENTAL STRESSORS ON THE WATER RESOURCES OF INTENSIVELY MANAGED HYDROLOGIC SYSTEMS.[2]

2.1. INTRODUCTION

The critical zone supports life on Earth. In this physical space, bounded by the outer extent of the vegetation and the deep geologic layers with flowing groundwater, many complex processes take place providing the nutrients and energy that the ecosystems depend on to survive (Brantley et al., 2007). Watersheds, viewed as small components of the critical zone, are complex systems with surface and subsurface spatial connections and coupled hydrological and biochemical systems. Studying watershed responses to selected environmental stressors can lead to a better understanding of their impacts on the ecosystem, which can facilitate the decision-making process aimed to mitigate their effects. (Serveiss et al., 2004).

Water fluxes are one of the main drivers of the evolution of the critical zone since they regulate its chemical, biological, and physical processes (Chorover et al., 2011). In turn, the ability of the ecosystem to deliver the services that support human life depends on how the critical zone evolves in response to natural and anthropogenic stressors (Kumar et al in press). For instance, overland runoff and tile drainage generate nonpoint sources of pollution that is considered the most important cause of water quality impairment in the United States (Arabi et. al., 2007). Soil losses caused by extreme rainfall-runoff events deteriorate soil productivity, affecting crop yield, while washed fertilizers transported from croplands impair water quality and compromise aquatic habitats (Yan et al., 2015) of stream networks. These problems are further aggravated in intensively managed watersheds where cropland and urban areas are the principal land use types.

Watershed Management Practices (WMPs) such as crop rotation, riparian buffers, and wetland construction among others, are typically implemented to address water problems such as flooding, excessive sediment load, and water quality impairment in intensively managed

[2] Chapter 2 is a reprint of the article: Botero-Acosta, A., Chu, M.L, Stumpf, A.J. 2018. Impacts of environmental stressors on the water resources of intensively managed hydrologic systems. Hydrological Processes. 32:2947-2962, which has been published in final form at https://doi.org/10.1002/hyp.13244 and the copyright is owned by Hydrological Processes journal.

catchments. The quantification of watershed responses to these practices is achieved through assessment endpoints such as streamflow or species concentration at the outlet. However, evaluating their effectiveness represents a challenge due to the difficulty of identifying their individual contribution to certain assessment endpoints (Serveiss et al., 2004). For instance, a stream species concentration measured in the field will most likely be the cumulative impact of multiple anthropogenic stressors (Christensen et al., 2006) taking place over a period of time. The effectiveness of these practices and their corresponding watershed responses rely on the spatial and temporal connections between the physical, biological, and chemical systems that are difficult to identify at a watershed scale. Isolating the impacts of specific management practices or a combination of them is deemed impossible through field experimentation alone. Although, the impacts of important natural stressors, such as climate change, cannot be assessed through field experiments alone, they are predicted to significantly impact the hydrologic responses that will adversely affect the surface and groundwater resources (Maxwell and Kollet, 2008). Nonetheless, a comprehensive characterization of the water fluxes in the critical zone at a watershed scale can lead to a better understanding of its responses to environmental stressors and can help evaluate the effectiveness of a WMP.

Modeling has largely facilitated impact assessment studies, enabling the investigation of the relationship between stressors and systemic responses. Risk-based conceptual models (Gentile et al., 2001; Serveiss et al., 2004) and conceptual hydrologic models (Bhaduri et al., 2000; Hundecha and Bárdossy, 2004; Tang at al., 2005; Grantham et al., 2010; Getahun and Keefer, 2016) have been applied in cause-and-effect studies to quantify the watershed performance under scenario-based analysis. However, it is crucial to choose models that accurately represent the temporal and spatial attributes of the system, in order to obtain realistic results, especially in intensively managed landscapes. Additionally, models should be able to simulate the spatiotemporal heterogeneity of the hydrologic processes (Kirchner, 2006). The level of complexity of the model should be sufficient to properly conceptualize not just the important processes in the system, but also the proposed WMP, taking into account the limitations of the data. This task is challenging since conceptual models that are easy to parameterize can result in high levels of uncertainties, while physically-based models that are deemed more appropriate require intensive data inputs and are computationally demanding. For intensively managed watersheds with agriculture as the primary land use, conceptualizing WMPs in models is even

more challenging, since the temporal and spatial representation of vegetation changes have to be represented in addition to the changes in hydrologic controls. Moreover, these vegetation changes themselves may affect the hydrologic characteristics of the watershed.

The main objective of this study was to use the physically-distributed watershed model MIKE-SHE (Refsgaard and Storm, 1995) to simulate the responses in an intensively managed watershed under different WMPs (e.g., crop rotation, wetlands, riparian buffers). In particular, the effects of tile drainage, a common practice in poorly drained landscapes, was studied to identify the effects of tile drainage presence on surface and groundwater resources. Future climate scenarios were also simulated to assess the impacts of WMPs under changing climatic conditions. The modeling framework was developed for the Upper Sangamon River Basin (USRB), which lies within the Intensively Managed Landscapes Critical Zone Observatory that is studying how human activities have impacted critical zone processes, specifically the effects of land alterations on the transport of sediment, water, and nutrients flow across the surface and through the subsurface (Kumar et al. in press). In accordance with the Illinois Environmental Protection Agency, Lake Decatur (located at the downstream end of the USRB (Figure 8) is listed as an impaired water body because of high levels of nitrate-nitrogen and phosphorus (Bekele et al., 2014). A baseline model was created with the current watershed conditions over which new scenarios were simulated. Streamflow and water table depth below ground level (*bgl*) at three gauging stations were used as assessment endpoints for the simulated scenarios. Results obtained from this study will facilitate the identification of the most suitable practices and their locations for enhancing water resources at the USRB.

2.2. METHODS

2.2.1. STUDY AREA

The USRB encompasses an area of approximately 2400 km^2 in central Illinois, USA (Figure 8) and receives an average annual precipitation of 1020 mm. Outflow from the USRB drains into Lake Decatur, a man-made reservoir which was constructed in 1922, and is the main water source for the City of Decatur (population 73,000) and the Village of Mt. Zion (population 5,800) (USCB, 2016). The USRB has undergone significant alterations from human activities. A study of the historic changes in the basin indicated that its channel network has been extended by more than a factor of three since the 1820s, mainly during human settlement and by agricultural

activities (Rhoads et al., 2016). The same study showed that in 1820, the USRB was 90% prairie and 10% forest; with forested areas mainly found along the riparian zones. Wetlands used to occupy approximately 50% of the total land area prior to European settlement as opposed to the current 2%. Presently, almost 90% of the watershed area is under row crops, primarily corn and soybeans (Bekele et al., 2014). The transformation of prairie and savannah into agricultural cropland occurred with the installation of ditches and tile drains that were used successfully to drain flat, poorly drained soils in the USRB, which significantly altered its hydrologic responses. As a consequence, the water entering Lake Decatur stems from groundwater pathways rather than from surface runoff, with drain tiles being the primary pathway for water and nutrient transport (Rejesus and Hornbaker, 1999).

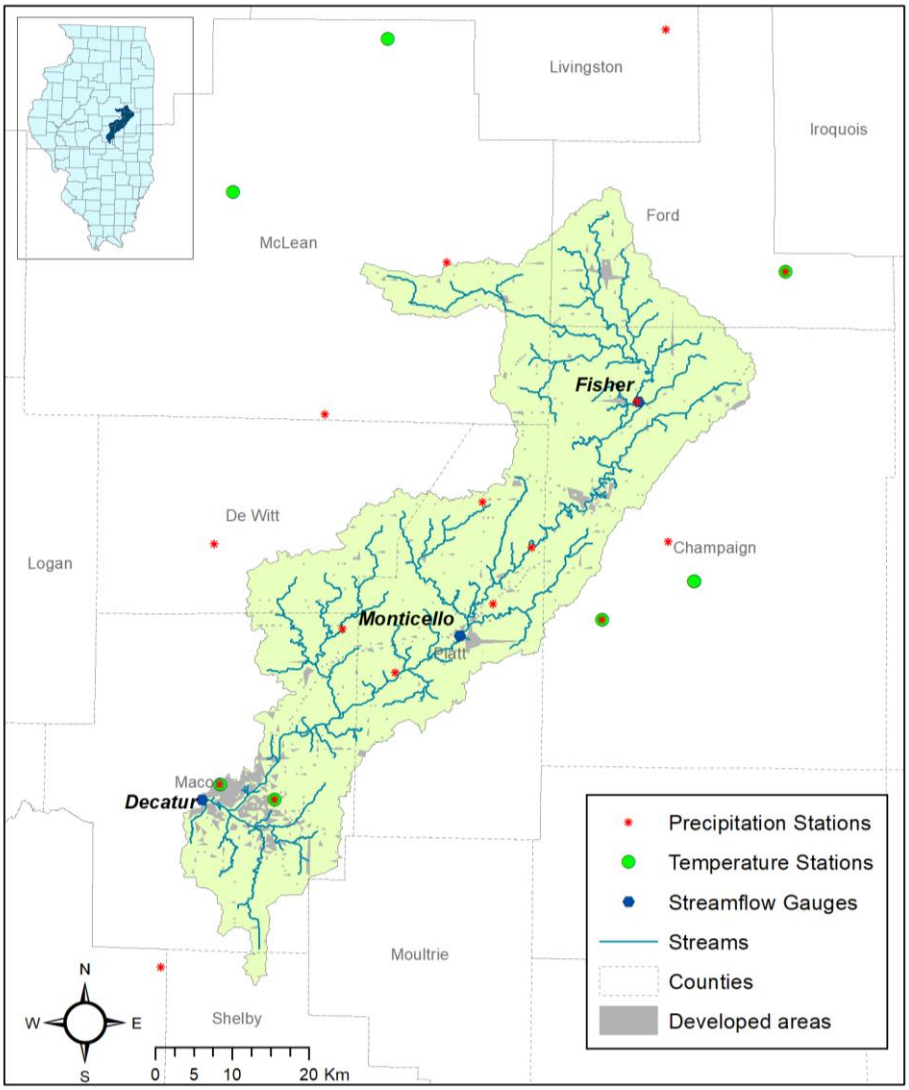

Figure 8. The Upper Sangamon River Basin (USRB) (Botero-Acosta et al., 2018)

2.2.2. HYDROLOGIC MODEL

2.2.2.1. Input Data and Model Setup

The baseline simulation for the WMP scenarios was created using the fully distributed, physically-based model MIKE-SHE coupled to the hydrodynamic one-dimensional model MIKE 11. The watershed was discretized into a 300 x 300 meter grid and the parameters were obtained from the physical properties of the watershed. The 300 x 300 m resolution was selected based on the resolution of the input layers and the computational requirements of MIKE SHE. The water flow was simulated through four systems or compartments: overland zone, unsaturated zone, saturated zone (including tile drainage), and streams. Inputs required to parameterize the overland zone included topography, climate, land use, Manning Surface Coefficient (M) related to each land use type, and runoff coefficient for paved zones. Daily precipitation and temperature time series data were obtained from the National Oceanic and Atmospheric Administration (NOAA) ground base database (NOAA, 2016). Stations from the USRB and its neighboring watersheds with recorded available data for the 1998-2015 period and a temporal coverage higher than 90% were considered. Sixteen stations were selected for precipitation data while seven stations were chosen for air temperature data. Missing values from the precipitation and temperature time series were filled in by means of the Inverse Distance Weighting method, while daily reference evapotranspiration was estimated by applying the modified Makkink formulation (De Bruin and Lablans, 1998). The land cover types found in the USRB are: urban, forest, pasture, wetlands, alfalfa, corn, and soybeans, the last two being the most prevalent (Figure 11a) (USDA, 2016). For each vegetation category, the Leaf Area Index (LAI), the root depth, and the crop coefficient (Kc) time series were spatially defined based on the 2014 Cropland Data Layer (USDA, 2016). The overland flow was simulated by solving the flow diffusive wave equation using a 2-dimensional finite difference method.

The subsurface components, the unsaturated and saturated zones, are explicitly coupled in MIKE-SHE. The unsaturated zone includes all the soil between the ground surface and the water table and hence, its changes as the groundwater table rises and falls. The unsaturated zone was characterized using the water retention curves of the soil profiles defined by the NRCS Official Soil Series Descriptions (NRCS, 2016). The representative soil series for each county was selected in accordance with its percentage of coverage over the county area. Four soil series were

selected as the most common in the seven counties within the USRB: Bryce, Sable, Drummer, and Flanagan (Table 3). The capillary pressure (in kPa) at field capacity and wilting point for all the soil types were set to 33 and 1500, respectively. The flow through this compartment was modeled by solving the Richards equation with a 1-dimensional unsteady finite difference method.

Table 3. Soil types used in the vadose zone characterization of MIKE-SHE.

Soil name	Location (by County)	Layer	Lower depth (m)	Soil moisture at saturation ( )	Saturated hydraulic conductivity (m/s)
Bryce	Ford	1	0.33	0.502	1.55e-5
		2	1.14	0.432	8.75e-6
		3	5	0.428	6.94e-7
Sable	McLean, DeWitt	1	0.36	0.469	4.39e-6
		2	0.51	0.466	2.86e-6
		3	0.71	0.441	2.15e-6
		4	0.99	0.451	3.53e-6
		5	1.22	0.446	2.14e-5
		6	1.42	0.474	1.12e-5
Drummer	Champaign, Piatt, Shelby	1	0.18	0.51	7.94e-6
		2	0.48	0.482	5.39e-6
		3	0.81	0.398	4.5e-6
		4	0.99	0.419	5.67e-6
		5	1.52	0.469	2.13e-5
Flanagan	Macon	1	0.46	0.546	7.17e-6
		2	0.58	0.487	9.69e-6
		3	0.97	0.518	5.53e-6
		4	1.14	0.518	4.81e-6
		5	1.52	0.455	2.32e-5

The saturated zone flow was simulated by a 3-dimensional unsteady finite difference solution of the Darcy flow equation. Required inputs for the saturated compartment included: lower level elevation of geologic layers, hydraulic conductivities in each direction (a 3x3 diagonal tensor), specific yield, and initial potential head. If subsurface drainage is included, the model further requires the drainage depth and time constant coefficient. The bottom elevation of the modelled geologic units was delineated according to the glacial stratigraphy the Upper Sangamon River Basin (Figure 9), characterized by its extreme complexity and heterogeneity (e.g., Anders et al., 2018). The geologic units mapped in the study area were simplified into two layers (Figure 9). They do not include the regionally important Mahomet aquifer, as its hydrostratigraphic unit is not exposed along the Sangamon River valley at the selected endpoint locations. This means that the top up the upper confining layer of the Mahomet aquifer is the

bottom of the modeled geologic layers. The upper geologic unit in the model, the Henry-Ashmore layer, is principally composed of till and sand and gravel of the Henry Formation and Ashmore Tongue (Figure 9). The lower layer includes the Glasford and Pearl Formations (Glasford-Pearl layer) that are comprised of till, sand and gravel, and silt and clay (Figure 9). These layers were spatially characterized from 22 geologic cross sections drawn based on the work of Stumpf and Atkinson (2015), from which the lower level elevation of each layer was extracted and interpolated across the study domain by the Inverse Distance Weighting method. The latter, predicted the lower level elevations of the entire domain using the values from the cross sections, giving greater weight to those cross sections closest to the prediction location (Figure 10).

A preliminary four-year running period indicated that the water table stabilized after 1 year at a depth of 2 m *bgl*, which was used as the initial condition for the water table depth. As the geologic units in the USRB were grouped into two main aquifer layers, their hydraulic properties (horizontal and vertical hydraulic conductivities and specific yield) were adjusted to achieve the equivalent value that best represented the saturated zone behavior.

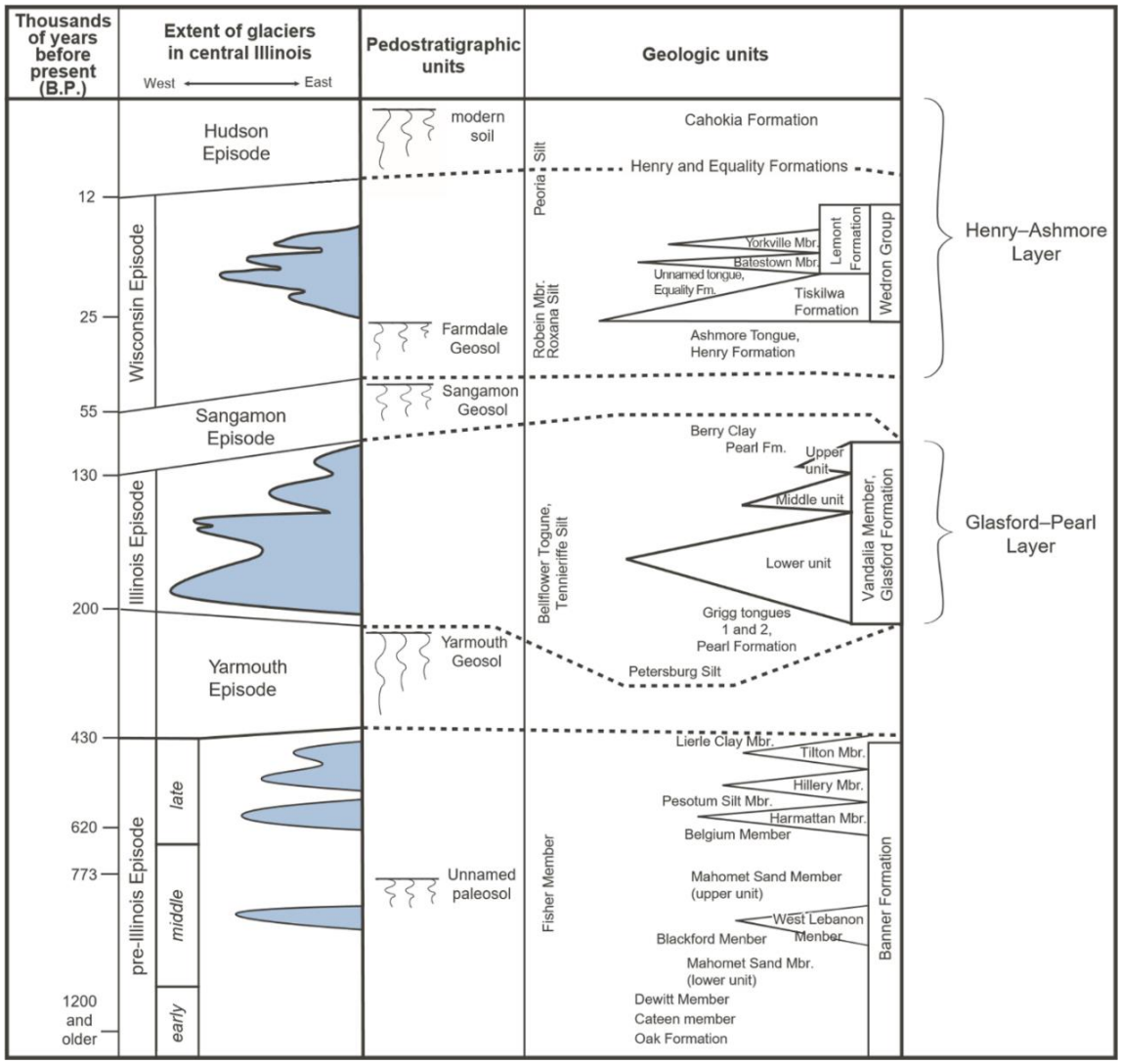

Figure 9. Schematic diagram of the glacial stratigraphy in the USRB, including the two aquifer layers. Also shown are the geologic and pedostratigraphic units, and diachronic classification. Modified from Stumpf and Dey (2012). ©2012 University of Illinois Board of Trustees. Used with permission of the Illinois State Geological Survey (Botero-Acosta et al., 2018).

The tile drainage was activated in the saturated zone module at 1 meter below the ground level and its drain time constant was adjusted so that the simulated daily and cumulative discharges matched the measured at the three stream gauges at Fisher, Monticello, and Decatur (Figure 8) (USGS, 2017). The drain time constant characterizes the density of the drainage network and the permeability around the drains (DHI, 2009). It is a conceptual parameter that acts as leakage coefficient between the soil and drain. The drainage outflow is then calculated as

a linear reservoir and is equal to the water table height above the drains multiplied by the drain time constant (Zhou et al., 2013).

When the water reached a cell linked to the river network, the 1-dimensional hydrodynamic model, MIKE 11, simulates the propagation of the hydrograph in the river. The river network topology used to create the MIKE 11 model, was built from a 30-meter resolution DEM (USGS, 2016). The flow through the 113 branches of the USRB river network was simulated by kinematic routing.

MIKE-SHE/MIKE 11 is a physically-based model with most parameters directly measured from field experiments. However, the performance of the model was still evaluated to ensure that the conceptualization of the saturated zone and the drain time constant adequately simulated the hydrologic response of USRB. Model performance was assessed using three metrics: (a) Nash-Sutcliffe (NS) - to evaluate general agreement between the measured and simulated hydrographs, (b) Pearson's correlation coefficient (r) - to estimate the correlation between measured and simulated daily streamflow, and (c) cumulative flow error - to estimate the water balance discrepancy at the end of the simulation period.

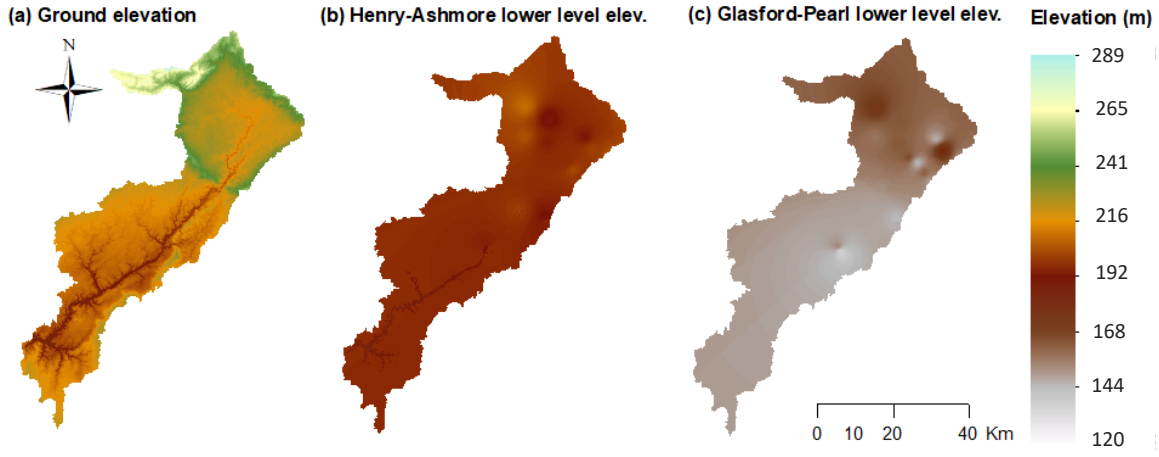

Figure. 10. The geologic layers used to conceptualize the saturated zone of USRB. (a) ground elevation from DEM, (b) lower level elevation of Henry-Ashmore layer and (c) lower level elevation of Glasford-Pearl layer (Adapted from Botero-Acosta et al., 2018).

2.2.3. ENVIRONMENTAL STRESSORS

The USRB baseline model was modified in order to simulate its responses to scenario-based environmental stressors. Combinations of WMPs and projected climate scenarios were implemented in the model. The assessment endpoints were the streamflow and water table depth

bgl at the three streamflow gauging stations: Fisher, Monticello, and Decatur (Figure 8). The baseline model was simulated from 1998–2015 period using the first two years to set-up the initial conditions of the model.

2.2.3.1. Watershed Management Practices

The natural, pre-settlement landscape of the USRB have been largely modified by human activities that in turn altered the response of the critical zone to natural stressors by modifying the fluvial processes and groundwater flow systems (Rhoads et al., 2016). The extensive row crop production, the tile drainage installation, and the complete loss of wetlands, have been the most important changes that the USRB has experienced, converting its natural landscape and ecosystem into one with intensive and extensive water, sediment, and nutrients fluxes. Lake Decatur has become the collector of these fluxes (e.g., Blair et al., 2018). Nearly 200,000 tons (0.83 tons/ha) of sediments reach the lake every year. In fact, Illinois Environmental Protection Agency issued eight warning alerts in 13 years period (between 1979 and 1992) due to high nitrate concentration caused mainly by non-point source pollution (Rhoads et al., 2016). Studying how these anthropogenic stressors modify the surface and groundwater resources will facilitate the understanding of watershed processes and the current and future behavior of the critical zone.

To create a more comprehensive scenario-based modeling framework to evaluate the impacts of WMPs on water resources in USRB, 19 scenarios (Table 5) were simulated using the baseline MIKE-SHE model. The WMP variations used in these scenarios were: (1) tile drainage removal, (2) wetlands construction, (3) forested riparian buffer, (4) crop rotation at Fisher subwatershed, (5) crop rotation at Monticello subwatershed, and (6) crop rotation at Decatur subwatershed.

Tile drainage largely affects water flow through the critical zone. For the first WMP modification, the tile drainage system was completely deactivated from the model to determine how the watershed would have responded if this alteration had not been done. All the other components (e.g., land use, climate, and saturated and unsaturated zones parameters) remained the same as in the baseline model.

The USRB used to have approximately 50% of its area covered by seasonal wetlands before European settlement (Rhoads et al., 2016). Currently, most of it is used for row crops, and less than 2% of the USRB contains wetlands. For this reason, the second WMP modification applied

to the watershed was conceived to assign 49% of the area originally used for row crops production as wetlands (Figure 11b). The choice of this WMP was also prompted by its popularity among the different environmental organizations in Illinois, and is one of the management practices to address high nitrate loads (Bekele et al., 2014; Getahun and Keefer, 2016). However, its effectivity has not been properly quantified yet. In order to recreate the conditions before settlement, the wetlands were placed over poorly draining soils and the existing tile drains were removed. The surface area and drainage area ratio of the wetlands varied from 16.9% to 93%. A retention storage of 150 mm was adopted for the wetlands (Blick et al., 2004). Moreover, implementing wetlands in MIKE-SHE entailed modifying the Manning (M) coefficient and the vegetation maps. The herbaceous vegetation properties (LAI, root depth, and Kc) time series were used in lieu of the original vegetation cover.

The third WMP variation consisted of creating a 300-meter wide buffer around the river network within which the row crop areas were replaced by forest (Figure 11c). The width of the buffer corresponds to the width of the cells in MIKE SHE and it is also within the recommended width for riparian buffer zones (Fischer and Fischenich, 2000; Hawes and Smith, 2005). The Manning (M) number and vegetation properties for the forest category were used for these cells.

The last three WMPs are non-structural in nature that farmers can implement without state level interventions. In these WMP scenarios, the model domain was divided into three subwatersheds: Fisher, Monticello, and Decatur, in accordance with the respective streamflow gauges. The scenarios were created by randomly modifying the land use of approximately 30% of each subwatershed area (or approximately 10% of the total USRB area) originally used for corn production to implement a two-year corn-soybean rotation (Figures 11d, 11e, and 11f), in which year one was for corn production and year two for soybean production. The LAI, root depth, and Kc time series were modified accordingly to implement the rotation schedule.

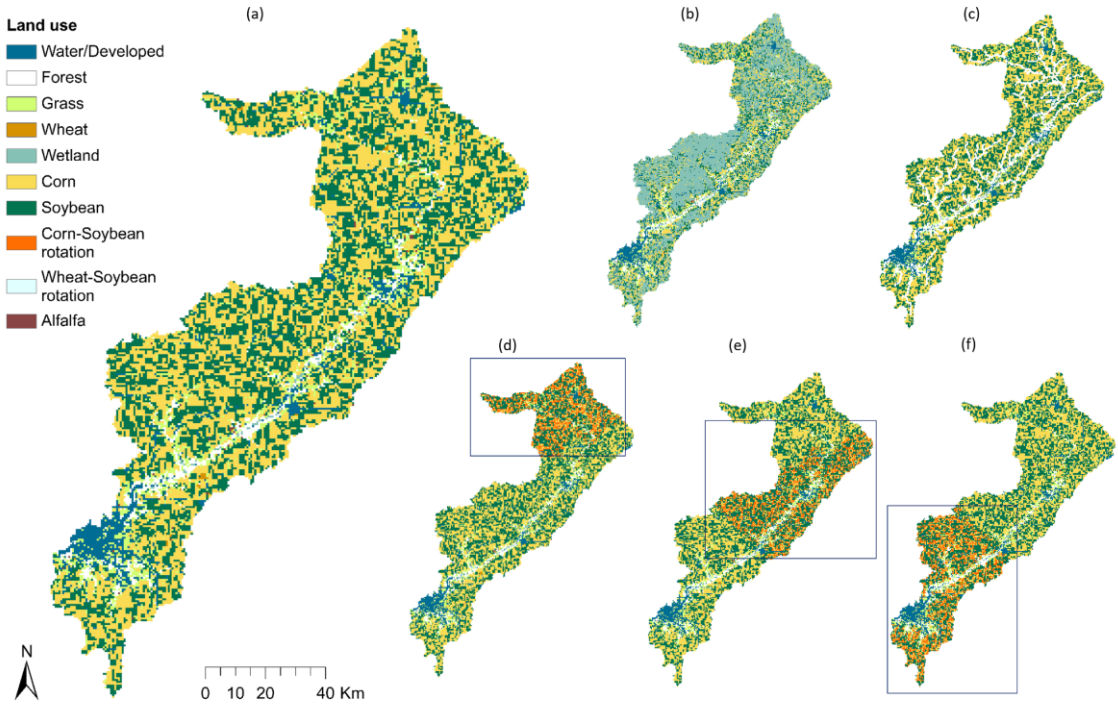

Figure 11. Watershed Management Practice (WMP) variations implemented in this study. (a) Current land use (baseline), (b) WMP 2: Constructed wetlands, (c) WMP 3: Forested riparian buffer, (d), (e) and (f) WMP 4, 5, and 6: Crop rotation at Fisher, Monticello and Decatur subwatersheds respectively (Botero-Acosta et al., 2018)

2.2.3.2. Climate change

Considering the impacts of climate change on the water resources over the long term will allow managers and policy-makers to take action to mitigate the future water-related problems. Considering climate change impacts on groundwater is critical to understanding processes of recharge and drought (Maxwell and Kollet, 2008). Climate change impact on the hydrologic cycle was evaluated by simulating the streamflow and water table under projected climate scenarios. Future climate projections were simulated for the period 2048–2065 with the first two years being allocated for the initialization of the model.

The Coupled Model Intercomparison Project (CMIP), an international mission to better simulate future climate by comparing existing climate models, was used to generate future climate data. The Geophysical Fluid Dynamics Laboratory (GFDL) from the National Oceanic and Atmospheric Administration (NOAA) has contributed to this project with three climate models. The downscaled climate data of precipitation and temperature (CMIP5, 2017) from the

three GFDL models for the climate stations (Figure 8) across USRB were extracted and studied. The average values at all locations showed that models GFDL-CM3 and GFDL-ESM2M generated the most critical projections with the former simulating the highest and the latter the lowest average values for precipitation and temperature during the simulation period. They were therefore used to generate the future climate in this study. The GFDL-CM3 model focuses on the role of (1) aerosols, (2) aerosols-cloud interactions, and (3) atmospheric chemistry, while the GFDL-ESM2M, from Earth System Models (ESM), comprises (1) atmospheric biogeochemical processes, such as aerosols, clouds physics and precipitation and (2) land processes that affect carbon dynamics as evaporation, and streams and oceanic fluxes (GFDL, 2017). The projection chosen for both models was the RCP 8.5 (Representative Concentration Pathway 8.5), which comprises of high population growth along with changes in technology and energy intensification, leading to a rise in energy demand and greenhouse gas emissions. The projection RCP 8.5, among all the RCPs, has the highest greenhouse gas emission (Riahi et al., 2011).

Although daily precipitation and temperature time series for future climate conditions were available at CMIP5 (2017), the reference evapotranspiration was not available. A polynomial regression analysis ($R^2 = 0.67$) was conducted between the historic reference evapotranspiration (1998-2015) and the corresponding temperature and precipitation of that period to obtain an expression to estimate the future daily reference evapotranspiration at the USRB. The historic reference evapotranspiration was computed using the modified Makkink equation (De Bruin and Lablans, 1998) using the following equations:

$$ET_{ref} = 0.65 \frac{s}{s+\gamma} \left(\frac{R_s}{L}\right) \quad \text{Eq. 7}$$

$$s = \frac{4098 e_a}{(237.3+T_{ave})^2} \quad \text{Eq. 8}$$

$$e_a = 0.6108 e^{\frac{17.27 T_{ave}}{237.3+T_{ave}}} \quad \text{Eq. 9}$$

where:

ET_{ref} is the reference evapotranspiration (mm/day), s is the slope of the temperature-saturation vapor pressure curve (kPa/^{o}K), γ is the psychrometric constant (0.067 kPa/ ^{o}K at sea level), R_s is the incoming short wave radiation (W/m^2), L is the latent heat of vaporization (2.45x10^6 J/kg), T_{ave} is the average temperature, and e_a is the air's saturation vapor pressure (kPa). The historic (1998-2015) average and maximum daily reference evapotranspiration and

the one computed from the polynomial regression for the 1998–2015 period were then compared for verification measures. The Makkink equation resulted in a mean and maximum reference evapotranspiration of 2.5 and 6.5 mm/d, respectively, while the polynomial regression resulted in 2.5 and 6.4 mm/d for mean and maximum values, respectively.

The current climate data for the period 1998–2015 was found to have lower average values of daily precipitation, temperature, and reference evapotranspiration than the future scenarios CM3 and ESM2M for the 2048-2065 period. The projected average precipitation was higher than the current by approximately 14% for CM3 and 1.5% for ESM2M, while the future average temperature increased from 11.25°C to 15.01°C for CM3 and to 13.33°C for ESM2M. This trend was mimicked by the reference evapotranspiration with increases of 27% for CM3 and 16% for ESM2M (Table 4).

Table 4. Statistical characteristics of the current and future climate scenarios.

	Daily Precipitation in USRB (mm)			Daily Temperature in USRB (°C)			Reference Evapotranspiration rate in USRB (mm/d)		
	Average	**Max**	**Min**	**Average**	**Max**	**Min**	**Average**	**Max**	**Min**
Current climate (1998-2015)	2.73	158.20	0.00	11.25	32.80	-25.30	2.56	6.49	0.05
GFDL-CM3 (2048-2065)	3.10	106.10	0.00	15.01	39.36	-21.43	3.26	9.46	0.00
GFDL-ESM2M (2048-2065)	2.77	110.49	0.00	13.33	36.45	-21.86	2.96	9.20	0.00

The impacts of WMPs and projected climate were evaluated through 19 scenarios (Table 5). The current watershed land use and climatic conditions were used as the baseline model (Scenario 1). The separate impacts of projected climates were assessed in Scenarios 2 and 3 while the impacts of the individual WPMs were evaluated in Scenarios 5, 8, 11, 14, and 17 (Table 5). The WMP modification number 2, tile drainage removal, was not used for future climate conditions since it is not feasible to uninstall the tile drainage system. It was only simulated with the current climate data with the aim of quantifying the effects of tile drainage over the watershed response. The combined effects of the future climate and WMPs were evaluated in the remaining scenarios.

Table 5. Applied scenarios.

	% Modified area*	Current climate (1998-2015)	GFDL-CM3 (2048-2065)	GFDL-ESM2M (2048-2065)
Current WMP	-	Scenario 1**	Scenario 2	Scenario 3
WMP 1 - Tile drainage removal	80.4	Scenario 4	-	-
WMP 2 - Wetland construction (Figure 11b)	49.0	Scenario 5	Scenario 6	Scenario 7
WMP 3 – Riparian buffer (Figure 11c)	13.7	Scenario 8	Scenario 9	Scenario 10
WMP 4 - Crop rotation Fisher (Figure 11d)	7.4	Scenario 11	Scenario 12	Scenario 13
WMP 5 - Crop rotation Monticello (Figure 11e)	8.9	Scenario 14	Scenario 15	Scenario 16
WMP 6 - Crop rotation Decatur (Figure 11f)	9.6	Scenario 17	Scenario 18	Scenario 19

* With respect to the current land use

**Baseline

2.3. RESULTS AND DISCUSSIONS

2.3.1. HYDROLOGIC MODEL

MIKE-SHE is a physically-based model whose parameters are measurable in the field. However, a comparison between measured and simulated values was made to evaluate the performance of the model in simulating the response of the watershed (similar to Botero-Acosta et al., 2017). The equivalent parameters of the saturated zone, as well as the drain time constant, were adjusted to improve the agreement between the measured and simulated discharges at the stream gauges in Fisher, Monticello, and Decatur (Figure 8) for the period 2009 to 2012. Horizontal and vertical hydraulic conductivities were adjusted to 4.8 x 10^{-6} m/s and 4.8 x 10^{-5} m/s respectively for the Henry-Ashmore layer, and 3 x 10^{-4} m/s and 1.6 x 10^{-8} m/s for the Glasford-Pearl layer. The hydraulic conductivities for the upper unit of the Glasford Formation vary over a wide range, from 10^{-4} and 10^{-9} m/s degrees of magnitude, due to the spatial variation in the sediment types (Atkinson et al., 2014). The time constant parameter for the drainage was adjusted to 1 x 10^{-7} s^{-1} to obtain reasonable model performance metrics. This value was within the ranges estimated from different studies quantifying the MIKE-SHE drainage time constant, which varied from approximately 1x 10^{-6} s^{-1} to 9 x 10^{-8} s^{-1} (Zhou et al., 2013). Nash-Sutcliffe of approximately 0.6, 0.8, and 0.7 and cumulative errors of 1.9%, 14.7% and 4.5 % were obtained for the simulated streamflow at Fisher, Monticello, and Decatur, respectively (Figure 12). The long-term (1998–2015) performance of the model in reproducing the streamflow was also

evaluated using Nash-Sutcliffe and Pearson's correlation coefficient. The Nash-Sutcliffe was found to be 0.41 in Fisher, 0.55 in Monticello, and 0.59 in Decatur while the Pearson's coefficient was 0.67 in Fisher, 0.75 in Monticello, and 0.79 in Decatur.

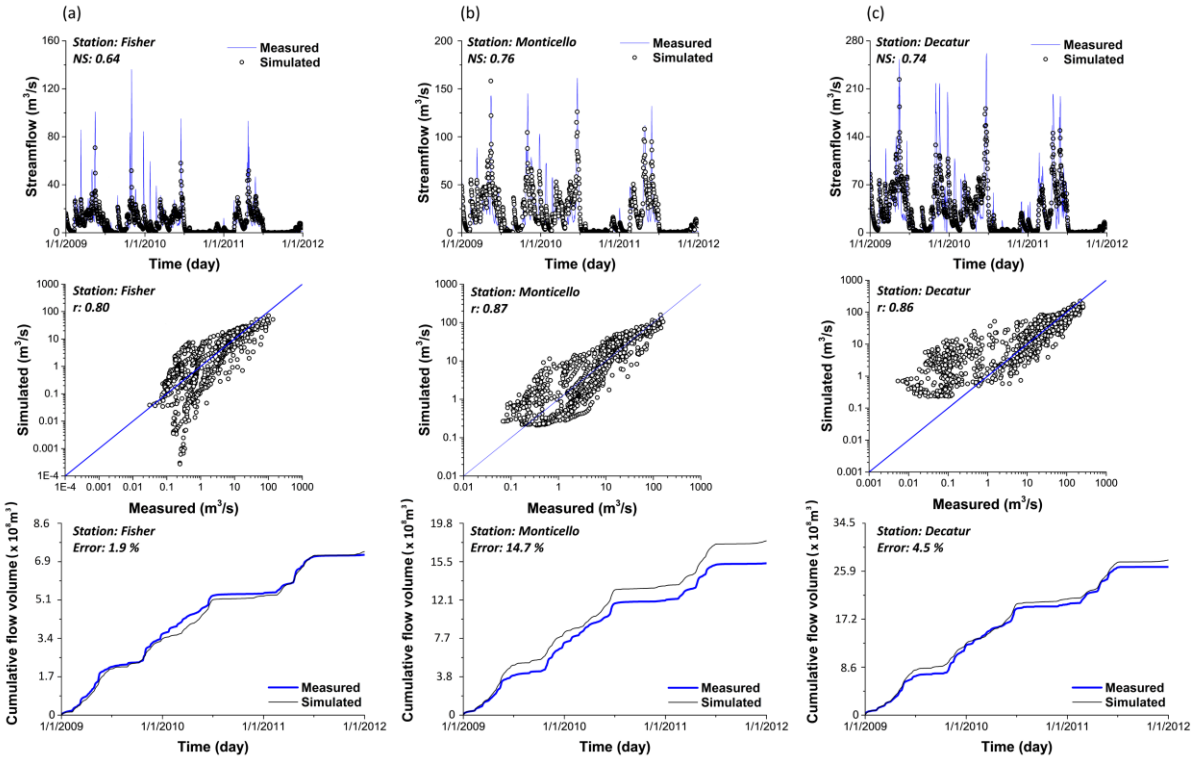

Figure 12. Model performance metrics for the three streamflow gauges. (a) Fisher, (b) Monticello, and (c) Decatur (Botero-Acosta et al., 2018)

2.3.2. ENVIRONMENTAL STRESSORS

The baseline, corresponding to the current hydrologic conditions in the USRB, consisted of the current land use and climate data for the 1998-2015 period (Scenario 1). The average daily streamflow at Fisher, Monticello, and Decatur stations were found to be 5.2 m^3/s, 12.3 m^3/s, and 19.3 m^3/s, respectively (Table 6). During the period of simulation, no visible trend was observed in the daily streamflow in the three gauging stations although, a notable wet period occurred in 2008 and a dry period in 2012. The average water table depth *bgl*, on the other hand, was simulated at 1.0 m at Fisher, 1.94 m at Monticello, and 1.15 m in Decatur. The annual behavior of the water table depth showed a very steady pattern for Fisher and Decatur of approximately 1.0 m *bgl*, as opposed to Monticello, which fluctuated from 1.0 to 2.0 m. The response of the water table depth was consistent with the changes in streamflow for the period of simulation.

Table 6. Streamflow and water table depth for the baseline model (Scenario 1) at Fisher, Monticello and Decatur stations.

	Streamflow		Water table depth *bgl*	
	Average (m^3/s)	Max (m^3/s)	Average (m)	Max (m)
Fisher	5.21	61.08	1.10	2.36
Monticello	12.26	128.61	1.94	2.73
Decatur	19.33	253.22	1.15	2.46

2.3.2.1. Impact of drains

The eighteen scenarios (Scenarios 2 to 18), were adopted with the aim of quantifying their impacts on streamflow and water table depth with respect to the baseline model at Fisher, Monticello, and Decatur. The effects of tile drainage removal (Scenario 4) was investigated under current climate conditions only, given the infeasibility of having them removed in the future. The goal was to understand how this anthropogenic stressor introduced many years ago into the USRB have modified the natural behavior of the watershed. Simulation results reveal that the drain removal decrease the average daily streamflow at Fisher by approximately 1% and approximately 9% at Monticello and Decatur, mainly because of the removal of tile drained water flowing to the main waterways. These changes were relatively small compared to the large effects on the maximum observed discharge, which increased by up to 400% when drains were removed (Table 7). This might be the effect produced by extreme rainfall events and the condition of the soil moisture when these events occurred; saturated soils, easily occurring when no tile drainages were installed, decrease the buffering effect on extreme rainfall events creating large OL flow to the rivers. As expected, the average water table depth below ground level decreased by 30% to 50% when the subsurface drains were removed (Table 8), which means the phreatic level was brought up to the surface when no tile drainage was installed. Even negative values of the water table depth were found at Fisher and Decatur, indicating that without the drains, the water table could rise above the ground level. The probability density function (*PDF*) of the assessment endpoints variables, streamflow and water table depth, were constructed to visually evaluate the water fluxes variations for each scenario. Figures 13a and 13b exhibit the effects of tile drainage removal on the average daily streamflow and water table depth at Decatur. Parallel results to that in Decatur were found in Fisher and Monticello and were not shown. Drainage removal decreased the frequency of streamflow ranging from 5 m^3/s to 500 m^3/s and increased the frequency of extreme events (lower than 0.01 m^3/s and larger than 500

m^3/s) (Figure 13a). Notwithstanding the relative increases in the frequency of extreme events (Figure 13a) and the reported increases in the maximum observed discharge (Table 7), the total amount of water reaching the outlet of the USRB every year was reduced (Figure 16a). The yearly cumulative flow volume at Decatur decreased for all the simulated years with respect to the baseline, with a maximum reduction of 24% (Figure 16). This is explained by the drastic drop in the relative frequencies of streamflow ranging between 5 m^3/s to 500 m^3/s and the increase in frequency of flow lower than 5 m^3/s, facts that also explain the reported reduction in the average streamflow at the three stations (Table 7). The *PDF* for the water table depth showed an increase in frequency for smaller water table depths *bgl*, bringing the phreatic level up (Figure 13b). It can be observed how the highest frequency of water table depth shifted to the left when the drains were disabled. The rising of the water table above the ground surface can be seen through the relative frequency of water table depths of 0 m and less (Figure 13b), behavior that was not observed in any of the other scenarios. The shift in the *PDF* of the water table depth allowed crop production in USRB by draining the excess groundwater. However, tile drainage also increased the frequency of daily streamflow ranging from 5 to 500 m^3/s (Figure 13a), which can be one of the main causes of water quality impairment in Lake Decatur since the drains provided a faster flow pathway for contaminants. This issue is exacerbated by agricultural activities, causing non-point source pollution from fertilizers and pesticides. In fact, Lake Decatur has high concentrations of fertilizers, pesticides, and sediments transported by the USRB streams and drained water, exceeding the drinking water standards for nitrate-N (Bekele et al., 2014). Although studies focusing on the impacts of tile drainage on water quality are numerous, very little literature was found about its effects on water resources quantity. Results from Calsamiglia et al. (2018) reported that tile drainage in a Mediterranean watershed increased the connectivity along the main channel, enhancing subsurface flow towards the river and fostering a more efficient draining of excess water. Wesstrom et al. (2000), and Wiskow and ven der Ploeg (2003) who developed studies in southern Sweden and northern Germany respectively, found that the construction of subsurface tile drains increased peak flows, a fact that was confirmed by the results reported here (higher relative frequencies of streamflow ranging between 5 m^3/s to 500 m^3/s when drains were included).

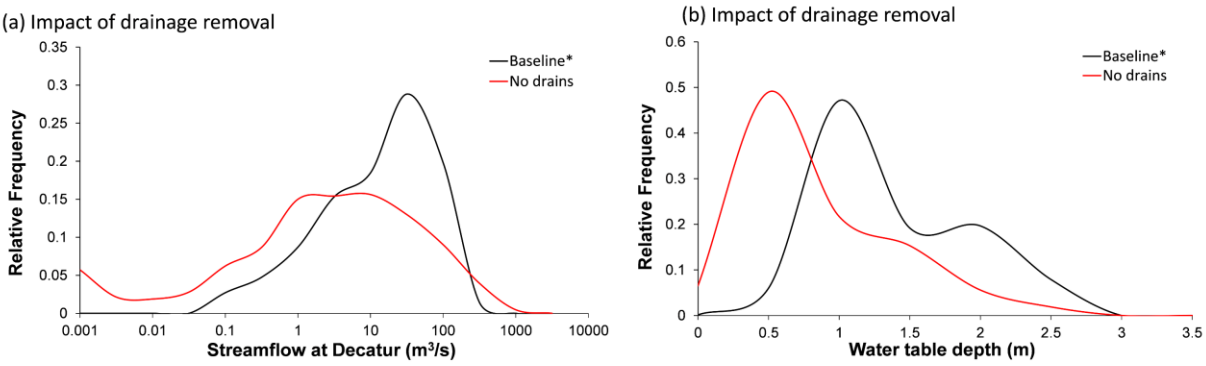

Figure 13. Tile drainage removal effects (Scenario 4). *PDF*s of (a) streamflow and (b) water table depth below ground level (*bgl*) at Decatur under current climate conditions. * Current land use and current climate (Botero-Acosta et al., 2018)

2.3.2.2. Impacts of future climate

The impacts of climate change were evaluated by comparing Scenarios 1, 2, and 3, that is, the baseline and the two climate projections with the currently applied WMPs. In general, future climate scenario CM3 (Scenario 2) increased the average daily discharge by approximately 12% in Decatur (Table 7) resulting from the presence of extreme flow events or outliers. An increase of approximately 78% of the maximum streamflow at Decatur was observed for this climate projection (Table 7). On the other hand, the climate projection ESM2M (Scenario 3) reduced the average streamflow at Decatur by almost 8% and also the maximum value by 32%. The relative change in the total cumulative flow volume in Decatur for the 15-year simulation period was computed for the two future climate models. An increase of 3.6 % with respect to the baseline was encountered for the CM3 model, while a decrease of 7.8 % was found for ESM2M. The difference in responses from these two climate conditions can be due to the differences in the projected precipitation from the two climate models. CM3 increased the average precipitation by 13% with respect to the baseline, in contrast with the 1.5% for ESM2M. The climate impacts on surface water at Fisher and Monticello were similar to that in Decatur, where CM3 caused an increase in the streamflow while ESM2M resulted in a reduction. The water table depth experienced similar effects between both future scenarios where the average water table depth *bgl* increased by approximately 10% in Decatur, up to 9% in Fisher, and up to 23% in Monticello (Table 8).

Overall, the impacts of both climate scenarios were to decrease the frequency of the most likely streamflow in Decatur (~60 m^3/s) (Figure 14a) while increasing the frequency of

streamflows smaller than 3 m^3/s. For the CM3 model, an additional increase in the frequency of extreme events (>500 m^3/s) was observed. On the other hand, the frequency of deeper water table (approximately 2.5-m depth) showed an increase at Decatur (Figure 14b) implying a decrease in groundwater resources due to the projected climate. These results agreed with the reported future climate impacts on water resources. Eckhardt and Ulbrich (2003) showed that under warmer climate conditions, the groundwater recharge and the streamflow of a catchment in Germany could be reduced by 50%, especially during summer. Taylor et al. (2012) estimated the global groundwater depletion during the 2001-2008 period showing that North America and Asia had the most pronounced groundwater depletion amounting to approximately 18% and 76% of the total global groundwater depletion, respectively. This shows the importance and high demand of groundwater in the US, which is expected to increase in the coming century with the reduction in surface water for domestic and industrial purposes. With the projected decreases in groundwater, this can result in water stress in the USRB if no mitigation strategies are implemented before then.

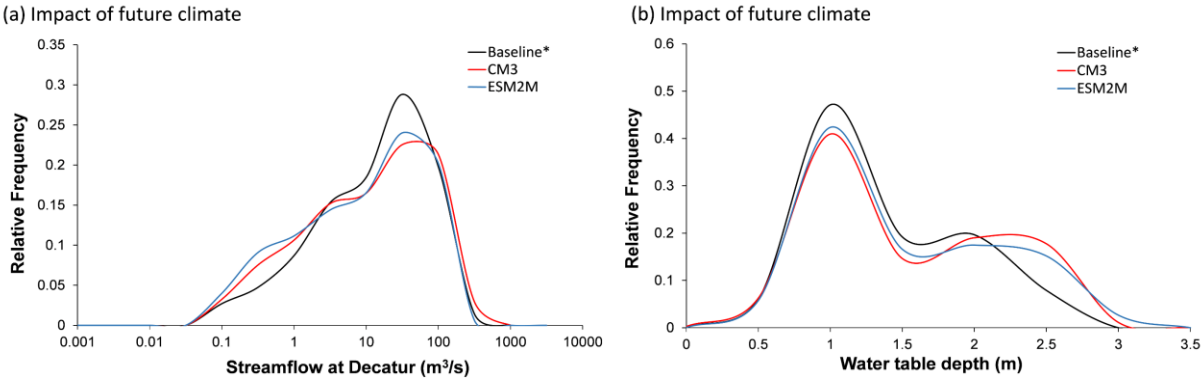

Figure 14. Climate change effects under current land use (Scenarios 1, 2 and 3). *PDF*s of (a) Streamflow and (b) water table depth *bgl* at Decatur. * Current land use and current climate (Botero-Acosta et al., 2018)

2.3.2.3. Impacts of WMPs

The impacts of WMPs were quantified by implementing the constructed wetlands, forested riparian buffers, and crop rotation at Fisher, Monticello, and Decatur subwatersheds. The streamflow and the groundwater were simulated by modifying land use input data over the study domain that led to changes in (1) plant uptake conditions (by changing the daily LAI, root depth, and Kc) and, (2) overland flow (by changing the Manning coefficient (M) and retention storage).

The variables related to the plant cycle varied accordingly to the development stage of the vegetation. These changes on the surface are seamlessly propagated to the unsaturated and saturated zones in MIKE SHE. Wetlands and forested riparian buffers under current climate conditions (Scenarios 5 and 8) decreases the average streamflow with respect to the baseline in the three stations, with reductions ranging from 13.4% to 18.3% (Table 7), generally presenting higher reductions for the wetlands. The cumulative flow volume is predicted to decreases with respect to the baseline in all the simulated years for both scenarios (Figure 16a), with reductions by up to 30% and 24.6% for the wetlands and riparian buffer, respectively. These results reflect the effects of the changes in the M, LAI, root depth, Kc coefficients and, in the wetlands case, the retention storage. For wetlands for instance, the retention storage was set to 150 mm, M decreased by 37%, LAI was increased by up to 54% while Kc was decreased by up to 18% from the start of plant development to harvest. For forested buffers, M decreased by 17% to 77%, LAI was increased by up to 56%, and Kc decreased by up to 36%. These changes resulted in reducing the overland flow and increasing the evapotranspiration. However, the maximum streamflow was increased by 10% for riparian buffers at Fisher, and up to 243% for wetlands at the three stations, with the highest increase observed at Fisher as well (Table 7). The fact that it is the smallest subwatershed (25% of the total USRB area) and has the highest elevation change could render the Fisher subwatershed prone to higher extreme values, due to a smaller travel time to reach the subwatershed outlet. The increases in the maximum streamflow obtained for the wetlands scenario, although not as high, were comparable to the ones found for the no-drains scenario. In both cases, the removal of tile drainage on almost half of the original cropland in the wetlands scenario and on the entire domain for the no drains scenario, resulted in a decrease of the average and an increase in the value of the maximum daily streamflow. Even though the large increase observed in the maximum streamflow for the wetlands, the net water flowing out of the USRB did not increase (Figure 16a); this is explained by the fact that the relative frequencies for large streamflow did not increase with respect to the baseline (Figure 15a), and that the maximum streamflow value had very low frequency. Golden et al. (2016) also reported the streamflow attenuation caused by wetlands. The simulation of the streamflow in 579 subbasins in North Carolina, USA, led to the conclusion that seasonal and annual streamflow decreases as the extent of wetlands increases. Literature has also reported the dampening effects of riparian buffers on streamflow. Wenger (1999) stated that riparian buffers moderate the

streamflow during flood events, one of the reasons why buffers help control stream sediment load. Similarly, according to Parkyn (2004), the main function of riparian vegetation in large rivers is slowing the flood flows, while in small streams it is shading and filtering.

Crop rotation scenarios (Scenarios 11, 14, and 17) did not result in significant changes on the average and maximum daily streamflow except when the crop rotation was implemented in Monticello (Scenario 14) where the maximum streamflow increased by 77% to 115% at the three stations (Table 7). However, this increase in maximum streamflow did not affect significantly the net amount of water flowing out of the USRB. The yearly cumulative flow volume at Decatur had an increase of up to 5.3% with respect to the baseline when the crop rotation was implemented at Monticello subwatershed (Figure 16a). Likewise, crop rotation implemented at Fisher and Decatur increased up to 4.8%, and 3%, respectively. The minor effects of the increase in the maximum streamflow over the cumulative flow volume for Scenario 14, can be explained by the fact that the frequency of extreme events did not increase with respect to the baseline, similar to what was observed for the wetlands. The *PDF* of streamflow for all WMPs under current climate conditions (Figure 15a) showed that all WMPs had a similar behavior to the baseline, with the exception of the wetlands (Scenario 5), which showed a slightly higher frequency around the most likely streamflow value. Hence, even though the maximum streamflow increased, it has a minute impact on the overall water balance of the watershed.

None of the WMPs caused any significant changes on the average water table depth, with the exception of the wetlands scenario (Table 8). This result was expected, since riparian buffer and crop rotations scenarios comprised surface WMPs that may have limited impacts on the groundwater resources, while the reduction in the tile drainage area for the constructed wetlands would certainly affect the water table level. A reduction of 13%, 5%, and 6% on the water table depth *bgl* was observed for wetlands scenario at Fisher, Monticello, and Decatur, respectively (Table 8). In general, the *PDF*s for all WMPs scenarios showed a similar behavior to the baseline (Figure 15b), except for the wetlands (Scenario 5) that registered the rise of the phreatic level, and the crop rotation implemented at Decatur subwatershed (Scenario 17), which increased the frequency of the average water table depth (around 1 m below the ground level) (Figure 15b). The reported effects of the wetlands over the phreatic level agrees with the findings of Hensel and Miller (1991) in northeastern Illinois. After experimental wetlands were constructed, an increase in the groundwater level was observed due to seepage. Numerical predictions of seepage

for wetlands situated over sand and gravel were reported to be 60 to 150 times the seepage of a wetland over clayey till (Hensel and Miller, 1991). Furthermore, Van der Kamp and Hayashi (1998) affirmed that wetlands are focal points of groundwater recharge and are of main importance for sustaining groundwater resources in Canadian semi-arid northern prairies.

2.3.2.4. Impacts of WMPs and future climate

The WMPs scenarios were then tested under the two future climate conditions: the CM3 and the ESM2M climate projections. The USRB reacted differently to the WMP under future climate scenarios. The wetlands under the CM3 climate projection (Scenario 6) did not significantly affect the average daily streamflow (Table 7) although it posted reductions of up to 4.2 % in the three stations. The water table depth increased at Monticello and Decatur by 7.8 % and 3.6 % with respect to the baseline, respectively (Table 8). The constructed wetland under the ESM2M climate projection (Scenario 7) resulted in a reduction in the average daily streamflow by 20% to 24% in all the stations. Varying effects were observed for the average water table depth where an increase of 12% was observed at Monticello, while Fisher experienced a decrease of 7% and Decatur did not present changes with respect to the average water table depth of the baseline. It can be noted the scenarios under ESM2M climate projection resulted in an increase in precipitation of only 1.5%, while the evapotranspiration increased by 16%, which could have caused the reduction in water flux. The forested riparian buffer had the same impacts as the constructed wetlands where reductions in the average streamflow were expected to reach up to 30% for both climate projections (Table 7). This is accompanied by an increase in the average water table depth of up to 40% (Table 8).

The crop rotation scenarios under the CM3 climate projections (Scenarios 12, 15, and 18) resulted in an increase in the daily average streamflow from 8% to 14% at the three stations (Table 7). Similarly, the magnitude of extreme streamflow increased from 89% to 117% (Table 7). The larger amount of rainfall water of this projection, along with the shorter life cycle of soybean, reduced the amount of evapotranspiration, causing an increase in surface water fluxes. This scenario contrasts with the effects of the same WMP under the climate projection ESM2M (Scenarios 13, 16, and 19) for which reduction in average and maximum streamflow were predicted. In both climate projections, the crop rotation scenarios increased the average water table depth, especially in Monticello where increases of up to 23% were predicted (Table 8).

The *PDF*s of daily streamflow at Decatur under CM3 and ESM2M climate projections (Figures 15c and 15e) showed similar behavior for the crop rotation scenarios regardless of where they were implemented. In general, the frequency of the most occurring streamflow events was reduced with respect to the baseline in all WMPs except in constructed wetlands. The frequencies for water table depths greater than 2 m in Decatur showed an increase for both CM3 and ESM2M projection and all WMPs. The occurrence of water table depths to up to 3.5 m *bgl* from the latter projection were also expected. For the wetlands scenario, an increase in the frequencies of water table depths smaller than 0.5 m, exhibited the effect of the partial drainage removal. When the crop rotation was implemented at Decatur (Scenarios 18 and 19), the frequency of the average water table depth (at 1 m *bgl*) tended to be higher than the other scenarios (Figures 15d and 15f). This was also observed in the current climate scenario for the same WMP (Scenario 17) suggesting a smaller impact of land use changes at the lowlands of USRB over the groundwater resources at Decatur. The impacts of climate change over the watershed response to WMPs is evident when comparing the *PDF*s of the streamflow and water table depth for current climate conditions (Figures 15a and 15b) and future climate projections (15c, 15d, 15e, and 15f). The frequency of low flow events seemed to increase with projected climate and a deeper water table was also expected to be more frequent.

The yearly cumulative flow volume at Decatur for the 15-year simulation period showed that the ESM2M climate model reduced the total cumulative flow volume for all WMPs, with a maximum reduction of 20% for the wetlands scenario. On the other hand, CM3 decreased the total cumulative flow volume for the wetlands (by 10%) and the riparian forest (by 13%), and increased it for the three crop rotation scenarios (by 6%). This behavior can be explained by the large mean ET for the future scenarios, being 27% and 15% (for CM3 and ESM2M, respectively) larger than for the historic climate.

The purpose of implementing the WMPs in USRB was to mitigate the impacts of agricultural activities on the river system by reducing the nutrient and sediment transport. Riparian buffers and wetland construction were intended to decrease mean flowrates by increasing evapotranspiration and trapping nutrients and sediments while crop rotation was implemented to reduce the nutrient load. For their intended purposes, the WMPs were perhaps effective with the general reduction in the average and maximum streamflow. However, their impacts under projected climate scenarios may not offer long term relief since increases in surface water fluxes

were also predicted in the future. The impacts of varying the location of land management practices did not result in significant changes in streamflow and groundwater flow. Crop rotation (between corn and soybeans) is a common practice in central Illinois that farmers have adopted, this practice reduces fertilizer application rates since soybean is a nitrogen fixer and does not require application of additional nitrogen fertilizer. Similar to the scenarios for wetlands and riparian buffers, the impacts in the USRB to crop rotation could be negative under the projected climate scenarios because the change in the maximum streamflow is predicted to be greater than 100%.

The biggest threat to the groundwater resources in USRB is the future climate changes. The simulated results in this study only considered the possible changes to the groundwater flow system due to changes in water fluxes brought about by surface alteration. Projected groundwater extraction was not considered but is expected to exacerbate the depletion of the groundwater resources as we approach the mid-century. For example, between 2012 and 2014, 16 irrigation pivot systems were added to the approximately 70 already existing in the USRB (Bridges et al. 2015). During their peak usage, groundwater withdrawals is more than double the per day usage in the cities of Champaign-Urbana (~23 million gallons per day).

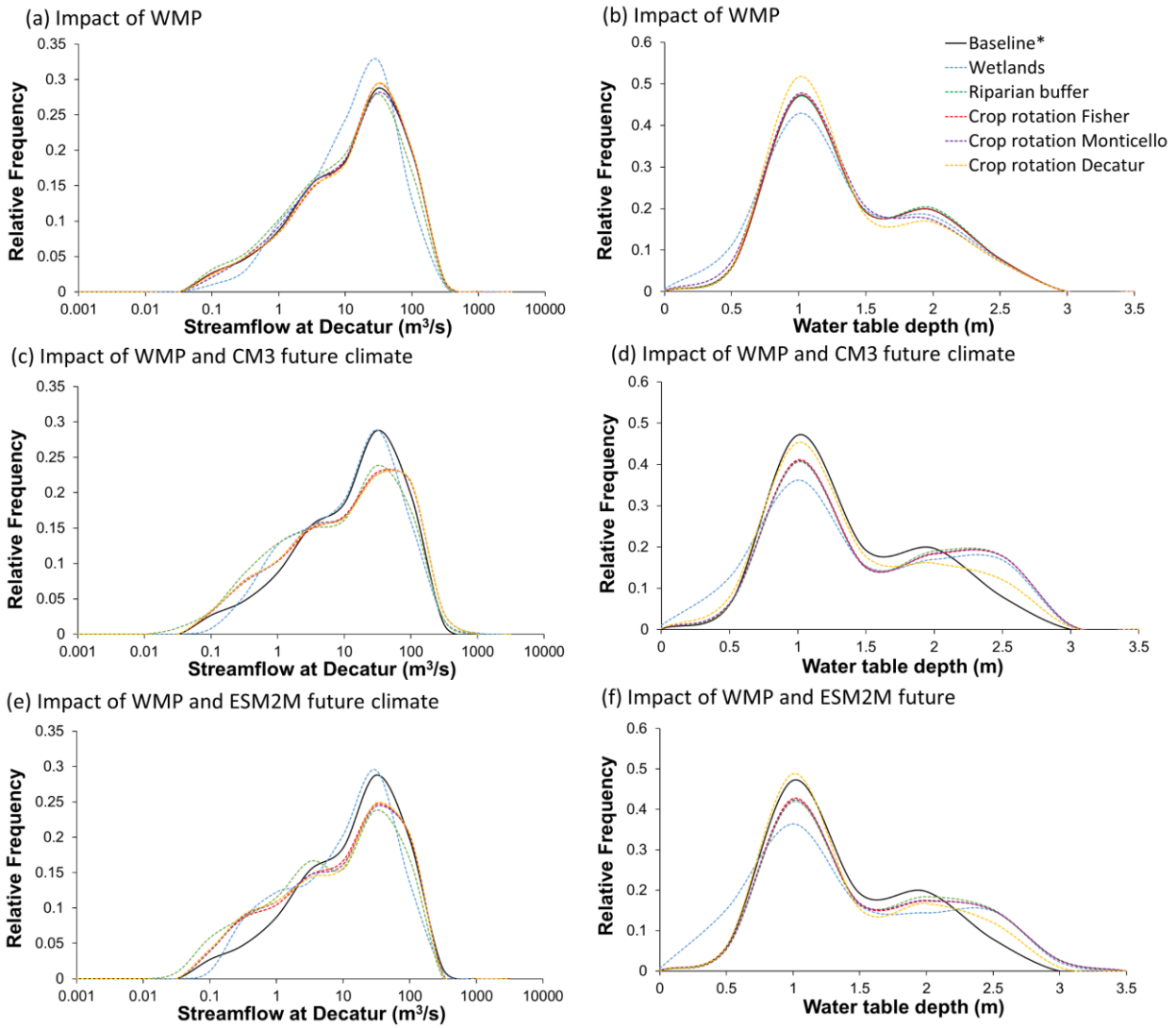

Figure 15. The impacts of WMPs under current and future climate conditions (Scenarios 5-19). *PDF*s of (a), (c) and (e) streamflow and (b), (d) and (f) water table depth *bgl* at Decatur. *Current land use and current climate (Botero-Acosta et al., 2018)

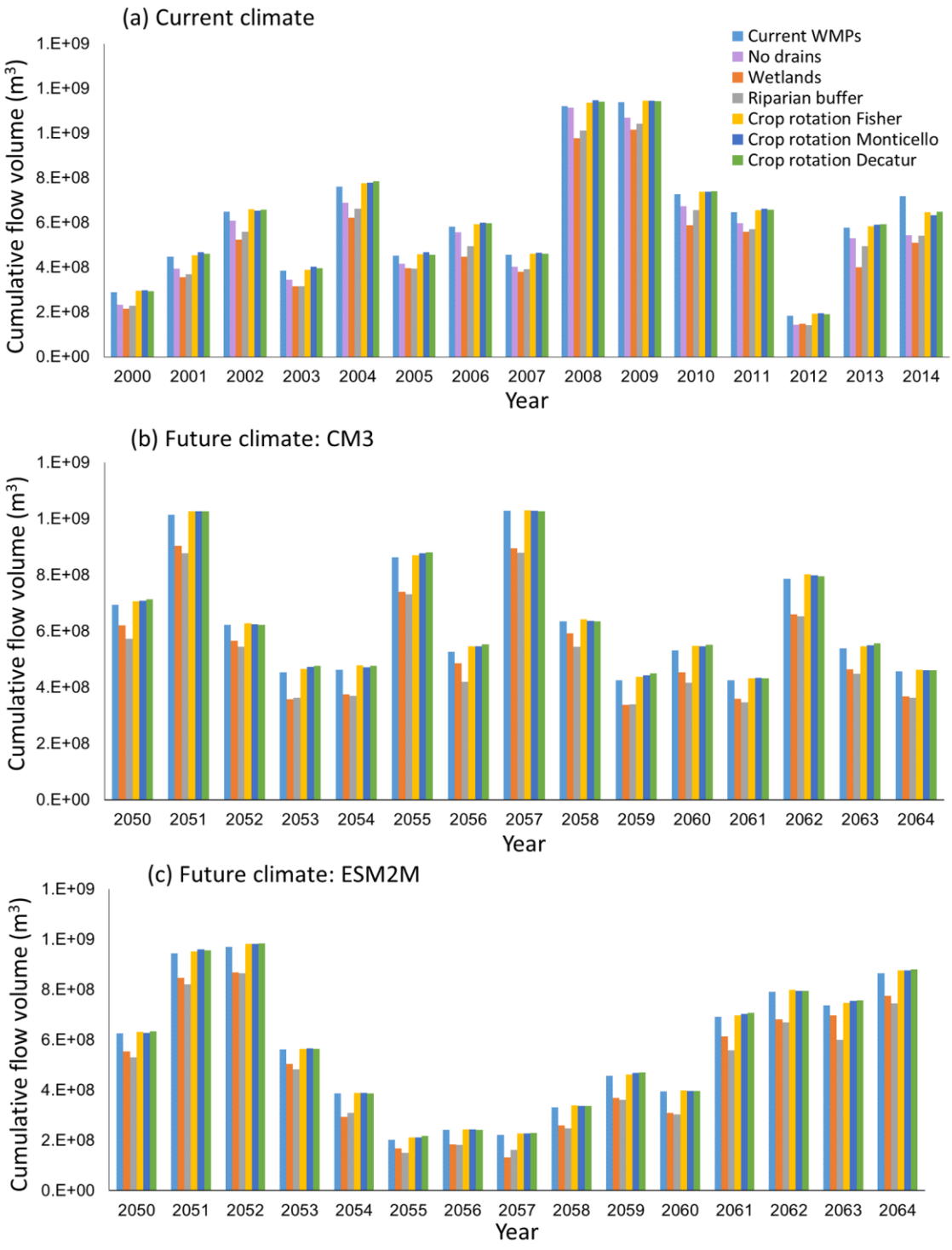

Figure 16. Impacts of WMPs on the annual cumulative flow volume at Decatur under (a) current climate, (b) CM3 and (c) ESM2M future climate models (Botero-Acosta et al., 2018)

Table 7. Percentage of change of the average and maximum streamflow for the 19 simulated scenarios with respect to the baseline at Fisher, Monticello and Decatur stations.

STREAMFLOW	FISHER STATION						MONTICELLO STATION						DECATUR STATION					
	Current climate		GFDL-CM3		GFDL-ESM2M		Current climate		GFDL-CM3		GFDL-ESM2M		Current climate		GFDL-CM3		GFDL-ESM2M	
Scenario	Ave. (%)	Max. (%)	Ave. (%)	Max. (%)	Ave. (%)	Max. (%)	Ave. (%)	Max. (%)	Ave. (%)	Max. (%)	Ave. (%)	Max . (%)	Ave. (%)	Max. (%)	Ave. (%)	Max. (%)	Ave. (%)	Max. (%)
Current WMP	**0.0**	**0.0**	8.3	103.1	-12.1	-1.0	**0.0**	**0.0**	10.1	112.1	-11.9	-8.9	**0.0**	**0.0**	11.8	77.5	-7.6	-31.9
No tile drainage	-1.2	328.6	-	-	-	-	-8.5	408.6	-	-	-	-	-8.8	372.5	-	-	-	-
Wetlands	-13.4	243.4	-1.2	169.6	-20.7	58.6	-17.6	167.0	-4.2	205.0	-24.1	53.4	-18.3	76.7	-2.8	165.2	-20.5	7.7
Riparian buffer	-15.7	10.6	-13.4	65.0	-30.6	-18.3	-15.1	-11.1	-10.5	48.9	-29.3	-20.2	-13.7	-24.8	-6.9	43.7	-23.5	-38.0
Crop rotation Fisher	2.6	41.5	12.5	112.8	-8.9	-0.4	1.1	5.3	12.2	117.1	-10.5	-8.7	0.7	-15.9	13.3	89.5	-6.7	-31.8
Crop rotation Monticello	0.6	115.3	8.5	106.7	-12.0	-0.5	2.0	97.5	12.7	117.8	-10.0	-7.4	1.4	77.0	13.5	92.1	-6.4	-30.6
Crop rotation Decatur	0.1	25.5	8.3	107.6	-12.2	-4.4	0.1	-2.8	10.2	114.0	-12.0	-6.3	1.1	-8.8	13.7	91.5	-6.3	-28.9

Table 8. Percentage of change of the average and maximum water table depth *bgl* for the 19 simulated scenarios with respect to the baseline at Fisher, Monticello and Decatur stations.

WATER TABLE DEPTH	FISHER STATION						MONTICELLO STATION						DECATUR STATION					
	Current climate		GFDL-CM3		GFDL-ESM2M		Current climate		GFDL-CM3		GFDL-ESM2M		Current climate		GFDL-CM3		GFDL-ESM2M	
Scenario	Ave. (%)	Max. (%)	Ave. (%)	Max (%)	Ave. (%)	Max. (%)	Ave. (%)	Max . (%)	Ave. (%)	Max (%)	Ave. (%)	Max (%)	Ave (%)	Max (%)	Ave. (%)	Max. (%)	Ave. (%)	Max. (%)
Current WMP	**0.0**	**0.0**	4.0	5.8	8.7	2.8	**0.0**	**0.0**	13.3	4.5	23.3	26.5	**0.0**	**0.0**	10.7	5.3	9.6	6.6
No tile drainage	-55.9	-8.3	-	-	-	-	-31.7	-4.5	-	-	-	-	-52.3	-11.7	-	-	-	-
Wetlands	-13.6	-5.5	-10.8	-0.6	-7.4	1.2	-5.3	-2.2	7.8	-0.6	12.4	15.3	-6.2	-0.7	3.6	4.8	0.0	6.1
Riparian buffer	0.5	-0.8	4.4	5.7	9.2	3.0	1.0	4.7	21.2	13.0	40.1	49.6	0.7	0.0	11.3	5.5	10.9	6.9
Crop rotation Fisher	-0.1	-0.7	3.5	5.5	7.8	3.0	0.5	0.0	12.4	4.2	22.6	26.3	0.1	-0.2	10.3	5.1	9.3	6.7
Crop rotation Monticello	-1.4	-1.2	4.0	5.5	8.6	2.9	-3.3	0.1	12.9	5.3	22.7	26.3	-3.5	0.2	10.6	5.2	9.5	6.6
Crop rotation Decatur	0.1	-0.5	4.1	5.5	8.7	2.9	0.5	0.1	12.5	4.7	23.1	26.8	-4.0	-0.2	0.8	3.9	1.8	4.4

2.4. CONCLUSIONS

This study applied a physically-based distributed model to simulate the water fluxes under different environmental stressors at a watershed scale. The hydrologic model of the USRB, an intensively managed watershed in central Illinois, was created to simulate the baseline scenario (1998-2015) and then tested under selected stressors (WMPs and climate projections) with the aim of quantifying their impacts on the surface and groundwater resources. In general, wetland construction and riparian buffers resulted in the reduction of the average streamflow and the cumulative streamflow volume regardless of the climate projection implemented. Crop rotation scenarios performed differently in accordance with where they were implemented in the watershed and also with the climate projection used. However, crop rotation choice is not found to significantly affect the net amount of water flowing out the USRB, causing relative changes of approximately 5% with respect to the baseline. All WMPs for both climate projections show increases in the water table depth from the ground level to up to 40% when the forested riparian buffer was applied under ESM2M climatic conditions. These scenarios result in a negative impact on water resources in USRB if no mitigation strategies are implemented before then. The most significant changes in the depth to the water table was caused by the tile drains. It was estimated that the depth increased by 56% when tiles were installed. The lowering of the phreatic level allowed cropland production but also made high magnitude daily streamflow events more frequent, providing a faster flow pathway for contaminants and compromising water quality in Lake Decatur. Overall, the projected climatic conditions had significant impacts on the water table depth, especially at Monticello, where the effects of WMPs were prevalent when applied under future climate projections.

Evaluating the impacts of scenario-based changes considering projected climate changes, showed how WMPs will respond differently depending on the climatic conditions in which they were applied. Their overall effectiveness in implementing WMP is unclear under different climate projections. Therefore, a thorough evaluation is required during future watershed management projects. This study demonstrated that incorporating climate projections to the WMPs analysis allows resource managers to understand their long-term effectiveness. Moreover, studying environmental stressors' individual and combined impacts can lead to a more

comprehensive analysis of the risk and tradeoffs made for every managerial decision, which will enable a more efficient use of resources.

CHAPTER 3: IMPACTS OF ENVIRONMENTAL STRESSORS ON NONPOINT SOURCE POLLUTION IN INTENSIVELY MANAGED HYDROLOGIC SYSTEMS.[3]

3.1. INTRODUCTION

Agriculture has been categorized as one of the most important sources of surface and groundwater pollution in the U.S. (Tim and Jolly, 1994). Nonpoint source pollution resulting from tillage and the associated soil exposure in row crops, aa well as fertilizer applications, constitute a principal concern in highly altered watersheds. Less environmentally aggressive practices are being sought for implementation to address these issues. Reduced tillage, crop rotation, and cover crops are some of the Watershed Management Practices (WMPs) applied to make agro-production more sustainable. The application of these practices requires a combination of scientific, economic, social, and political assessments to be considered. For instance, it is necessary for agro-producers to be aware of the consequences of unsustainable practices, as well as to be trained and be technically competent in the implementation of new production practices. All these efforts should be strategically focused on the most effective way to optimize productivity while minimizing the environmental impacts for a sustainable agro-ecosystem.

When planning long-term environmental watershed programs, climate variability is an important factor to be considered. Climate fluctuations can introduce variability in transport processes, where the amount and timing of rainfall are key factors in the flux rates of solutes to streams (Carpenter et al., 1998). This is especially important since the energy of raindrops and the overland run-off after rainfall events are the main causes of soil particles' detachment, transport to and deposition in streams. Moreover, future climate conditions are expected to significantly affect groundwater fluxes (Botero-Acosta, 2018), which are major contributors of solutes to rivers. Nitrogen transported from agricultural lands to surface aquatic systems through overland run-off is less than 5%, while infiltration and leaching in loam and clay soils carry from

[3] Some contents of Chapter 3 are part of the article in review: Botero-Acosta, A., Chu, M.L., Huang, C. Impacts of environmental stressors on nonpoint source pollution in intensively managed hydrologic systems. Journal of Hydrology, *(In review)*. The copyright will be owned by Journal of Hydrology if accepted and published.

10% to 40% of nitrogen and 25% to 80% for sandy soils (Howarth et al.,1996 cited by Carpenter et al., 1998).

Hence, to effectively propose a sustainable watershed management plan, it is necessary to understand the system's behavior under varied environmental stressors like WMPs and future climate conditions. However, hydrologic systems are complex to study, due to the multifaceted interactions of surface and subsurface water fluxes with biochemical processes that vary in time and space. For instance, understanding how farming and industrial practices, or climate variables, affect watershed responses, and how these effects are propagated in time and space, require a holistic approach that accounts for the spatio-temporal interactions of the main processes in the system. Computer models allow long-term watershed analysis in lieu of in-situ monitoring while also allowing the simulation of multiple changes in scenarios. Empirical equations to describe water fluxes have been widely used for simulating nonpoint source pollutants transport at a watershed scale. Some of the extensively used hydrologic models are: The Agricultural nonpoint Source (AGNPS) (Young, 1989), the Annualized Agricultural Non-Point Source Pollution (AnnAGNPS) (Chahor et al., 2014), the Generalized Watershed Loading Function (GWLF) model (Evans et al., 2002) and the Soil and Water Assessment Tool (SWAT) (Jiang et al., 2014; Shen et al., 2014, Zhai et al., 2014). However, the lack of physical representation of parameters in these models makes conceptualization of WMPs challenging. Moreover, simulations of systemic responses to environmental stressors should be able to account for changes in time and space, and to propagate them from the surface to the subsurface, and the river. This capability is jeopardized by the lumped or semi- distributed spatial discretization of empirical models and the constant parameters over the simulation period. For example, vegetation variables affecting evapotranspiration and plant uptake are not constant during the plant's growing stages, and the model should be able to sufficiently mimic the physical phenomena that are being represented, and to propagate their effects on the unsaturated zone moisture content, the infiltration process, and the aquifer recharge.

The objective of this chapter is to apply the mechanistic distributed model MIKE-SHE to simulate the effects of environmental stressors on the water quality of the Upper Sangamon River Basin (USRB) water bodies. For this, the hydrologic and transport model of the USRB was created applying the mechanistic distributed model MIKE-SHE. The Modified Universal Soil Loss Equation (MUSLE) was used to compute the distributed and time varying sediment inputs

from hydrologic and environmental variables, while distributed and time varying inputs of nitrate-nitrogen were created in accordance with the registered fertilizer application schedule for corn in Illinois. Eighteen scenarios were created by combining WMPs and climate cases and simulated to estimate the impact of environmental stressor over non-point source pollution at the USRB.

3.2. METHODS

3.2.1. STUDY AREA

As in Chapter 2, the USRB was chosen as the study area. Presently, almost 80% of the watershed area is allocated to grain crops, primarily corn and soybeans. The transformation of prairie and savannah into agricultural cropland occurred with the installation of ditches and tile drains that were used successfully to drain flat lands with poorly drained soils in the USRB. All these modifications altered the hydrologic and transport characteristics. High loads of nutrients and sediments derived from croplands, and transported by OL run-off and tile drainage, impaired Lake Decatur water quality. Nitrate-N concentrations have exceeded drinking water standards (Bekele et al., 2014) and the lake capacity has reduced significantly due to the sedimentation of suspended solids. By the 1980s, one-third of the original capacity had been lost (Rhoads et al., 2016). Approximately, 200,000 tons of sediments are delivered yearly to Lake Decatur (Rhoads et al., 2016). Efforts are being made to repair the damages that nonpoint source pollution has brought to the USRB. A dredging project is currently taking place to recover Lake Decatur's capacity by 2019 (Rhoads et al., 2016), and environmental agencies such as the Illinois State Water Survey and the Illinois Environmental Protection Agency, are taking actions in the watershed planning (IEPA, 2017; Bekele et al., 2014) to reduce agricultural practices' impacts on water quality. According to the Illinois Nutrient Loss Strategy (IEPA, 2017), a reduction of 15% in nitrate-nitrogen load is targeted by 2025 and a final goal of 45% load reduction it is expected to be met over time.

To study the effects of WMPs over the USRB, a watershed model was set up using the mechanistic distributed model MIKE SHE, coupled with the hydrodynamic river model MIKE 11. Hydrologic and transport processes were included in this model to account for nonpoint source pollution in the USRB. The Water Movement (WM) on the OL, UZ, and SZ were simulated and three streamflow measuring stations: Fisher, Monticello and Decatur, (Figure 8)

(USGS, 2017), were used as assessment endpoints to determine the capacity of the models to represent the system. Additionally, the transport processes for sediments and nitrate-nitrogen were simulated and verified with the measured loads at the stream.

The verified model was used to simulate the baseline scenario (1980-2015 period) under the current conditions of the watershed and measured climate data. Afterwards, scenario-based modeling was implemented in order to quantify the effects of WMPs on the water quality of the URSB. The streamflow, nitrate-nitrogen load, and sediment load were used as assessment criteria at the Fisher, Monticello and Decatur endpoints.

3.2.2. HYDROLOGIC MODEL

The hydrologic processes taking place in the USRB were simulated with the mechanistic, distributed model MIKE SHE, which fully integrates surface and subsurface sub-models (Figure 17). The WM in the OL, UZ, SZ and rivers were simulated by solving the partial differential equations describing mass flow and transfer of momentum. The parameters used in these equations were measured from the physical system. The basic model input data for the model are: climate data, model domain, topography, and physical parameters for each of the simulated hydrologic processes.

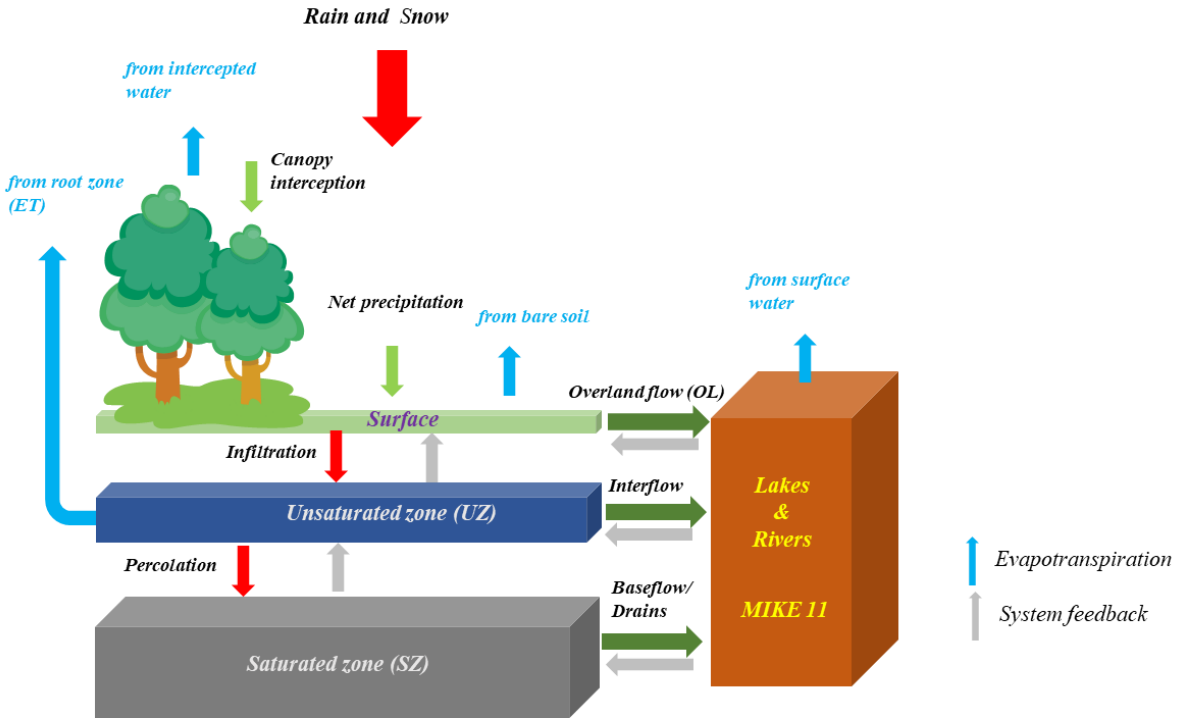

Figure 17. MIKE SHE/MIKE 11 compartments.

The climate data are one of the most important inputs for the model. Rainfall is the main driver of all hydrologic processes, from surface runoff to aquifer recharge, while temperature, solar radiation, and wind speed affect evapotranspiration, a main process in the water cycle. Daily values of precipitation, temperature, and reference evapotranspiration were required as station-based inputs. Sixteen precipitation stations in the USRB and its neighboring watersheds and seven temperature stations were used (NOAA, 2016) (Figure 8) as main climate inputs. Missing values from the time series were filled using the Inverse Distance Weighting method. Reference evapotranspiration was estimated from solar radiation and temperature data by means of the modified Makkink's equation (de Bruin & Lablans, 1998).

The model domain was discretized into 300x300-m grids to take into account the spatial variability of the physical parameters in the USRB. A topographic map was created from the Digital Elevation Model (DEM) (USGS, 2016). A map of vegetation distribution for the USRB was created from the NASS-2016 (USDA, 2016) data layer and time series of Leaf Area Index (LAI), root depth, and crop coefficient (K_c) were defined for each vegetation type. Data for root depth and Kc were obtained from the CROPWAT database (FAO, 2016). The vegetation layer showed that the USRB has approximately 80% of its area devoted to row crops, specifically corn and soybean (Table 9), which have maximum LAI values of 3.1 and 4.9 respectively, maximum root depths values of 1 m for both crops, and maximum Kc values of 1.2 and 1.4, respectively.

Table 9. Land use baseline USRB.

Land use	Percentage
Open water/ developed/ barren	6.57%
Deciduous forest	3.93%
Grass/pasture	8.71%
Winter wheat/Other hay/not alfalfa	0.32%
Woody wetlands/herbaceous wetlands	0.35%
Corn	43.06%
Soybean	36.81%
Double crop winter wheat/soybean	0.01%
Alfalfa	0.23%

After a rainfall event, excess water from interception is represented as either infiltrating into the soil or running over the surface. The simulation of the OL run-off was undertaken by solving the flow diffusive wave equation using a 2-dimensional finite difference method. The location of

paved areas and the values of Manning coefficient (M) for each land use type were entered as grid-point values. On the other hand, the flow through the vadose zone was simulated with a 1-dimensional finite difference solution of the Richards equation. The water retention curves of the soil profiles defined by the NRCS Official Soil Series Descriptions (NRCS, 2016) were used to characterize the UZ in the USRB as described in Chapter 2. The movement of water percolating into the SZ was simulated with a 3-dimensional finite difference solution of the Darcy equation. The geological stratigraphy of the SZ was conceptualized as a two-layer system, the Henry-Ashmore layer and the Glasford-Pearl layer (Figure 10), following the method described in Chapter 2. Maps of the lower level elevation of each geological layer, horizontal and vertical hydraulic conductivities, specific yield, and the initial potential head were created and included in the SZ model. As the geologic units in the USRB were grouped into two main aquifer layers, their hydraulic properties were adjusted to achieve the equivalent value that best

represented the saturated zone behavior. As mentioned in Chapter 2, the initial water table depth was set to be 2 m below ground level (bgl) in accordance with a preliminary four-year run.

Drainage was simulated with a linear reservoir model, an empirical formula that requires a drain level and a time constant that accounts for the density of drainage network and the permeability around the drains (DHI, 2017a). In this method, the drainage flow was set proportional to the water table height above the drain level and the time constant value (Zhou et al., 2013). A map of a reference coding system was used to link draining cells to river recipient cells. This method is usually applied for flat watersheds with agricultural activities (DHI, 2017a). The drains were located in the USRB in accordance with the hydrologic group of the soils and the land use type (Sugg, 2007). SSURGO database was used to identify cells with soils having slow and very slow infiltration rates (Soil hydrologic groups C, D and dual soils A/D, B/D and C/D). Fifty-eight percent of the USRB was found to have poorly drained soils and most of this area was devoted to row crops production. After crossing soil and land use type data (USDA, 2016), fifty-two percent of the USRB area was determined to be suitable for tile drainage installation. The drainage was set at 1 meter below ground level and the time constant was adjusted to $3x10^{-7}$ s^{-1} to match the measured streamflow at Fisher, Monticello, and Decatur stations (USGS, 2017).

The 1-dimensional hydrodynamic model, MIKE 11, simulated the hydrograph propagation along the streams by solving the system of flow equations through an implicit finite difference

scheme. This model interacts with the OL, UZ, and SZ compartments at the river linked cells established by the river topology. A 30 x 30-meter pixel resolution DEM (USGS, 2016) was used to draw 30 river branches across the USRB. The upstream tributaries flow was simulated through kinematic routing, while the main branch (148.5 km length) flow was simulated by solving the fully-dynamic continuity and momentum equations. Four cross sections (Personal communication USGS) were included in the main branch and five more at Lake Decatur (ISWS, 1987; 2001). The manning coefficient (n) for the main branch bed and banks was set to 0.04 (ISWS, 1994).

3.2.3. TRANSPORT MODEL

The advection-dispersion equation (ADE) (Eq. 10) was applied to simulate the transport of soluble constituents in each compartment of the hydrologic model: OL, UZ, SZ, and channels. The advection part of the equation accounts for the transport of solutes due to the WM and the dispersion part includes the spreading of solutes caused by solute's concentration gradients and the complex microscopic variability of velocities in the medium. The water fluxes resulting from the hydrologic model are used as inputs to the transport model. For this reason, the WM simulations must be stored frequently enough to account for the temporal changes in solute transport. The MIKE SHE model accounts for sorption, attenuation of solute by exponential decay, and plant uptake processes. Decay was enabled in the OL flow model and both sorption and decay in the UZ and the SZ.

The transport of solutes in the SZ is governed by the ADE (Eq. 10) which requires the dispersion coefficient tensor (D_{ij}) and the groundwater velocity vector (v_i). When sorption and decay are included, the equation results in:

$$\frac{\partial c}{\partial t} = -\frac{\partial}{\partial x_i}(c v_i) + \frac{\partial}{\partial x_i}\left(D_{ij} \frac{\partial c}{\partial x_j} \right) - \frac{\rho_b}{\theta} \frac{\partial c^*}{\partial t} + \left(\frac{\partial c}{\partial t} \right)_{reac} + R_c \qquad i, j = 1,2,3$$

Eq. 10

where c is the concentration of the solute, ρ_b is the bulk density of the soil, and θ is the porosity. The last three terms account for the sources and sinks, where c^* is the mass of sorbed solutes per dry unit weight of solid, $\left(\frac{\partial c}{\partial t} \right)_{reac}$ indicates the net rate of production of the solute by

chemical and biological reaction, and R_c is the sum of external sources and sinks. The groundwater fluxes (q_i) (or Darcy's velocities in the SZ) computed by the hydrologic model were used to determine the groundwater velocity for the advective transport (Eq. 11).

$$v_i = \frac{q_i}{\theta_{eff}} \qquad \text{Eq. 11}$$

Eq. 10 can be modified to represent transport in the UZ, OL, and rivers. For example, the 1-dimensional version of this equation results in the ADE for the UZ; removing the third term in the right-hand side of the equation (Eq.10), which accounts for sorbed mass onto the porous media, and using a 2-dimensional version will give the ADE for OL; and finally, a 1-dimensional version of the OL-ADE will give the ADE for rivers. In each case, the x-direction is specific to the application.

The transport parameter values and the sources for both sediments and NO_3-N were entered into the model for each simulated compartment. The ADE was solved numerically by finite difference method. In the OL, SZ and UZ, a fully explicit scheme, with a backward differencing for advection and a central differencing for the dispersion term was applied, the equations were developed to third order. The ADE in the river was solved with a fully implicit scheme with a correction term added to reduce the third order truncation error.

To maintain the numerical solution stable and minimize the numerical dispersion, the time step used for each compartment (i.e., OL, UZ, and SZ) varied according to the behavior of the WM and the Courant stability criteria. The Courant number is defined as the ratio of flow rate to grid size, by keeping the Courant number value to less than and close to 1 it is guaranteed that solutes will not travel too far in one time step and will keep the numerical solution stable. For example, the movement of solutes in the river is faster than the movement of solutes through an aquifer. Hence, the time step of the river compartment must be much smaller than that for the groundwater one.

3.2.3.1. Sediments

The Modified Universal Soil Loss Equation, MUSLE, (Williams & Berndt, 1977; Sadeghi, 2004) was used to simulate the erosion processes occurring at the surface of the watershed (Figure 18). In this method, the value of sediment runoff in a month (Y, ton/mo) is expressed as the product of the: surface run-off factor, computed from the surface runoff volume accumulated

in a month (Q) and the peak runoff rate (q_p), soil erodibility (K), slope length (LS), crop factor (C) and conservation practice factor (P) (Eq. 12).

$$Y = 11.8\left(Q \times q_p\right)^{0.56} KCPLS \quad \text{Eq. 12}$$

After the hydrologic model was executed to simulate the WM through the watershed, results from the OL flow were used in the MUSLE equation to compute the monthly sediment yield across the watershed. This was entered into the model as equivalent daily maps of distributed sources for the sediment transport model. Finally, the water quality model was run to simulate the transport of sediments in the OL, UZ, SZ, and rivers. It is important to note that the hydrologic model and the transport model are independently executed. The former simulates the exchange between the groundwater and the surface flow, using the river model (MIKE 11), and the latter uses the WM results to calculate the solute fluxes between the watershed compartments.

In Eq. 12, the surface run-off factor represents the erosive force of raindrops due to their kinetic energy. Monthly maps of OL flow to the river were extracted from the hydrologic model to compute the surface runoff (Q) volume map, while the peak runoff rate (q_p) for each month of simulation was determined from the daily time series of OL flow rate from selected river branches. In order to create a map of peak runoff rates, the watershed was divided into 32 subwatersheds, each one corresponding to a river branch. The peak OL flow rate for a branch in a month was replicated in the cells within the corresponding subwatershed.

The K-factor accounts for the soil susceptibility to erosion; it depends on soil properties such as texture, structure, consolidation, cohesion, and permeability. In general, most erodible soils have high silt content while soils with high content of organic matter and high permeability or clay-rich soils are less erodible. The K-factor map was created from the SSURGO database (NRCS, 2017). The distribution of K values in the USRB ranges from 0.05 to 0.49. These values correspond to poorly drained silty clay loams and silt loams, the soil types found in the USRB (ISWS, 1996).

The C-factor map was created according to the land use types (Table 10) (Ward et al., 2016) and their distribution across the watershed. This factor accounted for the temporal variations of crops within a cyclical period of time. For example, a corn-soybean rotation cell has one unique C-factor that includes the effects of both corn and soybean crops and was applied for all months

of simulation. The P-factor was fixed to 1.0 since no strip cropping, contouring or terraces were implemented in the USRB. Finally, the LS-factor map was computed from the Digital Elevation Model (DEM) following the method proposed by Desmet & Govers (1996, cited by Luna, 2016). The Geographic Information System (GIS) tools: Flow accumulation and slope calculation, were used along with Eq. 13-15 in computing the L portion of the LS-factor as follows:

$$m = \frac{F}{(1+F)} \quad \text{Eq. 13}$$

$$F = \frac{\sin\beta / 0.0896}{3(\sin\beta)^{0.8} + 0.56} \quad \text{Eq. 14}$$

$$L = \frac{(A + D^2)^{m+1} - A^{m+1}}{x^m D^{m+2} (22.13)^m} \quad \text{Eq. 15}$$

where β and A are the slope and the flow accumulation values for each pixel, D is the pixel side size (e.g.: 300 meter) and x is the shape coefficient, set to 1.0 for uniformly gridded systems. The S portion of the LS-factor was computed using Eq. 16 for slopes smaller than 9% (McCool et al., 1987; Renard et al., 1997; Panagos et al., 2015a) which is the case for the entire USRB.

$$S = 10.8 \sin\beta + 0.03 \quad \text{Eq. 16}$$

Table 10. C-factor for selected crop types and tillage method (Ward et al., 2016)

Land use	Crop factor
Corn (conventional tillage)	0.4
Soybean (reduced tillage)	0.175
Soybean (conventional tillage)	0.45
Corn-Soybean 2-year rotation (conventional tillage)	0.42
Grass/Pasture (no-till)	0.005
Wetlands	0
Winter Wheat/Other Hay/not alfalfa (no-till)	0.005
Alfalfa (no-till)	0.005
Deciduous forest	0.041
Row crop-Winter wheat 1-year rotation (conventional tillage)	0.3
Soybean-winter wheat 1-year rotation (reduced tillage)	0.1
Corn (reduced tillage)	0.14

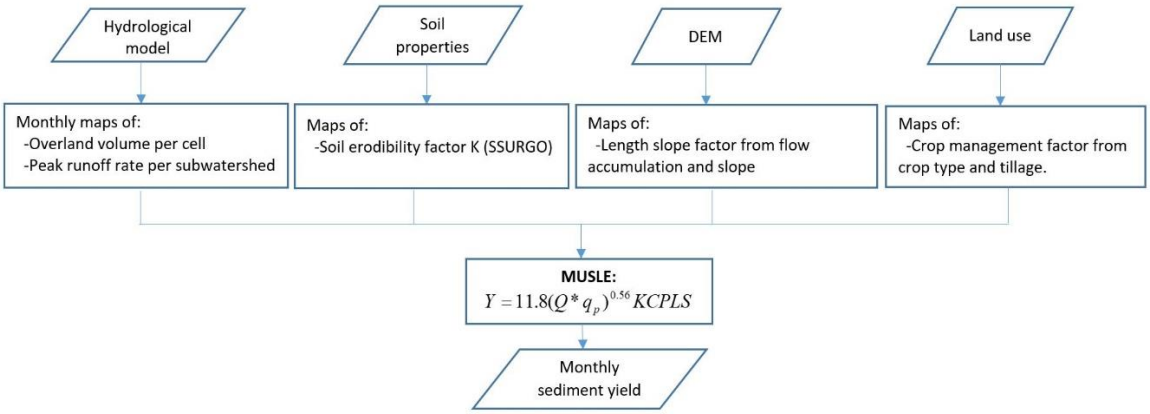

Figure 18. Methodology used to create the monthly sediment yield maps which were used to simulate surface sediment source for the transport model.

The monthly sediment yield was entered into the MIKE SHE model as daily source maps of mean step accumulated values in kg/day. For this determination, the monthly sediment yield computed with the MUSLE was divided by the number of days in the month. The sediment transport in the USRB was simulated with the conservative two-dimensional ADE as a suspended species in the OL compartment. Suspended species do not infiltrate to the UZ or SZ and they cannot be sorbed. A threshold concentration is used by the model to avoid unrealistic high species concentrations in the OL flow. The species will precipitate if this concentration is exceeded and put back into motion if the concentration falls below the threshold, similar to the concept of solubility. This effect is considered in the source/sink term of Eq. 10. This threshold will control the amount of eroded soil computed by the MUSLE that is actually transported and reaches the streamflow. According to Chinnasamy et al (2013) the sediment delivery ratio for the USRB ranges from 0.32 to 0.4. These values correspond to the ratio of the sediment delivered at the catchment outlet to on-site erosion throughout the basin.

The OL flow transports the sediment particles to the river network, where the MIKE 11 model takes over the cohesive sediment transport simulation. The ADE implemented for river transport has a lateral inflow term representing the input of sediment load from the OL and a source/sink term to account for erosion/deposition from the river bed. The R_c term in Eq. 10 will then be the combination of the inputs/outputs of lateral inflow and erosion/deposition (S_{ero} and S_{dep}).

The erosion and deposition rates depend on the hydraulic conditions and the concentration of sediments (Figure 19). The main parameters used to describe this process are: the free settling

velocity (w), and the critical shear stresses for erosion (τ_{ce}) and deposition (τ_{cd}). Deposition will occur when the bed shear stress is lower than the critical shear stress for deposition. Likewise, erosion will happen when bed shear stress is higher than the erosion critical shear stress. The rate of deposition is expressed as:

$$S_{dep} = \frac{wc}{h^*}\left(1 - \frac{\tau}{\tau_{cd}}\right), \tau \leq \tau_{cd} \qquad \text{Eq. 17}$$

Where h^* is the average depth through which particles settle and τ is the bed shear stress. The source term for erosion would be:

$$S_{ero} = \frac{M^*}{h}\left(\frac{\tau}{\tau_{ce}} - 1\right)^b, \tau \geq \tau_{ce} \qquad \text{Eq. 18}$$

Where M^* is the erodibility of the bed or erosion coefficient (g $m^{-2}s^{-1}$), h is the flow depth, and b is the erosion exponent, which describes the degree of non-linearity of the erosion rate (DHI, 2017b). Since the local bed shear stress is proportional to the squared flow velocity (V) (Eq. 19), critical shear stresses can be related to flow velocities, denoted critical velocities for erosion (V_{ce}) and deposition (V_{cd}). Erosion will then occur when flow velocity is larger than the V_{ce}, and deposition when flow velocity is lower than the V_{cd} (Figure 19).

$$\tau = \rho g \frac{V^2}{M^2 h^{1/3}} \qquad \text{Eq. 19}$$

Where ρ is the fluid density and M is the manning M coefficient.

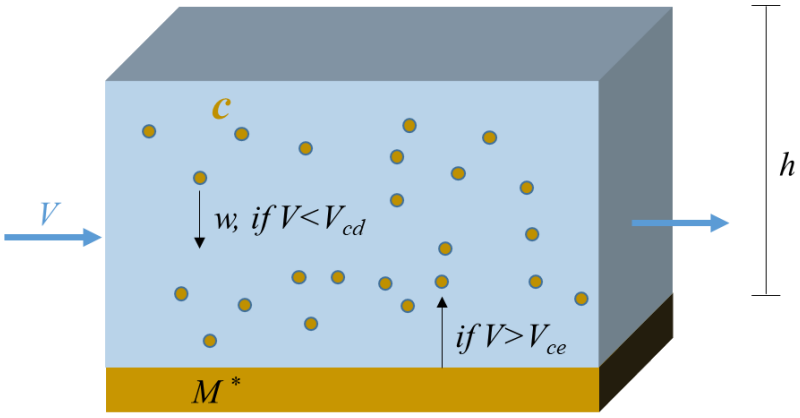

Figure 19. Erosion/deposition processes in the river.

3.2.3.2. Nitrate-nitrogen

The Illinois Environmental Protection Agency (IEPA) issued eight nitrate warnings in a 13-year period (1979 to 1992) due to exceedance of the maximum concentration level of nitrate-nitrogen (10 mg NO_3-N/l) in Lake Decatur. It is estimated that $6.5x10^6$ kg/yr of nitrates are lost from USRB by both point and non-point sources, from which $5.61x10^6$ kg/yr stemmed from non-point sources (IEPA, 2017). Three sources of NO_3-N were considered in this study: Non-point sources from fertilizers, point sources from facilities, and natural sources.

Nitrate-nitrogen non-point sources for the water quality model were created based on the fertilizer application schedule for corn crops in Illinois. The most commonly used fertilizer in Illinois is anhydrous ammonia (NH_3) which is injected at 25 cm depth and which dissolves and oxidizes quickly to form nitrate, highly soluble in water. This process is called nitrification and is accomplished by soil bacteria *Nitrosomonas* and *Nitrobacter*. The former oxidizes the ammonia to nitrite while the latter transforms the nitrite to nitrate. Both bacteria, commonly found in soils, require moderate soil water content and temperature to transform ammonia sources to nitrate within a few days of application (IPNI, 2015a). On the other hand, warm and wet soils with high concentration of organic material and NO_3 will foster the denitrification processes. Under anaerobic conditions and high carbon concentrations, microbial activity will transform the nitrate to nitrogen gas, which will be released to the atmosphere (IPNI, 2015b).

Daily maps of NO_3-N sources were created based on the application schedule of fertilizers in the USRB. It was assumed that the nitrogen applied to corn crops, either in the form of anhydrous ammonia or urea ammonium nitrate ($CO(NH_2)_2$+NH_4NO_3), would be converted to nitrate-N, which is highly soluble in water, and then transported throughout the OL, SZ, UZ, and rivers. Nitrogen application rates in the USRB vary from year to year depending on the producer's preferences. Six cases were identified to simulate this variation (Table 11). The IEPA (2017) reported that approximately, 207 kg/ha of nitrogen are applied yearly on Illinois corn crops, either through fertilizer or manure. Table 11 provides yearly application data for several individual cases, showing a maximum of 190.3 kg/ha of N, which has the same order of magnitude as the reported. The fertilizer inputs for the baseline period were set in accordance with information provided by the Illinois Fertilizer & Chemical Association (Schaefer, personal communication, 2018), as follows: from 1980 to 2008, Case 6 was applied; from 2009 to 2011, Case 1; and from 2012 to 2015, Case 2.

Table 11. Timing and rates of N fertilizer for corn crops in Illinois (Schaefer, personal communication, 2018).

	Date [I]	Form	Rate (kg of N/ha)
Case 1	November 10	NH_3	145.55
	April 1	UAN[II]	44.78
Case 2	April 1	UAN	111.96
	V6[III]	UAN	78.37
Case 3	Before April 1	NH_3 or UAN	190.34
Case 4	November 10	NH_3	111.96
	At planting [IV]	UAN	33.59
	V6	UAN	44.78
Case 5	At planting	UAN	55.98
	V6	NH_3 or UAN	134.35
Case 6	November 10	NH_3	190.34

I The timing is approximate and will differ from year to year depending on weather.

II UAN (Urea Ammonium Nitrate) is a solution of urea ($CO(NH_2)_2$) and ammonium nitrate (NH_4NO_3) in water.

III V6 Growth stage or 6th collar on the corn plant. Fertilizer in this stage is side dress. (5 weeks after planting)

IV Planting is usually made between April 15th -20th.

The USRB is reported as one of the eight watersheds in Illinois with the highest loading of nitrate-N and phosphorus from point sources (IEPA, 2017). Available annual data of nitrogen discharge for 9 facilities in the USRB (EPA, 2017a) (Table 12) were included as boundary conditions in the MIKE 11 model. Since the most common form of inorganic nitrogen in surface water is NO_3-N (Wall, 2013), the reported loads were assumed to be in nitrate-N form.

Natural sources such as fixation of atmospheric nitrogen by bacteria, decay of soil organic matter, and rainfall deposition, generate a background NO_3-N concentration. For groundwater systems, the background concentration of nitrate is usually considered to be less than 3 mg/L (ISWS, 1996). Since 22% of nitrate weight corresponds to NO_3-N, the initial NO_3-N concentration in the groundwater was set to 0.7 mg/L. Inputs from rainfall were considered to be 0.3 mg/L of NO_3-N in accordance with the data measured by the National Atmospheric Deposition Program (2018) from 1979 to 2016 at the nearest NADP station, near Bondville, 17 kilometers east of Monticello (Long: -88.3719, Lat: 40.0528).

Table 12. Facilities discharging Nitrogen to USRB streams.

Period	NPDES ID*	Facility Name	City	Mean Total Load (kg N/yr)
2007-2017	IL0023281	Gibson city wpcf	Gibson city	6792.74
2007-2017	IL0029980	City of Monticello STP	Monticello	9338.60
2007-2017	IL0024414	Mahomet STP	Mahomet	3538.38
2011-2017	IL0021016	Fisher STP	Fisher	2379.16
2011-2017	IL0046141	Sangamon valley pwd STP	Mahomet	2682.21
2013-2017	IL0035416	Solae LLC	Gibson city	719.36
2007-2017	IL0053325	Robert Allerton park	Monticello	60.43
2007-2017	IL0061425	Archer Daniels midland Decatur corn processing PLT	Decatur	160.36
2007-2010	IL0047643	Argenta-Oreana elementary	Oreana	3.76

*National Pollutant Discharge Elimination System (NPDES) permit number

The NO_3-N transport over the USRB was simulated by the reactive ADE. Nitrate decay and adsorption processes were included to simulate denitrification and NO_3-N adsorption to soil particles. In order to include complex biological and chemical reactions, the decay term was set to be dependent on soil water content and soil temperature (Boesten and van der Linden, 1991 cited in DHI, 2017a). First-order degradation with an exponential decay was included to simulate the attenuation of the solute, it was corrected by a temperature and a water content factors. The reaction term $\left(\frac{\partial c}{\partial t}\right)_{reac}$ in Eq. 10 was then expressed as:

$$\left(\frac{\partial c}{\partial t}\right)_{reac} = \frac{-ln2}{\lambda} * F_w * F_t * c \quad \text{Eq. 20}$$

$$F_w = \left(\frac{\theta}{\theta_s}\right)^B \quad \text{Eq. 21}$$

$$F_t = \begin{cases} 0, if\ T_s < 0°C \\ \frac{T_s}{5} e^{\alpha(5-T_{ref})}, if\ 0 \leq T_s \leq 5°C \\ e^{\alpha(T_s-T_{ref})}, if\ T_s > 5°C \end{cases} \quad \text{Eq. 22}$$

Where λ is the half-life of nitrate, F_w and F_t are the water content and temperature factors, respectively (Eq. 21 and 22) and c is the concentration of NO_3-N. The water content factor (Eq. 21) depends on the actual soil moisture (θ), the saturated moisture content (θ_s), and an empirical constant B. The temperature factor (Eq. 22) uses the actual temperature of the soil (T_s), the reference temperature (T_{ref}) at which the half-life was estimated and a constant α depending on

T_s, T_{ref}, the gas constant and the molar activation. When the temperature is above the reference temperature the rate of decay increases. For OL, the temperature of water is assumed to be the same as the air, while for the UZ and SZ the temperature is computed based on the air temperature using an empirical formula (Eq. 23) (Klein 1995, cited in DHI, 2017a).

$$T_s = T_{sy} + 0.346(T_{air} - T_{sy})e^{(2.7028z)} \quad \text{Eq. 23}$$

Where T_{sy} is the average daily soil temperature from the day before, T_{air} is the average daily air temperature for the current day and z is the depth.

The adsorption was simulated by the Freundlich Isotherm, the c^* in Eq. 8 would be expressed as:

$$c^* = K_f c^N \quad \text{Eq.24}$$

Where K_f and N were calibrated with measured NO_3-N concentration form grab samples.

The nitrate-nitrogen transport in the OL was modeled with a two-dimensional reactive ADE, where decay was allowed. Source terms in this compartment included: rainfall deposition and fertilizer inputs. One and three-dimensional reactive ADEs were applied for the UZ and the SZ respectively, both decay and adsorption processes were simulated in the porous media, and the background concentration of NO_3-N for groundwater was used as the initial condition. In the UZ, the plant uptake was represented as a sink term, and was computed as a function of the plant transpiration, plant's roots, soil moisture, and nitrate-nitrogen concentration. An empirical factor was used to include the root filtering capabilities and a factor of 1 was used for nitrate-nitrogen. Finally, the transport of NO_3-N along the river was simulated with a one-dimensional reactive ADE including decay. Point sources (Table 12) were included at the river branch closest to the facility location.

3.2.4. SCENARIOS

After setting up and validating the hydrologic and transport models, a scenario-based analysis was designed in order to simulate the watershed responses to selected WMPs (Table 14) and climate conditions. WMPs were proposed considering the information gathered at stakeholders' meetings (The Nature Conservancy) on 2017 and 2018. Two structural WMPs (constructed Wetlands and grassed riparian buffers), and three non-structural WMPs (crop rotation, cover crops, and reduced tillage) were selected. According to the information collected from the stakeholders and experts in management practices in the USRB, these WMPs appeared

to be the most feasible to be used by landowners or implemented as conservation practice by environmental agencies. Each of these WMPs were analyzed under current and future climate scenarios in order to identify the effects of climatic variations in the watershed hydrologic processes.

3.2.4.1. WMPs

Constructed wetlands: Storm water wetlands remove pollutants from overland runoff through vegetation filtering and settling processes. Wetlands are found to be long-lasting pollutant removal facilities that can effectively work even 20 years after construction (Groh et al., 2015). Potential wetland restoration areas were identified as those underlain with hydric soils, not currently developed, covered by water or forested. Hydric soils are characterized by being permanently or seasonally saturated. According to the IEPA (2007), most of the USRB are suitable for wetland construction. Results from the baseline were applied to locate the cells with accumulation of OL water. The daily OL depth maps from the baseline were added for the 1980-2015 period. Cells originally devoted to crop production or grass, and with and added OL depth higher than 10 meters were chosen as those suitable for wetland construction. In accordance with this selection, 3.4 % (921 cells) of the total USRB was converted to wetlands draining areas ranging from 180 ha to 3060 ha as shown in Figure 20. Location of wetland cells is presented in Figure 21a.

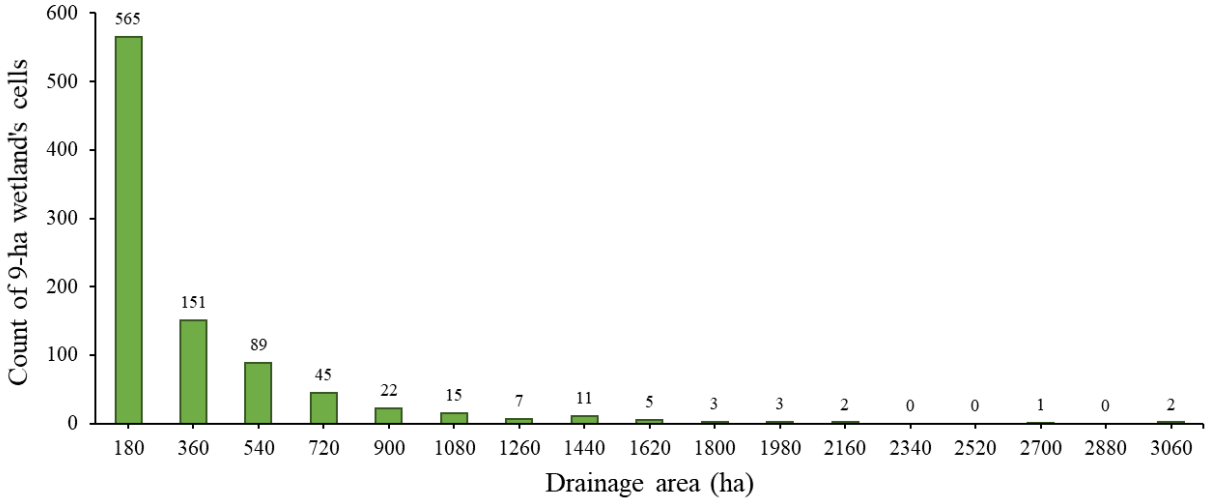

Figure 20. Absolute frequency of drainage area for wetland cells.

Flow in wetlands has specific characteristics that make it different from open channel flow. It is characterized as largely laminar, implying smaller dispersion values. Wetland vegetation is different from that of grassed channels, which results in greater variations in the velocity from point to point (Tsihrintzis and Madiedo, 2000). Wetlands were represented in the MIKE SHE model by modifying the manning number, the detention storage, the vegetation properties (Leaf Area Index LAI, crop coefficient Kc, and root depth), and the C-factor for the MUSLE. A Manning M value of 1.6 (n=0.6) was applied to wetlands grid cells (Tsihrintzis and Madiedo, 2000) and a detention storage of 60 cm was set in accordance to New Jersey Stormwater Best Management Practices Manual (2004) for a pond wetland. This representation of detention storage simulates infiltration and evaporation with a limitation on the amount of water flowing over the surface when the depth of ponded water is less than the specified value. The vegetation properties were set to those of herbaceous plants, and since wetlands and other inland waters are not prone to soil erosion (Panagos et al., 2015b), their C-factor was set to 0.

Grassed riparian buffers: Riparian buffers are areas next to the river with permanent vegetation that help stabilize soils and control pollutants mainly by reducing runoff flow rate and filtering sediments and nutrients (IEPA, 2007). The installation of a grassed riparian buffers in the model was assumed in grid cells along the streams originally used for crop production. Buffer width was set to 300 m, similar to that applied in Chapter 2 (Figure 21b). The vegetation properties, the OL manning coefficient, and the MUSLE C-factor were modified in order to include their effects in the model.

Crop rotation: Agricultural practices and tile drainage are the most important aspects affecting nitrate-nitrogen stream loads. It has been reported that NO3-N concentrations downstream from agricultural lands were nine times larger than the concentrations downstream of forested zones. Among the agricultural lands, annual row crop lands had NO3-N losses ranging from 30 to 50 times higher than those growing perennial crops (Randall and Mulla, 2001). Corn crops in Illinois have yearly nitrogen application of approximately 190.3 kg/ha, which represent the main source of NO_3-N in the USRB. For this reason, a two-year corn-soybean rotation was simulated as an alternative crop system in replacement of continuous corn croplands. This cropping system was included in the MIKE SHE model through the vegetation properties time series and into the transport model by the C-factor in the MUSLE and the fertilizer application schedule (Schaefer, personal communication, 2018) (Table 13). In this

scenario all the corn crops (approximately 40% of the total area, Table 9) were converted to corn-soybean rotation (Figure 21c).

Table 13. Nitrogen application schedule for Corn-Soybean rotation (Schaefer, personal communication, 2018).

Date	Form	Fertilizer Inputs (Kg of N/ha)
Year 1 (Soybean)		
NONE	-	-
Year 2 (Corn)		
March 23th	NH_3	156.91
At planting [I]	UAN	50.43

[I] planting is usually made between April 15th -20th.

Cover crops: One-year rotation with cover crops was simulated as an alternative crop system. Winter wheat serves as overwintering cover crop to prevent erosion, add organic matter and scavenge excess nutrients. If planted in September, winter wheat can absorb 44 kg N/ha by December (SARE, 2012). Winter wheat was included in the simulation between regular growing seasons of row crops of either corn or soybean. Since it works well in reduced-tillage systems (SARE, 2012), no additional tillage, from the one contemplated in the original row crop needed to be considered. This WMP was implemented by modifying vegetation variables time series and the MUSLE C-factor.

Reduced tillage: Conservation tillage requires at least 30% of residue cover from the previous crop to be retained (IEPA, 2007). This land cover intercepts raindrops at the surface, reducing their impact and associated dislodging of soil particles. It creates a preferential flow path through the unsaturated zone, increasing infiltration, and reducing runoff and sediment movement. Conventional tillage is usually used for corn crops in the USRB, while Soybean crops are managed with either conventional or reduced tillage (IEPA, 2007). The baseline for the USRB was set to run with the Manning M (inverse of the Manning number, n) for row crops (Chow, 1959) for both Soybean and Corn cropland (M=28). The effects of conservation tillage were represented in the MIKE-SHE model through the OL manning number, the detention storage, and the MUSLE C-factor. In accordance with the findings and recommendations by Mohamoud (1992), a detention storage of 2.2 mm was used for reduced-till cells and a manning M of 7.7 (n= 0.13). The MUSLE C-factor was set in accordance with Table 10.

Table 14. WMPs description

Type	Description		Implementation site	WMP cases
Current state	Current state	Land use as described in Table 9. Row crops under conventional tillage	-	1. Current state
Structural WMP	Constructed wetlands	Treatment system using wetland assemblage. Wetlands intercepting overland water.	Cells with cumulative OL depth > 10 m in the baseline (1980-2015) AND originally devoted to crops or grass.	2. ~ 3.4 % of total area
	Grassed riparian buffers	Strip of grass located in the riparian zone to intercept runoff from upslope pollutant sources and filter it.	All the cells along the riparian zone **originally devoted to row crops**.	3. The riparian zone (~12% of total area)
Non-Structural WMP	Crop rotation	2-year corn-soybean rotation.	Areas originally devoted to Corn.	4. ~40% of total area (area devoted to corn)
	Cover crops	1-year row crop-winter wheat rotation under conventional tillage.	Locations with SPI in the 50th percentile or higher originally devoted to row crops.	5. Area that meets SPI conditions originally under row crops ~25% of total area
	Reduced-till	Leave previous crop's residues for row crops.	Locations with SPI in the 50th percentile or higher originally devoted to row crops under conventional tillage.	6. Area that meets SPI conditions originally under conventional tillage ~25% of total area

The cover crops and reduced-tillage WMPs were applied where they were most influential (Figure 21d, e). The sensitive areas for sediments and nutrients transport were selected by identifying the cells devoted to row crops with large stream power index (SPI) values. The SPI is a secondary topographic index that estimates the erosive power of the water movement (used as well in Chapter 1). It is computed as the natural logarithm of the product of the specific catchment area for each cell (A_c) and the local slope (S) (Eq. 25).

$$SPI = Ln(A_c S) \quad \text{Eq.25}$$

The SPI for the USRB ranged from -9.3 to 20.8. Cells with SPI values equal or larger than the 50th percentile (3.4) and originally used for row crop production (approximately 25% of the entire watershed area) were chosen for the implementation of cover crop and reduced tillage WMPs.

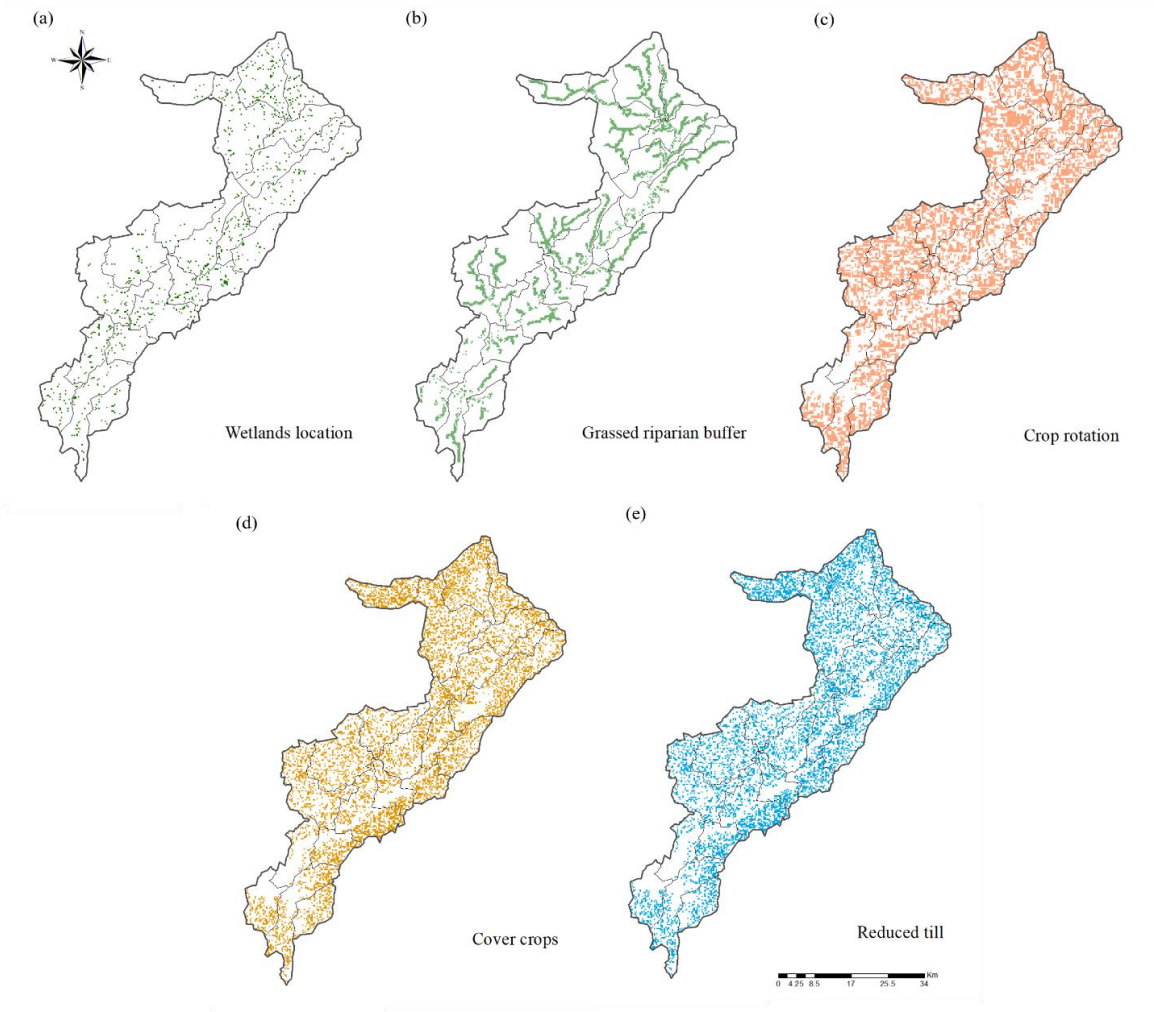

Figure 21. Location of WMPs modifications.

3.2.4.2. Future climate scenario

The inclusion of climate as a natural stressor allows the study of the combined effects of WMPs and climate on the systemic response of the USRB. The Illinois Nutrient Loss Reduction Strategy phase I milestone is to reduce the reported load of NO_3-N for 1980-1996 (404 million lb/yr) by 15% by the year 2025, and its ultimate goal is to reduce the Mississippi River Basin NO_3-N load by 45% over time (IEPA,2017). Climate data for the 2020-2055 were extracted from the Coupled Model Intercomparison Project (CMIP), an international program with the mission of simulating future climate and comparing existing climate models. The Representative Concentration Pathway 8.5 (RCP 8.5) was chosen to for the future climate scenario. The RCPs are greenhouse gas concentration trajectories (concentration vs. time) used along with the

climate model. They affect the change in atmosphere's energy due to greenhouse gases. RCP 8.5 is comprised of high population growth along with energy usage intensification, leading to a rise in energy demand and attendant greenhouse gas emissions. The projection RCP 8.5 has the highest greenhouse gas emission among all the RCPs, (Riahi et al., 2011).

CMIP5 consists of 32 global circulation models (gcm) from different climate groups across the globe. These models have a "historic" period of simulation for evaluation purposes (before 2005), after which the forcing from each model starts altering the greenhouse gases emissions to the atmosphere (Taylor et al., 2012). Data from the 32 models were analyzed in order to assess their capability to simulate climate trends in the USRB. The downscaled climate data simulated by the 32 models were compared with the observed data for the years1980-2005 at the NOAA Decatur station (Lat: 39.85, Long: -88.95). The monthly observed and simulated data for rainfall and temperature were statistically tested for the mean and the probability distribution through the 2-sided t-test and the 2-sided Kolmogorov Smirnov (KS) test, respectively. The monthly precipitation showed p-values ranging from 0.25 to 0.98 for the t-test, and from 0.03 to 0.91 for the KS test, while the monthly temperature p-values ranged from 0.58 to 0.99, and 0.67 to 0.99, for the t-test and the KS test respectively. The null hypotheses of equal mean and probability distribution between the observed and simulated, for both precipitation and temperature, was accepted with a significance level of 0.05 (p-value > 0.025 for a 2-sided test) for all the models. The box plot charts (Figures 22 and 23) and the means of the annual climate variables (Figures 24 and 25), show the dispersion of the simulated data compared to that of the observed data, and the difference of the means between simulated and observed data.

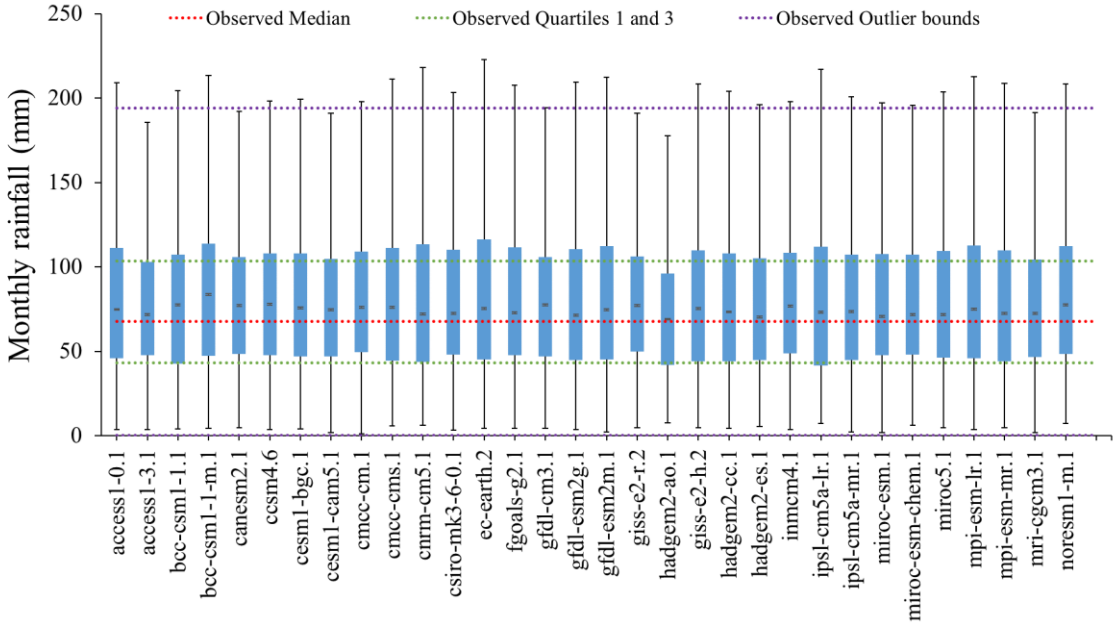

Figure 22. Box plots of the monthly rainfall (mm) simulated by the 32 CMIP5 models during the 1980-2005 period at the NOAA Decatur station. Dashed lines correspond to the observed quartiles for the same period.

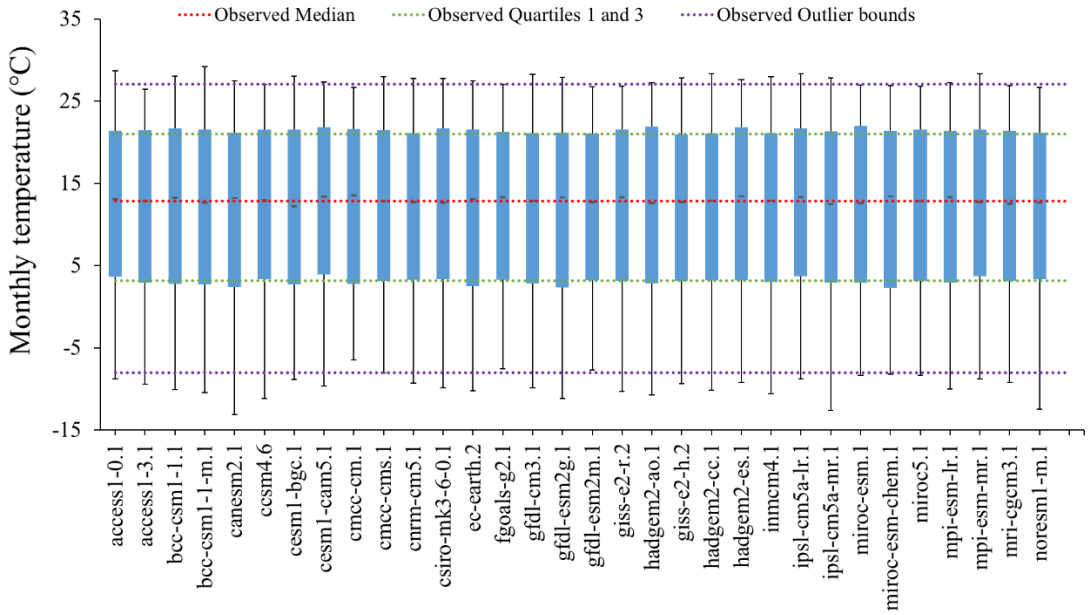

Figure 23. Box plots of the monthly temperature (°C) simulated by the 32 CMIP5 models during the 1980-2005 period at the NOAA Decatur station. Dashed lines correspond to the observed quartiles for the same period.

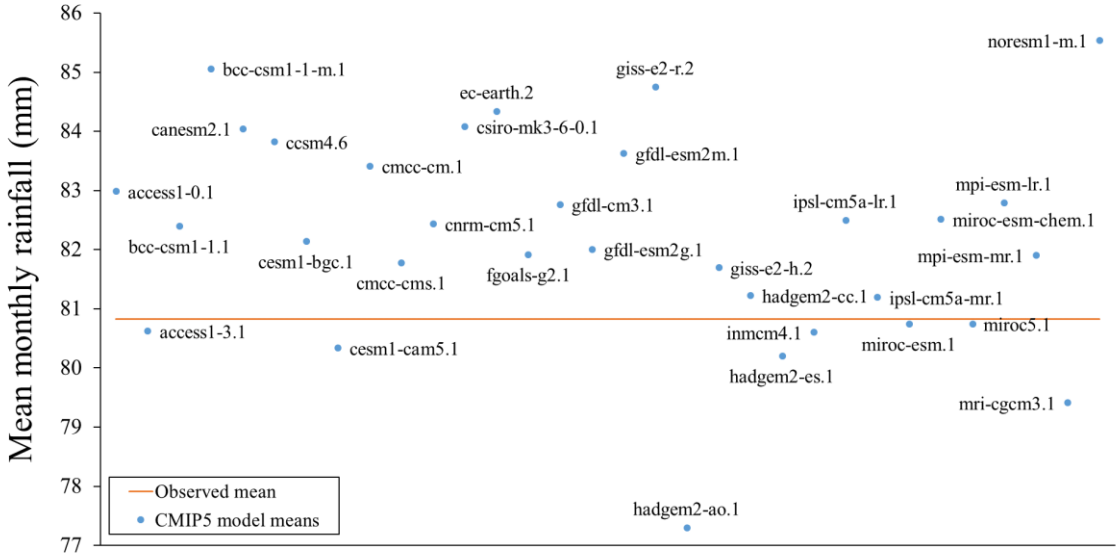

Figure 24. Observed and simulated mean monthly rainfall for the 1980-2005 period at the NOAA Decatur station.

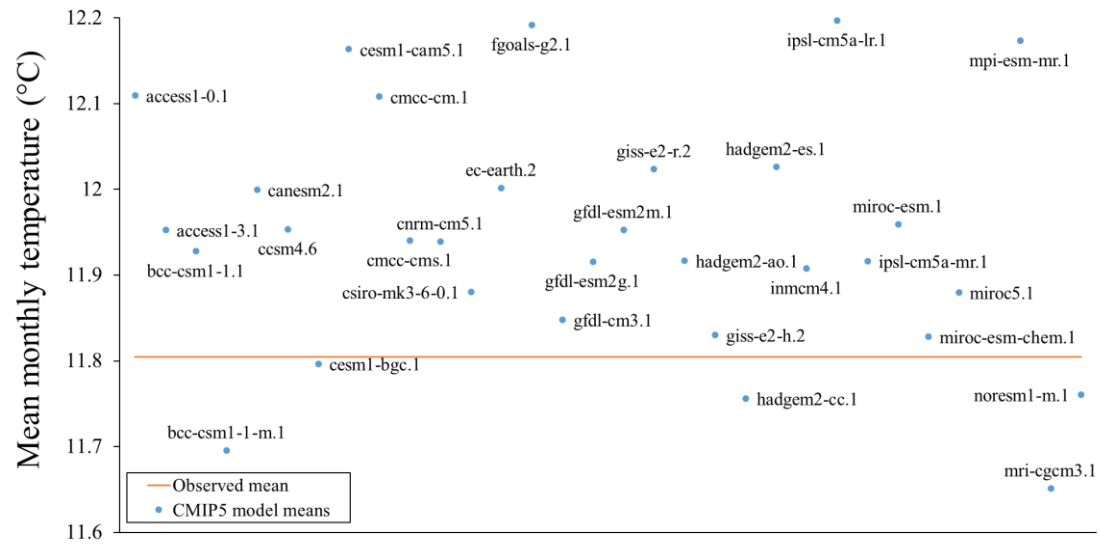

Figure 25. Observed and simulated mean monthly temperature for the 1980-2005 period at the NOAA Decatur station.

Additionally, a Taylor diagram was made for the monthly temperature and a double-mass curve for the monthly precipitation. The Taylor diagram (Taylor, 2001) is a polar coordinate diagram that evaluates in a concise way the correspondence of observed and simulated data by showing simultaneously the root mean square error (RMSE), the Pearson correlation coefficient, and the standard deviation (STD) of both observed and simulated. This technique presents the

performance and accuracy of the models in a visual way (Dong et al., 2018; Marta-Almeida et al., 2016; Chen et al., 2018; Curt et al. 2003). The monthly temperature for all the models showed correlation coefficients ranging from 0.94 to 0.96, RMSEs of approximately 3°C and STDs of approximately 10°C, very similar to the observed data (9.7°C) (Figure 26). On the other hand, a double-mass curve was used to check the consistency and the water mass balance of the simulated and observed monthly rainfall data (Figure 27). In general terms, the simulated cumulative rainfall at the USRB for the 32 models was shown to be consistent with the observed cumulative despite some cases of overestimations and underestimations and the Pearson correlation values (from 0.05 to 0.26 for the 32 models). The PBIAS was computed to further asses this observed behavior, PBIAS ranging from -0.04 to 0.05 were found for the 32 climate models, giving a very good performance of all the models to reproduce the cumulative amount of water entering the watershed system through rainfall, which is one of the most important aspects in the mass balance of the watershed.

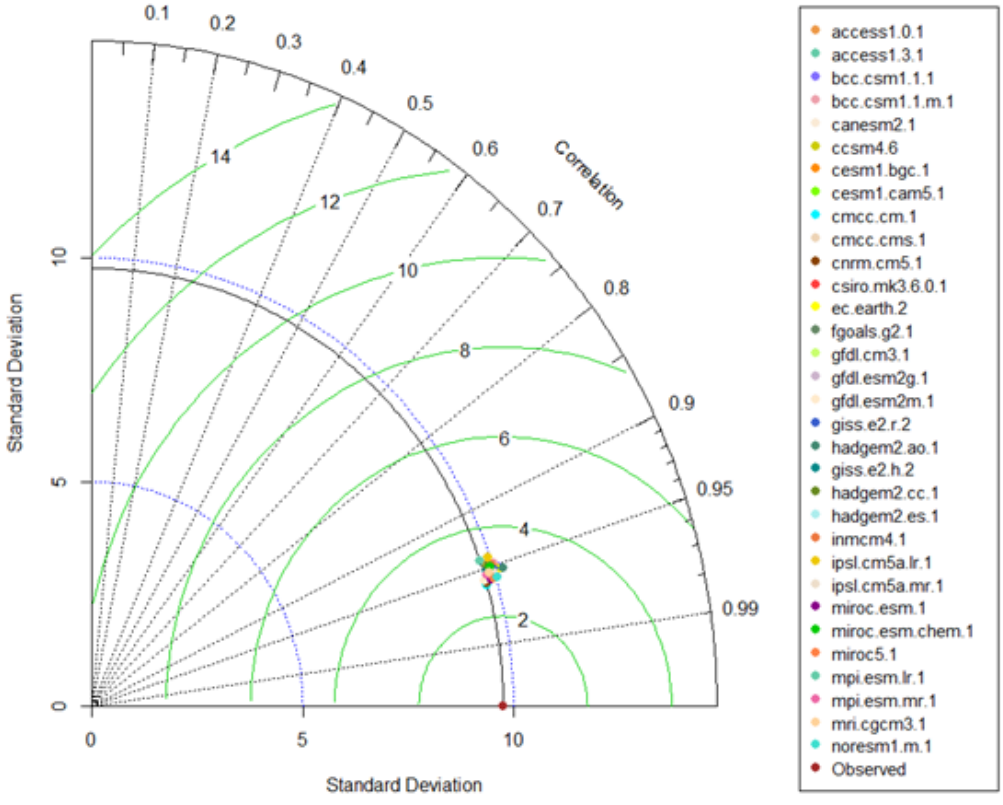

Figure 26. Taylor diagram of the monthly temperature (°C) of observed and simulated time series for the period 1980-2005. Correlation, standard deviations, and root mean square error (green continuous arcs) are presented. The continuous black arc represents the standard deviation of the observed data.

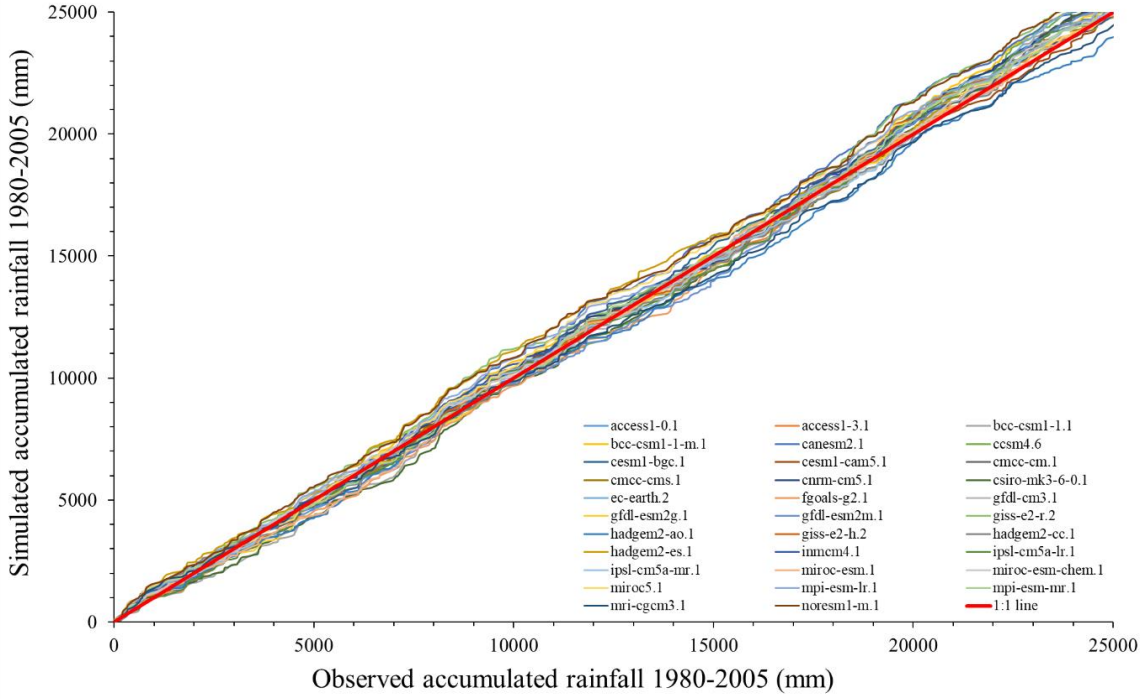

Figure 27. Double-mass curve of rainfall for the 1980-2005 period.

Since the 32 models had a satisfactory performance for the evaluation period and none of them appeared to be better than the others for this specific study area, the choice of a model to simulate the future climate at the USRB was made under a "critical scenario" condition. This is an agricultural watershed, and precipitation is one of the most important climatological variables that drives agricultural activities. Hence, it was used to identify the models having the driest and the wettest conditions (2020-2055). These two climate models were chosen to be the future climate scenarios to be used along with the WMPs variations. From the three gcm models with the highest total cumulative rainfall at Decatur station for the 2020-2055 period, the one with higher p-values for the KS and t-tests (from 0.77 to 0.91), and lower rainfall PBIAS (0.01) from the 1980-2005 analysis was "gfdl-esm2g.1.rcp85". On the other hand, the driest climate model whose cumulative rainfall was predominantly lower than all the other models for the 2020-2055 period was "access1-0.1.rcp85". It has p-values ranging from 0.36 to 0.97 for the KS and the t-tests, and rainfall PBIAS of 0.02 for the 1980-2005 analysis. Both climate models were verified to be among the wettest and driest, respectively, at other locations across the watershed.

Although daily precipitation and temperature time series data for future climate conditions were available at CMIP5 (2017), the reference evapotranspiration data were not available. A polynomial regression analysis, similar to Chapter 2, was conducted to obtain an expression to estimate the future daily reference evapotranspiration values from temperature and precipitation data for the USRB. Data for the 1998-2015 period were used for this purpose, yielding an R^2 of 0.67 and a reasonable reproduction of the historic evapotranspiration dynamics. The mean and maximum daily reference evapotranspiration computed through the modified Makkink formulation (De Bruin and Lablans, 1998) and the one computed from the polynomial regression for the 1998-2015 period were compared as verification measures. The Makkink equation resulted in a mean and maximum reference evapotranspiration of 2.5 and 6.5 mm/d, respectively, while the polynomial regression resulted in 2.5 and 6.4 mm/d for mean and maximum values, respectively.

The statistics of historic and future climate data at the Decatur station are presented in Table 15 in order to identify the general behavior of the future climate scenario with respect to the current one. The current climate data for the period 1980-2015 was found to have lower mean values of daily precipitation, temperature, and reference evapotranspiration than the future scenarios GFDL-ESM2G.1 (GFDL) and ACCESS1-0.1 (ACCESS) for the 2020-2055 period. The projected mean precipitation for GFDL was approximately 6% higher than the current, while ACCESS had a mean precipitation 14% lower than the observed for the 1980-2015 period. The future mean temperature increased from 11.95°C to 13.38°C for GFDL and to 14.69°C for ACCESS. For its part, the mean reference evapotranspiration increased by 9% for GFDL and by 23% for ACCESS (Table 15). Monthly values of the climate variables are plotted in Figure 28. The historic climate was shown to have the wettest period in the months of May and June, with a peak of 112 mm/month, while the future climates showed the wettest period around March to May and July, with the largest peaks being 117 mm/month and 98 mm/month for GFDL and ACCESS, respectively. Monthly temperature and evapotranspiration reached their maximum from June to August for the three climate cases, the ACCESS model being the highest among the three.

Table 15. Characterization of climate used scenarios

	Daily Precipitation in USRB (mm)			Daily Temperature in USRB (°C)			Reference Evapotranspiration rate in USRB (mm/d)		
	Mean	**Max**	**Min**	**Mean**	**Max**	**Min**	**Mean**	**Max**	**Min**
Current climate (1980-2015)	2.75	148.30	0.00	11.95	33.35	-27.50	2.64	7.22	0.00
GFDL-ESM2G.1.rcp85 (2020-2055)	2.92	84.77	0.00	13.38	35.59	-19.35	2.96	7.88	0.00
ACCESS1-0.1.rcp85 (2020-2055)	2.36	93.10	0.00	14.69	37.55	-21.04	3.25	8.66	0.00

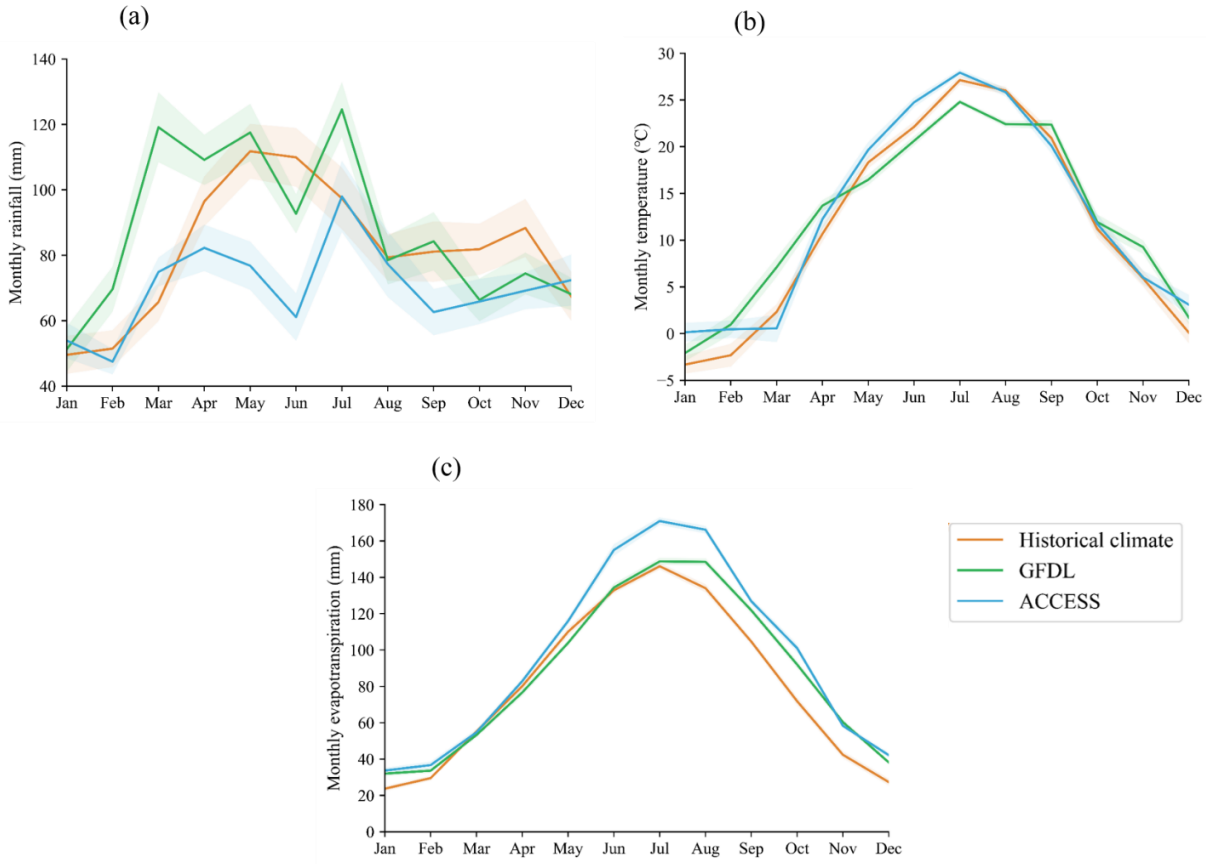

Figure 28. Monthly values of (a) rainfall, (b) temperature and (c) evapotranspiration for the selected climate cases. The band represents the standard error with 68% of confidence level.

3.3. RESULTS AND DISCUSSION

3.3.1. HYDROLOGIC MODEL

The flow parameters of the OL, UZ, SZ and rivers compartments in MIKE-SHE are measurable in the field. Nonetheless, certain processes and simplifications, such as drainage routing and geological layers conceptualization, required the adjustment of a few parameters in order to improve the model performance. Daily measured streamflow data (USGS, 2017) for the 1995-1999 and 2011-2015 periods at three stream gauges: Fisher, Monticello and Decatur (Figure 8) were used to evaluate the hydrologic model performance. Decatur's streamgauge station, corresponding to the outlet of the USRB, had a mean streamflow of 20.73 m^3/s for the 1980-2015 period, while Monticello and Fisher average streamflows are 13.81 m^3/s and 6.31 m^3/s, respectively (Table 16). The Nash-Sutcliff (NS) efficiency, the cumulative error and the Pearson's correlation coefficient (r) were computed to evaluate the agreement, the correlation, and the water balance difference between measured and simulated time series, respectively for two time periods.

Table 16. Statistics from available measured daily streamflow data.

		Streamflow (m^3/s)		Period	
USGS Station Code	**Station**	**Mean**	**Max**	**Start date**	**End date**
USGS-05570910	Fisher	6.31	261.93	1/1/1980	12/31/2015
USGS-05572000	Monticello	13.81	396.44	1/1/1980	12/31/2015
USGS-05573540	Decatur	20.74	543.68	10/1/1982	12/31/2015

To improve the agreement between the measured and simulated streamflow, the equivalent hydraulic conductivities of the Henry-Ashmore and the Glasford-Pearl layers were adjusted as described in Chapter 2. On the other hand, the drain time constant was set to $3x10^{-7}s^{-1}$, a value that agrees with the findings presented in Zhou et al. (2013) and the recommended range in the MIKE-SHE manual ($1x10^{-7}$ s^{-1} to $1x10^{-6}$ s^{-1}) (DHI, 2017a). The model was run for the two evaluation periods with a 2-year period to set up initial conditions and the efficiency metrics were computed. Generally, good agreement between observed and simulated daily streamflow was found (Figure 29 and 30). The NS for the three stations and two evaluation periods ranged from 0.54 to 0.72, the error from 2.2% to 8.5% (absolute values), and the correlation coefficients were found to be between 0.73 and 0.85.

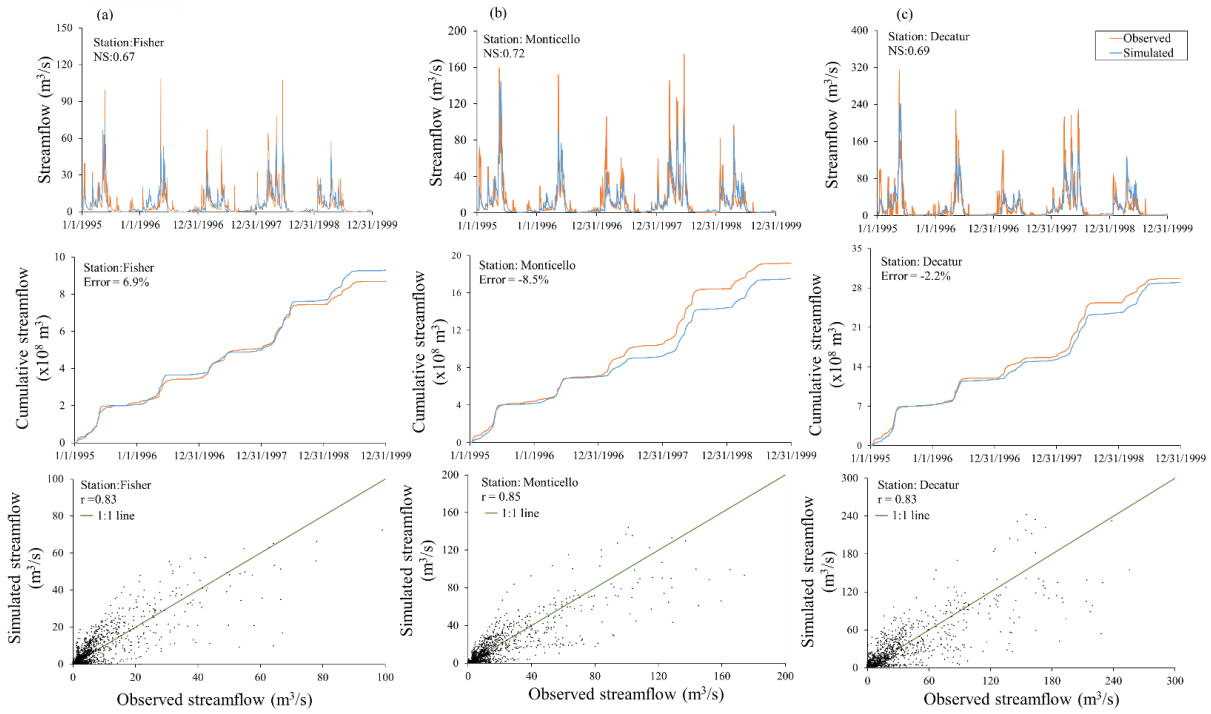

Figure 29. Hydrologic model performance at three streamflow gauges for the period of 1995-1999. (a) Fisher, (b) Monticello, and (c) Decatur.

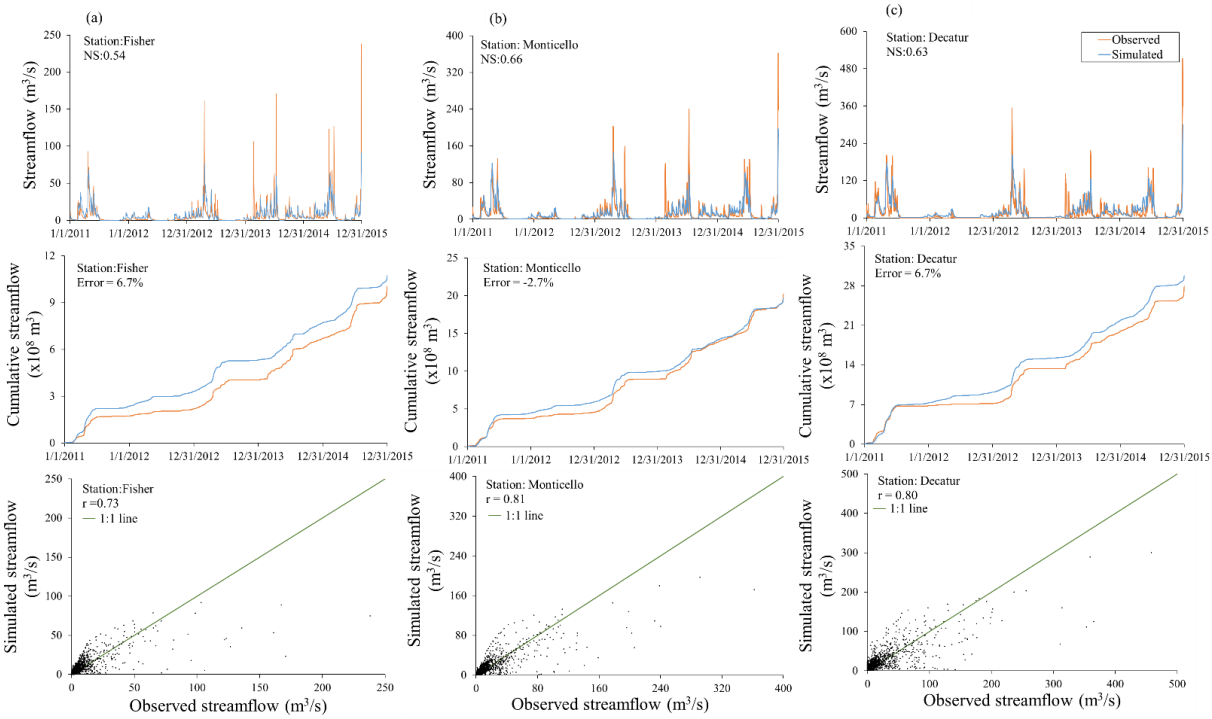

Figure 30. Hydrologic model performance at three streamflow gauges for the period of 2011-2015. (a) Fisher, (b) Monticello, and (c) Decatur.

3.3.2. TRANSPORT MODEL

Similar to that of streamflow, the transport simulation was performed using a physically-based equation, the ADE (Eq. 10). As in the flow simulation, certain simplifications and processes required the adjustment of some transport parameters. This was the case of the SZ layers equivalent transport parameters and the inclusion of processes not explicitly incorporated in the model, such as denitrification and sediment traps. The performance of the transport model for NO_3-N and sediments was evaluated by comparing the simulated load with the observed load from grab samples. Load represents the total mass of a pollutant reaching certain location per unit of time and it is commonly used to assess transport models (Li et al., 2010; Talebizadeh et al, 2010; Zhang and Zhang, 2011, Strauch et al., 2013, Spieles & Mitsch, 2000, Abbaspour et al., 2007). The model efficiency metrics were computed using the simulated values for days with grab samples. The PBIAS and Pearson correlation coefficient were computed to estimate the degree of over or underestimation of the model with respect to the observed data, and the collinearity of the two datasets, respectively. Two time periods, denoted *period I* and *period II*, were considered for each station and solute, the dates and length of these periods mainly depended on the availability of data (number of grab samples).

General transport parameters (non-species related), as porosity, dispersion (OL) and dispersivities (UZ and SZ) were adjusted. The porosity of both SZ layers was set to 0.2. These layers are composed by till, sand, gravel, and clay for which an equivalent porosity was adjusted. The OL dispersion coefficient was set to 0.075 m^2/s (Abbasi at al., 2003; Garcia-Navarro et al., 2000), while the UZ and SZ dispersivities were set to 0.05 m and 10 m, respectively. Values within the usual ranges used for these parameters were found in previous studies (Forrer et al., 1999, Adams & Gelhar, 1992, Neuman, 1990). The product of the dispersivity and the flow velocity gives the dispersion coefficient for the UZ and the SZ compartments.

3.3.2.1. Sediments

Given that sediment is defined as a suspended species, only the OL and the river flow compartments can transport it. The yearly mass balance was used in order to check the total amount of sediments entering the river from the OL compartment. The threshold concentration for the OL sediment concentration, explained in section 3.2.3.1., was adjusted in order to get results as close as possible to the reported yearly sediment load reaching Lake Decatur (200,000 ton/year) (Rhoads et al., 2016). The adjusted value was found to be $1x10^4$ kg/m^3, which

produced the transport of approximately 30% of the total in-site eroded soil computed at grid-cell scale to the river network. An examination of the daily OL concentration maps for sediments, showed that approximately 95% of the grid-cells presenting sediment transport had concentrations of up to 2 x10^3 kg/m^3.

The predominant soil types in the USRB are the Drummer silty clay and the Flanagan silt loam (Botero-Acosta, 2018), which is why cohesive sediments are expected to reach the main stem. According to ISWS (1994) the sediments reaching Lake Decatur are predominantly clay, which has very low settling rates in fresh water (Sutherland et al., 2013). A conservative ADE was applied to simulate the transport of cohesive sediments along the streams towards Lake Decatur. Once at the lake, the source/sink (Erosion/deposition) term was activated in order to include the lake's trapping effects of sediments and the lakeshore bank erosion. The sediment trap efficiency of the lake was reported to be 78% in 1983; this value represents the percentage of sediments held in the lake (ISWS, 1987). The trap efficiency depends on the spillway height. In 1956 the peak of sediment trap efficiency was reached due to the increase in the spillway height and hence, the increase in the lake volume (ISWS, 1987). In addition to this, sediment traps are being constructed since 2011 (Huffer, 2016, City of Decatur, 2017). Three traps located at the lake inlets capture incoming sediment before it reaches the main body of the lake. One of them treats 85% of the incoming water. On the other hand, ISWS (1987) reported lakeshore bank erosion as being responsible for contributing 2.2% of the total yearly sediment deposited in the reservoir. The main causes of this are the steep bluffs and the waves formed at the lake.

In order to simulate this effect in the sediment concentration at the outlet of the USRB, the free settling velocity (w), the critical shear stresses for erosion (τ_{ce}), and deposition (τ_{cd}), and the erodibility of the lake (M^*) were adjusted. The settling velocity was found to be 2x10^{-5} m/s. Settling velocities for particles with diameters ranging from 0.001 mm to 0.07 mm (a range that includes clay and silt), can be found to be between 6x10^{-7} m/s to 3x10^{-3} m/s (Cheng, 1997). A critical shear stress for deposition of 4.0 N/m^2 was found to reproduce the lake's sediment trapping effect as shown in the observed data and reported by ISWS (1987). Maximum bed shear stresses at the lake were found to be 3.8 N/m^2, having a τ_{cd} approximately equal to this value allowed continuous sedimentation at the lake, similar to Borsje et al. (2008). Since the $\left(1-\frac{\tau}{\tau_{cd}}\right)$ factor in Eq. 17 represents the probability of deposition happening (Lumborg and Vested, 2008),

having a large τ_{cd} signifies that the settling process is very likely to happen. On the other hand, the τ_{ce} and the M^* were adjusted to 0.5 N/m^2 and 0.2 g/ m^2 s, respectively. These values are in accordance with measurements from other studies about cohesive sediment erosion (Borsje et al., 2008) and are within the typical ranges proposed in the MIKE 11 manual for these parameters (DHI, 2017b).

The sediment transport model performance was tested by comparing the simulated sediment load for the days with available data (grab samples). The observed mean load at the outlet of the USRB (Decatur) was found to be 113.7 ton/day, 20% less than the load observed at the upstream station, Monticello (140.4 ton/day). The effect of sediment trapping of the lake and the recently installed sediment traps caused a load reduction at the outlet of the lake. By contrast, Fisher presented a mean sediment load of 61.5 ton/ day, less than half of the load observed at the following downstream station (Monticello) (Table 17). Simulated daily sediment load and observed grab sample loads for *Periods I* and *II* are presented in Figures 31 and 32. The PBIAS for the simulated loads at the three stations and two periods showed very good agreement with the observed load (0.83% to 5.54% in absolute values), except for Fisher station during *Period I*, which presented an underestimation of 23%. A PBIAS of up to 20% for sediment transport simulation was considered to be "good" and "satisfactory" up to 55% (Moriasi, 2015; ASABE, 2017). Additionally, it had a Pearson's correlation coefficient of 0.88 and a PBIAS of -4.5% for the *Period II* at the same station. The correlation coefficient for the three stations and two periods showed a good collinearity of observed and simulated values, ranging from 0.65 to 0.88.

Table 17. Statistics from measured total suspended solids (TSS) data. Measured streamflow was used for load computation.

			TSS load (Ton/d)		Period of samples collection	
USGS Station Code	**Station**	**Number of samples**	**Mean**	**Max**	**Start date**	**End date**
USGS-05570910	Fisher	153	61.53	1882.15	1/29/1980	5/1/1997
USGS-05572000	Monticello	190	140.48	1552.94	9/26/1996	8/5/2013
USGS-05573540	Decatur	129	113.73	3676.71	11/4/1982	4/24/1997

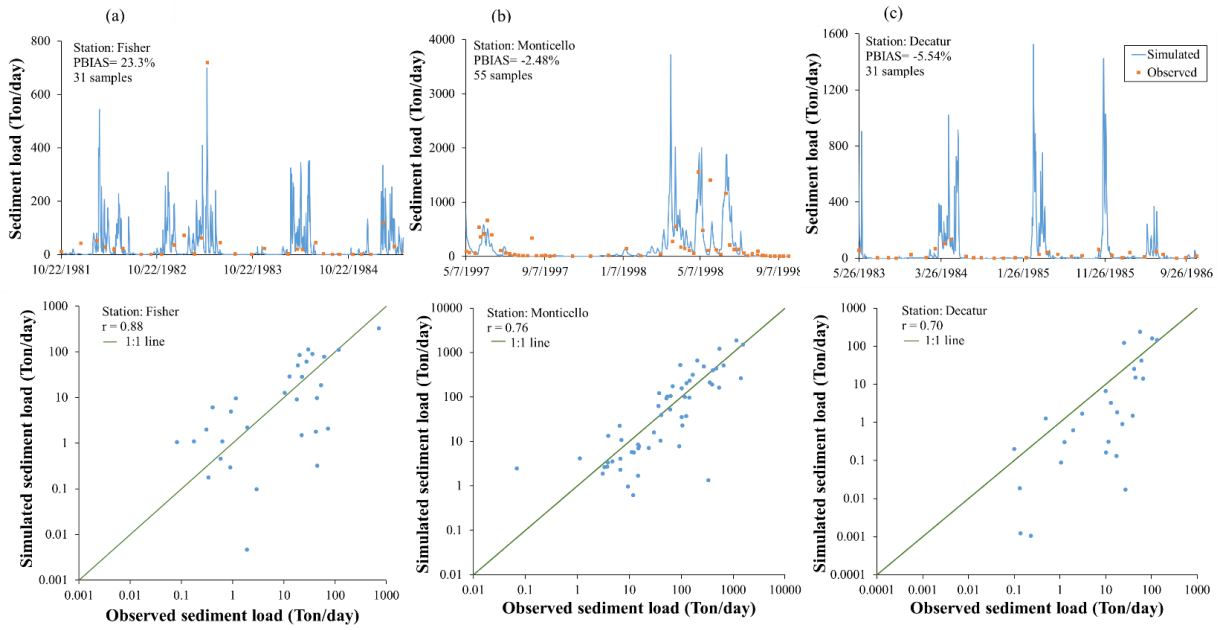

Figure 31. Sediment transport model performance at three gauges. (a) Fisher, (b) Monticello, and (c) Decatur *period I.*

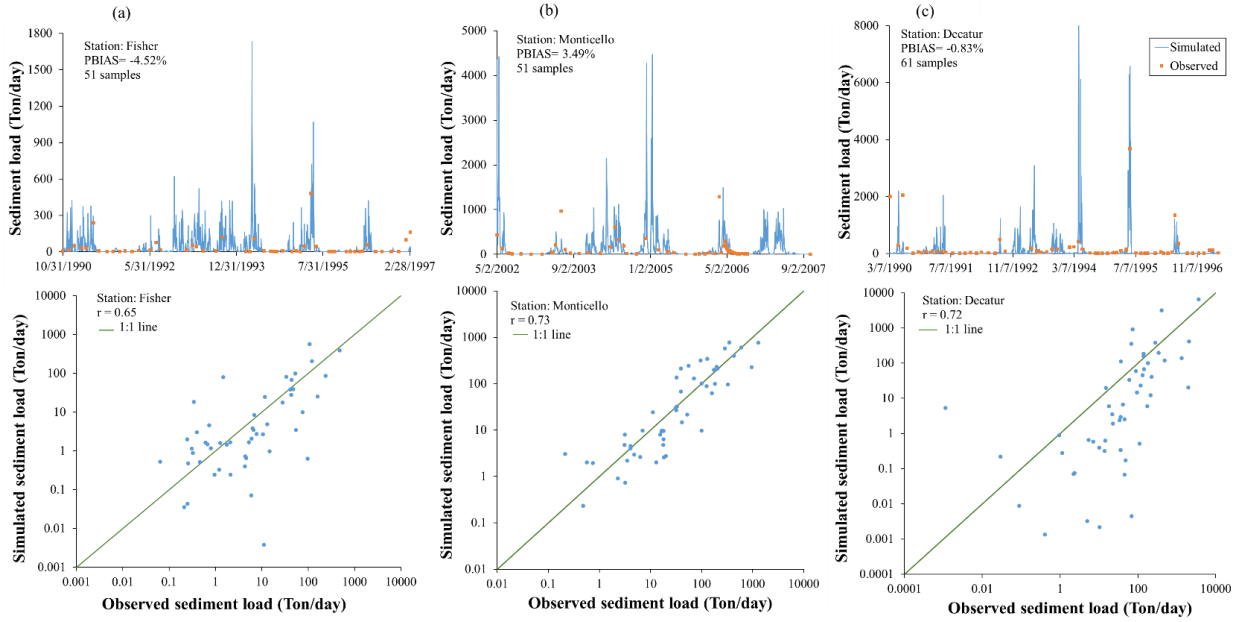

Figure 32. Sediment transport model performance at three gauges. (a) Fisher, (b) Monticello, and (c) Decatur *period II.*

3.3.2.2. Nitrate-N

Simulation of NO_3-N transport was also performed by the ADE. The dissolved nature of the NO_3-N allowed the transport to be simulated through the OL, UZ, SZ and rivers. Decay processes were included in all the watershed compartments, while sorption was simulated in the

UZ and SZ. Parameters of NO_3-N transport were adjusted to better reproduce the observed data. The half-life (λ) of the NO_3-N used in the decay reaction (Eq. 20) was set to 1.2 years with a reference temperature (T_{ref}) of 20°C. This value agrees with that of Klein et al. (2013), who stated that NO_3-N half-life was approximately 500 days for zones where organic substances were present. Empirical parameters B and α used in the water content and temperature decay correction (Eq. 21 and 22), were adjusted to 0.7 and 1, respectively. With regard to the adsorption process happening in the UZ and the SZ, the Freundlich isotherm (Eq. 24) parameters, K_f and N were set to $8x10^{-10}$ m^3/g and 0.78, respectively. These values agreed with the ones used by Hamdi et al. (2013) for Nitrate sorption in agricultural soils. The initial sorbed concentration in the UZ and the SZ layers ranged from $3x10^{-6}$ g/g to $2x10^{-5}$ g/g.

The transport model was run for the two evaluation periods, with a 2-year startup period ahead of each. Results were compared with the observed NO_3-N load obtained from the grab samples (Table 18). The observed mean of NO_3-N load at Decatur was found to be 13.1 ton/day, while Fisher and Monticello had 6.3 ton/day and 11.8 ton/day, respectively. Daily simulated time series and grab samples of NO_3-N load at Fisher, Monticello and Decatur stations for *Periods I* and *II* are shown in Figures 33 and 34. The PBIAS (in absolute values) and the Pearson's correlation coefficient ranged from 0.87% to 9.32%, and 0.55 to 0.91, respectively, showing a satisfactory behavior of the NO_3-N transport model.

Table 18. Statistics from measured NO_3-N data. Measured streamflow was used for load computation.

			NO_3-N load (Ton/d)		**Period of samples collection**	
USGS Station Code	**Station**	**Number of samples**	**Mean**	**Max**	**Start date**	**End date**
USGS-05570910	Fisher	157	6.34	87.47	1/29/1980	8/15/1997
USGS-05572000	Monticello	291	11.87	96.46	4/12/1991	8/5/2013
USGS-05573540	Decatur	136	13.17	110.26	11/4/1982	4/24/1997

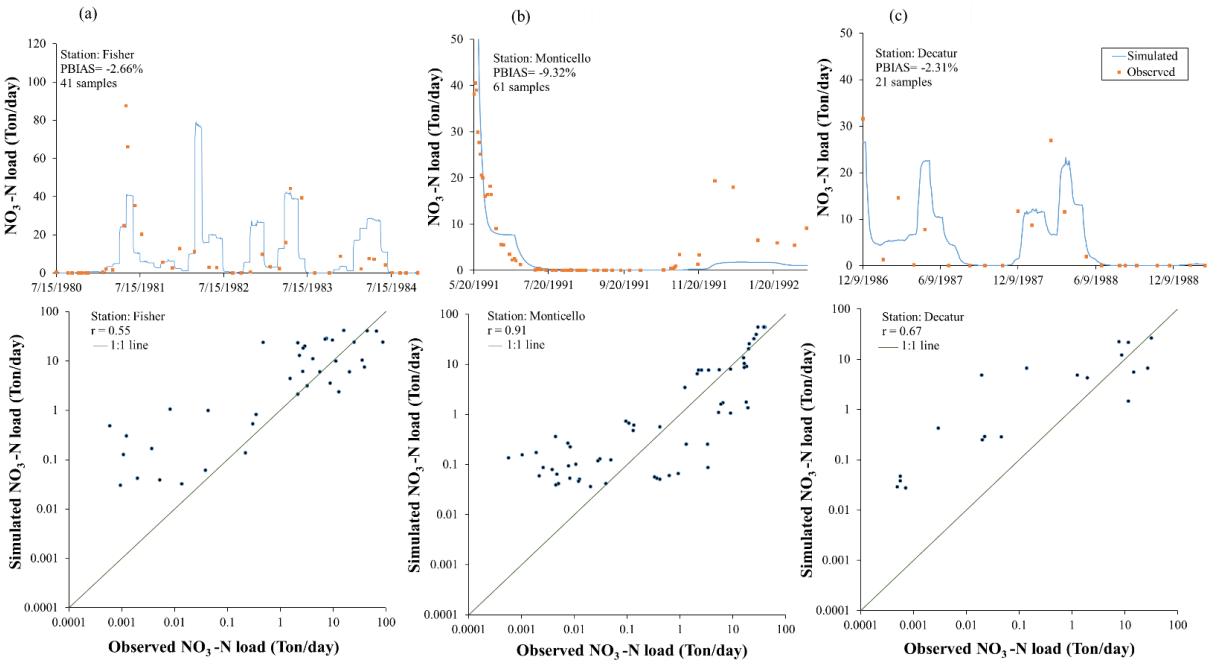

Figure 33. NO_3-N Transport model performance at three gauges. (a) Fisher, (b) Monticello, and (c) Decatur *period I.*

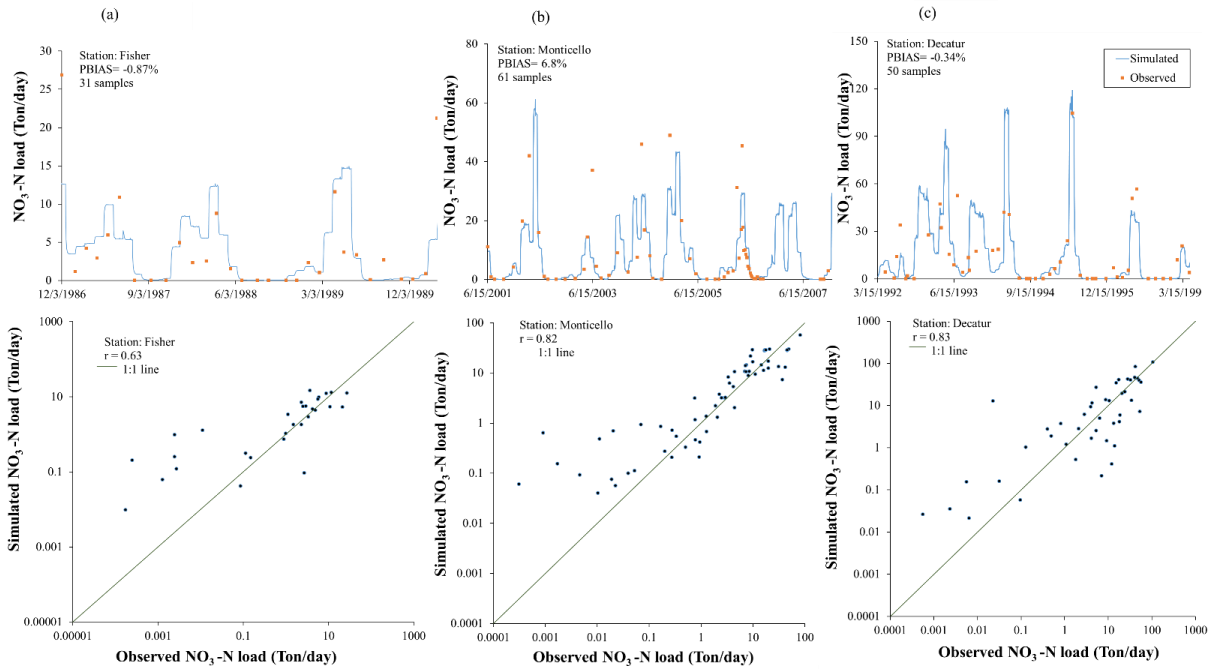

Figure 34. NO_3-N transport model performance at three gauges. (a) Fisher, (b) Monticello, and (c) Decatur *period II.*

3.3.3. BASELINE

The baseline model was simulated for the 1980-2015 period with a 2-year warming period. The current land use (Table 9) of the USRB and the historic climate were used for setting up the model. The NO_3-N inputs were created as explained in section 3.2.3.2: from 1980 to 2008, Case 6 (Table 11) was applied; from 2009 to 2011, Case 1; and from 2012 to 2015, Case 2. Sediment inputs were computed through the MUSLE equation and the WM outputs (Section 3.2.3.1). The C-factors applied for the baseline land uses are presented in Table 19.

Table 19. C-factor used in the baseline (Ward et al., 2016).

Land use	C-factor
Deciduous forest	0.041
Grass/pasture	0.005
Winter wheat/Other hay/not alfalfa (no-till)	0.005
Wetlands	0
Corn (conventional till)	0.4
Soybean (conventional till)	0.45
Alfalfa (no-till)	0.005

Results for the baseline at the three stations are presented in Table 20. The mean values of streamflow, sediment, and NO_3-N loads at the outlet of the watershed (Decatur) for the entire simulation period were found to be 20.7 m^3/s, 78.2 ton/day, and 14 ton/day, respectively. The mass balance report revealed that more than 95% of the total cumulative NO_3-N reaching the streams during the simulated period stemmed from tile drainage flow. Panno et al. (2008) reported that Nitrate transported to Illinois River tributaries mainly comes from tile-drained agricultural lands. The sediment trapping effect of the lake is manifested in the reduction of sediment load between Monticello and Decatur. The baseline results exhibited maximum and minimum monthly means (monthly median for the streamflow) at May and August, respectively, for the three studied variables (Figure 35a, b and c). These results are highly related to the monthly rainfall trends observed in Figure 28a for the historic climate, and were expected, given the relationship of rainfall with runoff, drainage flow, erosion and transport processes. Previous studies about the USRB water and nutrient's seasonal variation had also reported these trends for streamflow and nutrient load (Li at al., 2010; ISWS, 2000).

Table 20. Results baseline. Mean, maximum and minimum of streamflow, sediment and NO_3-N loads at Fisher, Monticello and Decatur.

	STREAMFLOW (m^3/s)			SEDIMENT LOAD (Ton/d)			NO_3-N LOAD (Ton/d)		
	Mean	**Max**	**Min**	**Mean**	**Max**	**Min**	**Mean**	**Max**	**Min**
FISHER	6.72	42.78	0.03	26.64	1730.64	0.00	7.13	78.91	0.00
MONTICELLO	12.72	93.30	0.64	165.34	16701.57	0.00	14.05	286.14	0.03
DECATUR	20.77	184.71	1.41	78.25	22073.60	0.00	14.04	311.65	0.02

3.3.4. ENVIRONMENTAL STRESSORS

The six selected WMPs and the three climates cases were combined in order to study the USRB response to individual and combined environmental stressors. A total of 18 scenarios were created (including the baseline; see Table 21) to simulate the impacts of: climate, WMPs and climate + WMPs, over the water quantity and quality in USRB. The daily discharge, sediment and NO_3-N loads were simulated through the MIKE SHE/MIKE 11 model. The relative change in the mean, maximum, and minimum values with respect to the baseline were computed (Tables 22, 23 and 24) to estimate the general effects of each scenario over the studied variables at the three measuring stations. Graphs of monthly values (Figures 35, 36 and 37) were created to analyze the seasonal trends and changes produced by the selected stressors at Decatur.

Table 21. Simulated scenarios.

	Current climate (1980-2015)	**GFDL (2020-2055)**	**ACCESS (2020-2055)**
WMP 1 – Current WMP	Scenario 1*	Scenario 2	Scenario 3
WMP 2 – Wetland construction	Scenario 4	Scenario 5	Scenario 6
WMP 3 – Grassed riparian buffer	Scenario 7	Scenario 8	Scenario 9
WMP 4 – Crop rotation	Scenario 10	Scenario 11	Scenario 12
WMP 5 – Cover crops	Scenario 13	Scenario 14	Scenario 15
WMP 6 – Reduced till	Scenario 16	Scenario 17	Scenario 18

*Baseline

The climate cases were applied by modifying the daily precipitation, temperature and evapotranspiration, while the WMP modifications were implemented as stated in Section 3.2.4.1. The fertilizer application schedule and rates for the future climate scenarios were set in

accordance with Case 1 (Table 11). This schedule was chosen since Case 1 is the currently most common application schedule in central Illinois (Schaefer, personal communication, 2018). For the corn-soybean rotation scenario, the fertilizer application schedule presented in Table 13 was used for both past and future scenarios.

3.3.4.1. Impact of future climate scenarios

An initial analysis of the climate impact over the streamflow, sediment, and NO_3-N load was achieved by comparing the results for the three climate cases under current WMP application (Scenarios 1-baseline-, 2 and 3 in Table 21). In this way the sole effects of the climate would be identified, since the WMP would remain as in the baseline. It was observed that the GFDL produced an increase of approximately 5% in the streamflow at the three stations, while ACCESS reduced it by 50% to 61% at the three stations (Table 22). The monthly variability of rainfall, temperature and ET (Figure 35a) resulted in the reduction in the monthly median streamflow for ACCESS in all the months, and the increase from January through May for GFDL. Additionally, the occurrence of the monthly streamflow peak for both future climates shifted from May (baseline) to April, a shift that was reflected in the graphs for the sediments and NO_3-N loads. The behavior of the streamflow monthly s reveals their relationship with the climate variables. GFDL showed a higher monthly rainfall than the baseline from January through May, while maintaining a similar evapotranspiration rate, after which, a higher evapotranspiration than the baseline was observed. For its part, ACCESS had less rainfall than the baseline for the majority of months, accompanied by higher monthly evapotranspiration rates.

Although the wettest climate (GFDL) showed a slight increase in the NO_3-N load for the months of January through May with respect to the baseline (similar to the streamflow) (Figure 35b), the reduction of load for the rest of the months caused a general decrease in the mean load for the simulated period (Table 23), with reductions of up to 11% at the three stations. A larger decrease was observed for the NO_3-N under the driest (ACCESS) climate, reaching load reductions by up to 74% (Table 23), this result was expected given the small amount of water available to drain to the streams (Figure 35a).

The effect of climate was observed to be stronger on the sediment load than the NO_3-N. The general impact of the driest climate was to reduce the sediment load by up to 91%, while the wettest increased it by up to 48% (Table 24). Figure 35c shows the high impact of climate over

the monthly mean sediment load and how it follows the monthly trend of the streamflow (Figure 35a). The accentuated effect of climate on the sediment load compared to the NO_3-N, is probably due to the nature of the sources for both species. Transport of both pollutants was influenced by natural events but sediment inputs to the model depended on the OL volume and the OL flow (MUSLE), while the NO_3-N inputs were solely dependent upon anthropogenic activities. With this in mind, climate variables (especially rainfall) were modifying the sources and the transport processes for the sediments, while the NO_3-N sources remained unchanged.

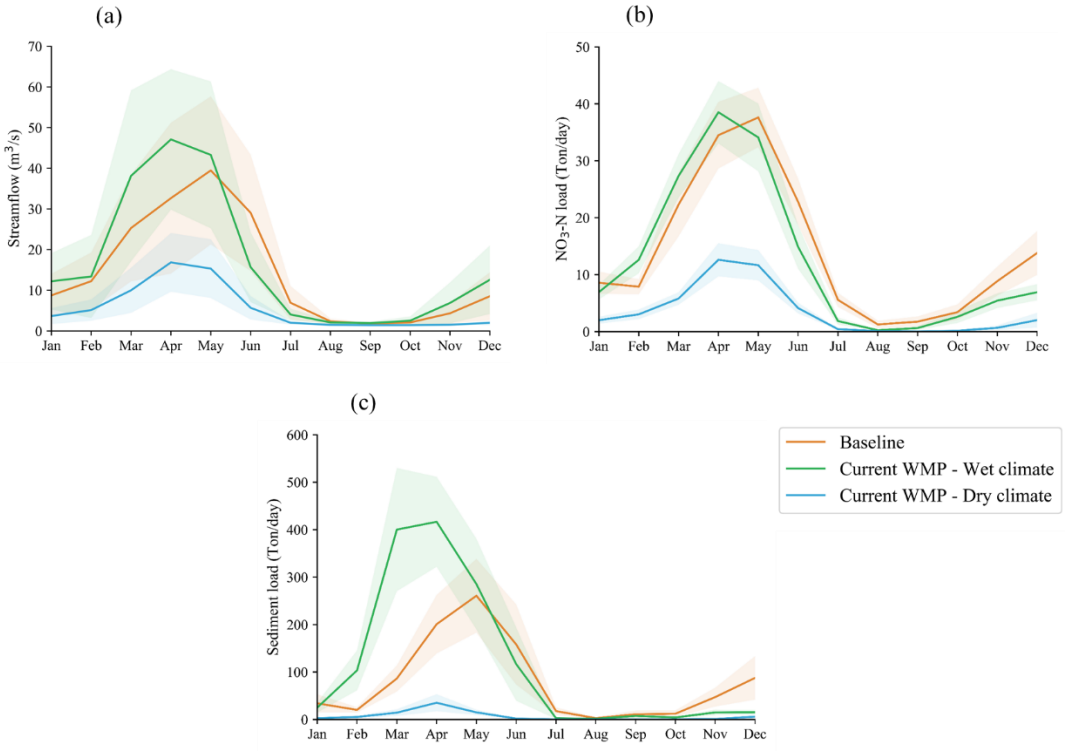

Figure 35. Impacts of climate over (a) streamflow, (b) NO_3-N load and (c) sediment load at Decatur. 68% confidence level band.

Table 22. Percentage of change of the mean, maximum and minimum streamflow for the 18 scenarios with respect to the baseline.

Streamflow	FISHER									MONTICELLO									DECATUR								
	A. Current climate 1980-2015			B. GFDL 2020-2055			C. ACCESS 2020-2055			A. Current climate 1980-2015			B. GFDL 2020-2055			C. ACCESS 2020-2055			A. Current climate 1980-2015			B. GFDL 2020-2055			C. ACCESS 2020-2055		
	Mean (%)	Max (%)	Min (%)	Mean (%)	Max (%)	Min (%)	Mean (%)	Max (%)	Min (%)	Mean (%)	Max (%)	Min (%)	Mean (%)	Max (%)	Min (%)	Mean (%)	Max (%)	Min (%)	Mean (%)	Max (%)	Min (%)	Mean (%)	Max (%)	Min (%)	Mean (%)	Max (%)	Min (%)
1. Current state	**0.0**	**0.0**	**0.0**	5.4	17.5	-2.0	-56.6	-32.3	-2.3	**0.0**	**0.0**	**0.0**	5.1	25.3	-2.0	-60.7	-33.7	-9.4	**0.0**	**0.0**	**0.0**	5.3	0.0	-1.8	-61.4	-40.0	-9.2
2. wetlands	0.6	3.3	1.3	6.6	18.6	-2.2	-56.1	-32.6	-2.2	0.1	7.5	-9.9	5.8	28.4	-11.6	-60.8	-32.6	-17.9	0.2	4.1	12.0	6.1	4.2	-13.8	-61.5	-38.0	-18.6
3. buffer	-14.6	-7.1	-0.9	-11.8	11.7	-2.3	-70.3	-44.4	-2.3	-13.5	-7.6	-1.0	-10.4	17.5	-3.1	-71.6	-46.5	-12.1	-11.5	-5.9	-0.7	-8.0	-6.4	-2.5	-70.3	-49.6	-11.7
4. crop rotation	-4.3	-0.2	-0.8	0.5	16.0	-2.0	-59.4	-33.3	-2.4	-4.7	0.1	0.1	-0.2	23.6	-2.8	-63.4	-35.4	-9.8	-4.7	4.1	-0.1	0.0	3.6	-2.3	-64.2	-41.5	-9.7
5. cover crops	-25.6	-20.1	-2.2	-24.0	0.7	-2.2	-77.5	-55.7	-2.2	-26.4	-15.6	-2.4	-24.8	4.4	-4.8	-78.9	-61.3	-19.6	-25.0	-6.8	-2.1	-23.4	-15.7	-3.8	-78.3	-65.0	-19.1
6. reduced till	-0.3	-1.0	1.3	5.3	16.9	-2.2	-56.3	-32.6	-2.2	-0.3	-0.4	0.1	5.0	24.7	-2.1	-60.4	-33.9	-9.3	-0.3	-1.1	0.0	5.2	-0.2	-1.8	-61.1	-40.1	-9.0

Table 23. Percentage of change of the mean, maximum and minimum NO_3-N load for the 18 scenarios with respect to the baseline.

NO_3-N Load	FISHER									MONTICELLO									DECATUR								
	A. Current climate 1980-2015			B. GFDL 2020-2055			C. ACCESS 2020-2055			A. Current climate 1980-2015			B. GFDL 2020-2055			C. ACCESS 2020-2055			A. Current climate 1980-2015			B. GFDL 2020-2055			C. ACCESS 2020-2055		
	Mean (%)	Max (%)	Min (%)	Mean (%)	Max (%)	Min (%)	Mean (%)	Max (%)	Min (%)	Mean (%)	Max (%)	Min (%)	Mean (%)	Max (%)	Min (%)	Mean (%)	Max (%)	Min (%)	Mean (%)	Max (%)	Min (%)	Mean (%)	Max (%)	Min (%)	Mean (%)	Max (%)	Min (%)
1. Current state	**0.0**	**0.0**	**0.0**	-8.9	-26.8	0.0	-64.4	-56.1	0.0	**0.0**	**0.0**	**0.0**	-11.1	-19.4	-100.0	-70.8	-58.9	-15.3	**0.0**	**0.0**	**0.0**	-9.9	-21.4	-4.5	-74.8	-59.1	-16.2
2. wetlands	-2.3	-1.6	0.0	-11.2	-27.3	0.0	-64.6	-56.7	0.0	-1.2	-0.9	-100.0	-12.3	-19.9	-100.0	-70.9	-59.2	-21.9	-1.6	-1.0	-100.0	-11.5	-21.0	-100.0	-75.0	-59.0	-31.8
3. buffer	-19.9	-13.8	0.0	-27.0	-35.2	0.0	-76.4	-65.5	0.0	-16.4	-10.7	-1.5	-25.8	-28.3	-4.2	-80.5	-67.2	-15.6	-17.3	-11.5	-100.0	-25.7	-29.2	-5.7	-83.3	-66.5	-19.9
4. crop rotation	-39.6	-5.0	0.0	-42.7	-30.8	0.0	-79.4	-65.7	0.0	-33.8	-3.6	-0.1	-40.9	-21.1	-100.0	-81.5	-65.8	-13.8	-40.9	-6.7	-1.7	-46.3	-24.1	-100.0	-86.5	-70.1	-18.5
5. cover crops	-24.6	-23.2	6.0	-32.5	-38.1	6.0	-82.0	-71.9	6.0	-27.4	-21.6	-5.3	-36.2	-37.1	-5.7	-87.7	-77.2	-23.8	-30.3	-24.7	-4.1	-38.1	-42.2	-100.0	-90.6	-78.3	-30.9
6. reduced till	0.1	-0.5	7.0	-8.6	-26.9	7.0	-64.2	-56.1	7.0	-0.1	-0.5	0.5	-11.0	-19.5	-100.0	-70.5	-59.1	-17.4	0.0	-0.2	0.1	-9.6	-21.5	-100.0	-74.5	-59.2	-16.1

Table 24. Percentage of change of the mean, maximum and minimum sediment load for the 18 scenarios with respect to the baseline.

Sediment Load	FISHER									MONTICELLO									DECATUR								
	A. Current climate 1980-2015			B. GFDL 2020-2055			C. ACCESS 2020-2055			A. Current climate 1980-2015			B. GFDL 2020-2055			C. ACCESS 2020-2055			A. Current climate 1980-2015			B. GFDL 2020-2055			C. ACCESS 2020-2055		
	Mean (%)	Max (%)	Min (%)	Mean (%)	Max (%)	Min (%)	Mean (%)	Max (%)	Min (%)	Mean (%)	Max (%)	Min (%)	Mean (%)	Max (%)	Min (%)	Mean (%)	Max (%)	Min (%)	Mean (%)	Max (%)	Min (%)	Mean (%)	Max (%)	Min (%)	Mean (%)	Max (%)	Min (%)
1. Current state	**0.0**	**0.0**	**0.0**	14.4	6.2	0.0	-82.6	-59.4	0.0	**0.0**	**0.0**	**0.0**	13.9	50.2	0.0	-82.9	-52.7	0.0	**0.0**	**0.0**	**0.0**	48.1	43.4	0.0	-91.4	-92.3	0.0
2. wetlands	-40.0	133.2	1.0	-41.9	45.5	0.0	-94.7	-95.0	0.0	-15.5	-59.4	0.0	-17.5	20.9	0.0	-89.3	-94.7	0.0	-12.6	102.8	1.0	9.8	139.6	0.0	-94.8	-96.2	0.0
3. buffer	-31.0	14.9	2.0	-39.2	40.4	0.0	-95.0	-87.4	0.0	-6.8	13.7	0.0	-14.8	32.6	0.0	-90.9	-69.1	0.0	-3.4	35.5	2.0	15.5	25.2	0.0	-95.7	-83.3	0.0
4. crop rotation	18.5	56.9	3.0	7.4	23.2	0.0	-87.0	-64.9	0.0	16.5	57.4	0.0	9.1	55.6	0.0	-86.1	-55.5	0.0	22.8	47.2	3.0	42.7	37.6	0.0	-93.7	-89.2	0.0
5. cover crops	-47.8	-15.6	4.0	-59.0	-60.7	5.0	-98.8	-98.4	6.0	-40.6	-33.6	4.0	-47.1	-50.1	5.0	-97.7	-98.6	6.0	-42.1	2.7	4.0	-34.8	-39.2	5.0	-98.9	-94.7	6.0
6. reduced till	-33.4	45.6	5.0	-36.4	-26.1	6.0	-91.4	-81.2	7.0	-25.6	-53.8	5.0	-26.7	-43.7	6.0	-90.9	-81.7	7.0	-26.9	-44.0	5.0	-9.0	-24.2	6.0	-95.2	-96.6	7.0

3.3.4.2. Impact of WMPs

The impact of WMPs was then assessed by comparing the streamflow, sediment, and NO_3-N loads of all the WMP cases under historic climate (Scenarios 1 -baseline-, 4, 7, 10, 13 and 16 in Table 21). Figure 36 shows the monthly averages of streamflow, NO_3-N and sediment loads at Decatur station, located at the outlet of the watershed and right downstream Decatur Lake.

Wetlands were located in cells that showed the highest OL depths, corresponding to those cells producing a large portion of the sediment inputs for the baseline. Sediment reductions ranged from 12% to 40% at the three stations (Table 24), with the higher reductions happening at Decatur in March, April and June (Figure 36c). By converting local depressions prone to flooding to wetlands, flow patterns were not altered significantly. This is the reason why the 3.4% of the total area turned into wetlands cells did not significantly modify the streamflow (Table 22). For its part, impacts over the NO_3-N were minimal given that NO_3-N is mostly transported through the drainage system (Table 23) (Figure 36a and b). It is important to mention that the storm water wetlands were not intercepting tile drained water, and hence, not affecting the NO_3-N transported through subsurface drainage to the streams. The reference coding system used to conceptualize the routing of drained water to the rivers was modified to remove tile drainage from wetlands. With no grid codes assigned to wetland cells, they were neither able to produce nor receive tile drained water. Special attention was paid to the increase in the maximum sediment load at Fisher (133%) (Table 24). The time series results showed that this value corresponded to an extreme event observed once during the simulated period, on 13/04/1994, occurring the day after the highest rainfall that was expected to increase erosion and transport processes. Fisher subwatershed is the smallest of the three and has the highest elevation change (Botero-Acosta et al., 2018) that might have limited its ability to buffer extreme events.

Similar to the wetlands, the reduced till scenario had very low impacts on the flow and the NO_3-N load. Relative changes of less than 1% were observed for both variables at the three stations with respect to the baseline (Tables 22 and 23). This effect was also manifested in the monthly average of these two variables (Figure 36a and b). According to the study developed by Haag et al. (2006) in a mesoscale basin, the effects of reduced tillage over the runoff and flood mitigation could be negligible if produced by rainfall events of moderate intensity and long duration (advective rainfall), contrary to high intensity events of short duration (convective rainfall) that could trigger its buffering effect. However, in basins as large as the USRB, even

convective rain events will drive minor impacts on the runoff and flood patterns, given their localized occurrence (Niehoff et al., 2002), making reduced-till effects hardly detectable. Regarding the minor reductions on NO_3-N load, a study funded by the USDA (Daryanto et al., 2017) reported that conservation-tillage practices by themselves do not impact NO_3-N loss from cropland, unless implemented along with other practices as cover crops or reduced fertilizer rates. Their findings indicate that the combined effects of no-till over the NO_3-N concentration and flow patterns of runoff and leaching may not affect NO_3-N load. For example, an increase in the concentration of NO_3-N on the runoff water, along with a proportional reduction of the runoff flow, would not impact the total load of NO_3-N being transported out of the cropland. With this in mind, it is expected that reduced till will not present major changes in the flow patterns at a watershed scale, nor will modifying NO_3-N inputs or transport processes. In contrast, erosion processes, simulated at a cell grid scales by the MUSLE would be affected by the modification of the C-factor to account for the soil cover effect. This can cause reductions in sediment inputs to the transport model, causing a sediment load decrease of up to 30% at the three stations (Table 24).

The grassed riparian buffer constructed along the streams on grid cells originally devoted to row crop caused the reduction of the streamflow by up to 14% (Table 22). At Lake Decatur, this effect was mostly manifested during the wettest months (April to June) (Figure 36a). Annual evapotranspiration of pasture is expected to be greater than that of row crops since crop growth has a duration of about 4 months while pasture was assumed to be available all year round. This cyclical behavior was introduced to the model through the LAI, root depth, and Kc time series of each vegetation type. Additionally, the LAI of grass was 33% larger than that of corn during fully developed plant stage. Reductions of NO_3-N load ranged from 16% to 20% at the three stations (Table 23). The mass balance of NO_3-N revealed a reduction of OL inputs to the river of 56% with respect to the baseline. Although drainage flow was the most common way of NO_3-N transport from inland farming areas to the river, NO_3-N contributions from OL flow were found to be significant along the riparian zone, due to its proximity to waterways. Removing fertilizer application along the riparian zone had a strong impact in the amount of NO_3-N reaching the streams through OL run-off and tile drainage flow. According to USDA (2007), grassed buffers can reduce nitrogen runoff by 10% to 60%, while forested buffers could reduce it from 40% to 100%. In contrast, we observed reductions of sediment loads of 31%, 7% and 3% at Fisher,

Monticello and Decatur, (Table 24). Pasture continuously covering the soil, with no-till practices, caused the reduction of erosion along the riparian zone. This effect was conceptualized in the model through the land cover factor (C-factor) reduction (from 0.4 for row crops to 0.005 for pastures). The denser riparian buffer network in upland areas (Figure 21b) might have caused a greater reduction effect at Fisher. Moreover, the localized erosion processes evinced in the wetlands scenario might have led to the low sediment load reductions at Monticello and Decatur riparian zones, showing the riparian zone as a minor contributor to sediment sources for the Monticello and Decatur subwatersheds. Note that the model does not include settling processes in the OL transport, as a result of which the reductions in the river sediment load are merely the effect of the reduction in the sources, simulated through the MUSLE equation.

The crop rotation had very little impact on the streamflow; reductions of approximately 4% were found at the three stations (Table 22) probably due to the increase in the evapotranspiration rate caused by a higher LAI of soybean with respect to corn during the developed stage of the plant. Regarding the NO_3-N load, corn-soybean rotation had the highest reduction among all the WMPs (Table 23) (Figure 36b). This was the result of removing fertilizer inputs for the soybean production year in 40% of the USRB. In contrast, this scenario was the only one increasing the sediment load at the three stations by up to 22% (Table 24). Soybean cropland have been reported to have higher soil losses than corn under conventional and no-till methods, while presenting very low impact in water flow patterns (Alberts et al.1985). This effect was introduced to the model through the C-factor, which increased by 5% for corn-soybean rotation with respect to only corn scheme. This fact might be explained by the plant dynamics and the way canopy develops through the first plant growth stages. Canopy morphology and soil coverage are the reasons for the difference between corn and soybean C-factors. The amount of soil coverage around a corn plant would be significant when six leaves have entirely emerged (approximately 30 days after planting), while soybean would need 50% of its canopy to be completely developed to have a comparable soil coverage (Alberts, 1985).

The last WMP to be analyzed is the implementation of cover crops. This scenario reported the highest reduction for streamflow (up to 26%) and sediment load (up to 47%), and the second highest for NO_3-N load (up to 30%), for the three stations (Tables 22, 23 and 24). The reductions occurred mostly during the wettest months, March through May (Figure 36a, b, and c). The water mass balance evinced a reduction of approximately 20% for both drained and OL water

contributions to the river, which in turn decreased erosion rates by reducing the OL flow and depth. The high evapotranspiration rate was the main cause of this, brought about by the 25% of the USRB area in which cover crops were implemented. The LAI, root depth and Kc time series reflected the effect of having a crop production all year long. This effect also led to a NO_3-N plant uptake 23% higher than in the baseline, in accordance with the NO_3-N mass balance.

To gain better insight on the level of impact of the WMPs, the percentages of change in streamflow and loads at Decatur, were weighted with the percentage of modified area for each scenario (Table 25). Higher weighed impacts (in absolute value), would mean larger effects in the study variable with less modifications on the current state of the watershed. To this end, if two scenarios have the same percentage of pollutant load reduction, the one with the least percentage of modified area would be considered to be more efficient than the other one. Considering this approach, the most efficient WMPs in reducing NO_3-N and sediments were the buffer and the wetlands, respectively.

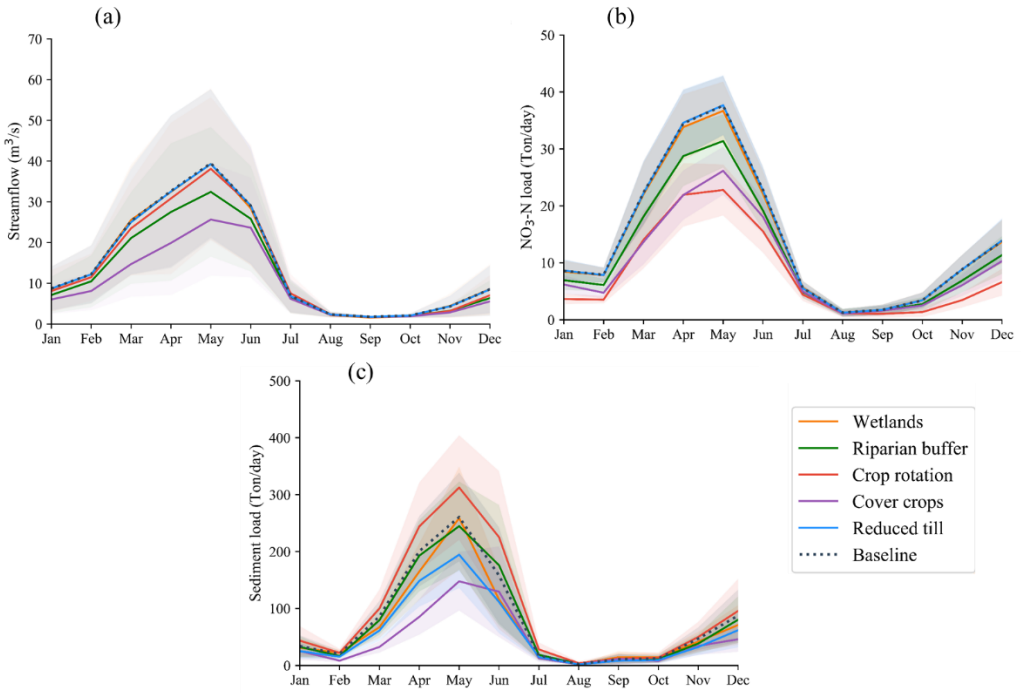

Figure 36. Impacts of WMPs over (a) streamflow, (b) NO_3-N load and (c) sediment load at Decatur. 68% confidence level bands.

Table 25. Absolute values of weighed impact of WMPs at Decatur under current climate (+ for increase, and – for decrease).

	Streamflow		NO_3-N		Sediment	
WMP	**+/- Impact**	**Weighed Impact**	**+/- Impact**	**Weighed Impact**	**+/- Impact**	**Weighed Impact**
Wetlands	+	0.05	-	0.48	-	3.71
Buffer	-	0.96	-	1.44	-	0.29
Crop rotation	-	0.12	-	1.02	+	0.57
Cover crops	-	1.00	-	1.21	-	1.69
Reduced till	-	0.01	+	0.00	-	1.08

3.3.4.3. Impact of WMPs and future climate

The combined effects of WMPs and climate were analyzed through scenarios 1 (baseline), 5, 6, 8, 9, 11, 12, 14, 15, 17, and 18 (Table 21). The relative difference in the average, maximum, and minimum streamflow, sediment, and NO_3-N load were computed at the three stations (Tables 22, 23 and 24), and monthly averages were plotted to visualize seasonal trends (Figure 37). As stated in the climate impact section, the monthly averages of the streamflow, sediment and NO_3-N loads for both future climates experienced a shift of the monthly peak from May to March/April (Figure 37). WMPs applied under the wettest climate (GFDL) showed diverse responses over the study variables. Wetlands and reduced till increased the average streamflow and NO_3-N load by up to 6% and 12%, respectively for the three stations (Tables 22 and 23). This effect is believed to be mainly produced by the climate as it was evinced that these two variables were barely affected by the WMP under historic climate (section 3.3.4.2.). In addition, the percent change for the scenario with current WMP under GFDL climate (Scenario 2) was very similar for both variables (approximately 5% for streamflow and up to 11% for NO_3-N), confirming that the observed effect was mainly caused by the climate conditions. For its part, the riparian buffer and the cover crops under GFDL climate decreased the average streamflow, although in a lower degree than under historic climate (Table 22). NO_3-N load reductions for the riparian buffer, crop rotation and cover crops were accentuated under the GFDL scenario (Table 23). By looking at the monthly average (Figure 37b) it can be observed that the months of November and December experience a load reduction not observed under the historic climate,

which coincides with months that also present drier conditions with respect to the historic scenario (Figure 28a).

Just as in the scenarios with historic climate, sediment load reduction under GFDL climate decreases as water flows downstream (Table 24). Reductions at Fisher for wetlands, riparian buffer, cover crops, and reduced till under GFDL ranges from 36% to 59%, while at Monticello are found to lie between 15% and 47%. At Decatur, wetlands and riparian buffer had no reduction effect on the sediment load with respect to the baseline, with increases of 10% and 15%, respectively, while cover crops and reduced till showed reductions of 35% and 9% with respect to the baseline. However, when comparing the relative changes in wetlands and riparian buffer, with the one for current WMP and GFDL (an increase of 48% of sediment load) (Table 24), the WMPs were found to have reduced sediment load more than the non-WMP scenarios.

As reported for the historic climate, crop rotation caused higher sediment loads than the baseline at the three stations (up to 43%, at Decatur). Although the GFDL climate was considered the wettest among the two future climates due to its higher average precipitation and lower average temperature, dry months (October to December) had a strong impact in the USRB response to the WMPs. Monthly sediment load peaks in March and April are found (Figure 37c) while there is virtually no load in the months of July through December. The highest reductions of NO_3-N and sediment loads under GFDL are achieved with crop rotation and cover crops, respectively.

The driest climate (ACCESS) reduced streamflow, NO_3-N, and sediment loads in the three stations by up to 78%, 90%, and 98%, respectively, with respect to the baseline. The highest reductions for the three variables were always obtained for the cover crops. However, the substantial reduction caused by all WMPs on the three studied variables when using ACCESS climate was that the reduction was mostly driven by the climate and not by the WMP. This can be confirmed when considering the reductions in the current WMP scenario with the same climate (61%, 75% and 91%, for streamflow, NO_3-N and sediments, respectively). In this case an imminent drought would be the main problem.

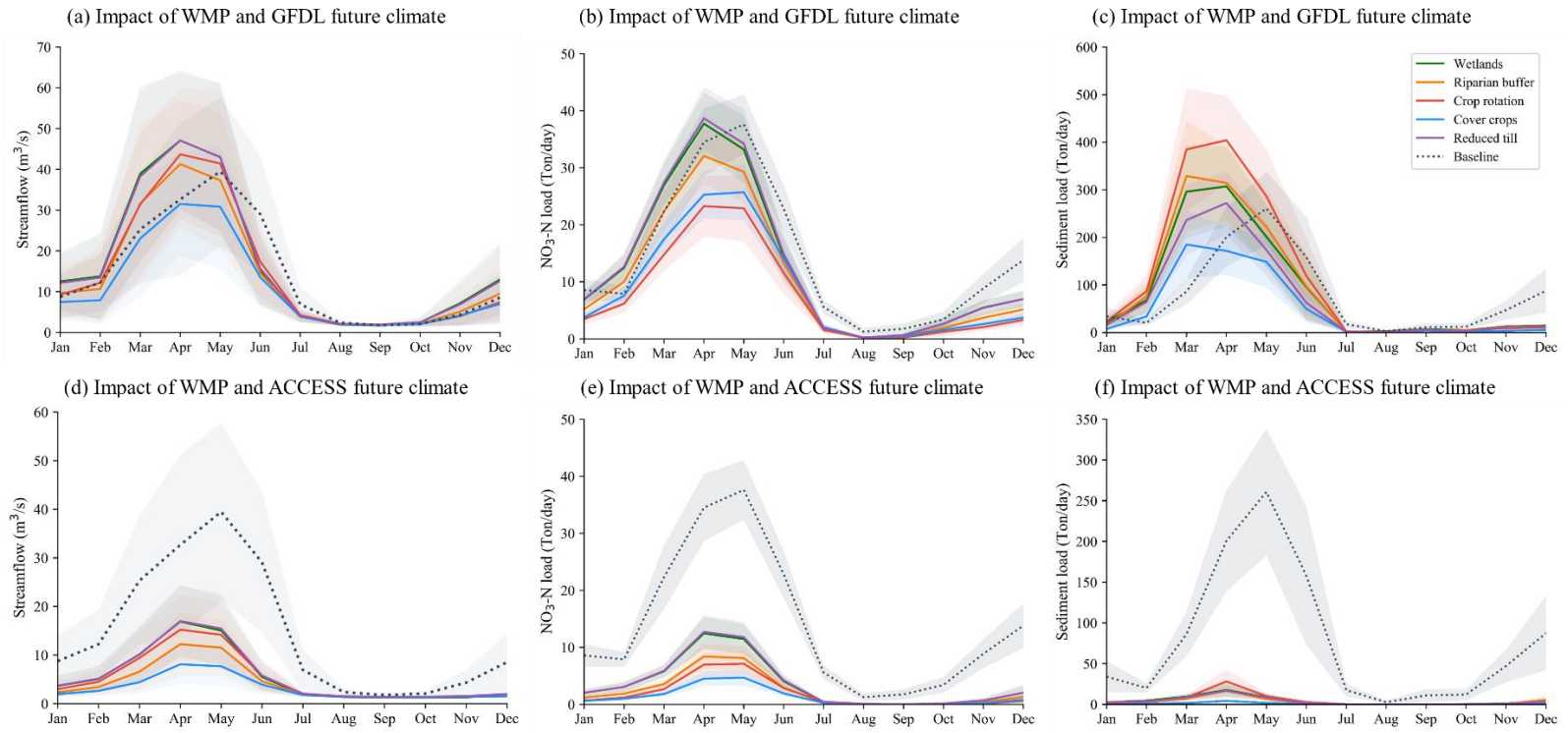

Figure 37. Impacts of WMPs and climate over (a) and (d) streamflow, (b) and (e) NO_3-N load, and (c) and (f) sediment load at Decatur, 68% confidence level bands.

3.4. CONCLUSION

The mechanistic distributed model MIKE-SHE was applied to study the effects of environmental stressors (anthropogenic and natural) over the non-point source pollution in the USRB, a highly managed watershed in Central Illinois. Cohesive sediment transport was simulated in the OL flow and rivers through the ADE, establishing an OL threshold concentration over which sediments would settle in OL flow allowing sedimentation and erosion at Lake Decatur. Sediment inputs were computed variedly in time and space using the MUSLE. Similarly, NO_3-N transport was simulated with the ADE as a dissolved species with transport and transformation in the OL, UZ, SZ (including drains) and river. Decay was included in all the compartments and adsorption in the UZ and SZ. NO_3-N inputs were created based on fertilizer application schedule and dosage. The hydrologic and transport model for NO_3-N and sediment were evaluated using daily streamflow and grab sample data at three gauging stations. Seasonal trends showed the highest monthly streamflow, NO_3-N and sediments loads from March to June for the baseline.

The conceptualization of erosion allowed the quantification of the effects of climate and WMPs over sediment load in the USRB. Erosion processes were found to be localized, occurring in the cells with high OL depth. This is the reason why a WMP implementation in a reduced area (3.4%, for wetlands) was found to have relatively high reductions compared to those other WMPs which required altering a larger portion of the watershed. In future studies, including the filtering effects of vegetation in the sediment transport model will allow a better understanding of the effects of riparian buffers and wetlands over the sediment transport dynamics. It is possible that the concentration threshold for the OL sediment transport had been overestimated due to the fact that no bank or bed erosion was considered, hence the inputs from the OL sediments were supplying the total sediment load.

Simulation of storm water wetlands allowed the study of their effects on the net OL transport of pollutants into streams. However, given the importance of drains in the conveyance of NO_3-N to the streams, it is recommended to use a conceptualization of the drainage system that allows it to be intercepted by wetlands without dewatering the latter or interfering with

drainage effectiveness. In this way, the effects of this WMP over the NO_3-N load would be better approached.

Generally, cover crops were found to constitute the WMP causing the highest reduction of streamflow and sediment with respect to the baseline for the three stations (up to 26.4% and 47.8%, respectively, and with minimums of 25% and 40.6%), while the crop rotation scenario had the highest NO_3-N load reduction (up to 40%), while increasing the sediment load. These performances were similarly observed for the future wettest climate, GFDL. According to the results of this study, the most suitable WMPs to apply in order to achieve the NO_3-N reduction goals proposed in the Illinois Nutrient Loss Strategy (IEPA, 2017) (15% by 2025 and 45% over time), assuming the future wettest climate condition, would be crop rotation or cover crops, at the risk of increasing stream sediment loads if the latter is chosen. However, based on the weighed impact of the area of implementation, the wetlands and the riparian buffer were found to be the most efficient for sediments and NO_3-N, respectively. The buffer effects over the NO_3-N load was caused by the removal of fertilizer application along the riparian zone (effected over 12% of the entire watershed) which reduced the amount of NO_3-N reaching streamways by OL and tile drainage flows. With this in mind, it is possible to affirm that non-structural WMPs caused the highest overall reductions of both pollutant loads, but structural WMPs were more efficient if the WMP effectiveness is normalized by modified area.

Under future dry conditions, climate was found to be the main factor controlling pollutants load in streams. A decrease of 78% in the average streamflow resulted in the reduction of OL and drainage flows and consequently in NO_3-N at the three gauging stations. In this case, non-point source pollution will not be the main problem anymore, but water shortage. The three WMP cases with the smallest streamflow reduction will be recommended to use for this climate condition (current WMP, reduced till or the wetlands -if located using the method proposed here in less than 4% of the total area). It is also possible under the ACCESS climate scenario, that the wetlands would serve as water and nutrient reservoirs for artificial irrigation.

The simulation of non-point source pollution at a watershed scale through a mechanistic-distributed model is a complex task, due to the interactions among the compartments, the physicochemical processes, and the conceptualization of non-point sources. Results from this study can be used as a tool for stakeholders and managerial agencies in the planning of short and long term recovery strategies for highly managed watershed. The gains and trade-offs of the

selected WMPs in terms of water quality, and the foresight of climate change impacts over their performances will allow a better and more efficient use of the resources.

3.5. LIMITATIONS AND INSIGHTS OF THE TRANSPORT MODEL

Simulation of transport processes through the numerical solution of the ADE is an important tool for engineers to predict the behavior of a pollutant in a water body (Abbott and Basco, 1989). The uni-directional movement of the pollutant by the mean flow (advection), and the spread of the pollutant in all directions caused by the concentration gradients and changes in velocity at a microscale (dispersion) can be applied to simulate the transport of any pollutant regardless of its nature. The main assumptions used to apply this equation are: complete mixing of the pollutant over the cross section and diffusion that follows Fick's law where the diffusive transport, included in the dispersion term, is proportional to the concentration gradients. These assumptions may not be realistic at a micro-scale since they do not provide a concentration profile across the cross-section. However, considering that the overall objective of this study was to simulate the changes in mean concentration of the pollutant at different locations, these assumptions resulted in reasonable representation of the transport processes.

In addition to the assumptions inherent to the ADE formulation, the fate of sediments and Nitrate-N was conceptualized through mathematical expressions that represented the effects of complex physical and biochemical processes occurring in natural environments. The sediment fate processes were simulated through the critical shear stress approach, which quantifies the sediments settling and eroding as a function of the near-bed turbulent velocities. The critical shear stresses for erosion and deposition are the thresholds to initiate the movement from/to the bed, which is assumed to be instantaneously triggered when the threshold is attained. On the other hand, nitrification process transforming nitrogen fertilizers to Nitrate, depends on the presence of Nitrobacter and Nitrozoma bacteria, as well as on the temperature and moisture conditions of the soil. This study simulated the transport of Nitrate-N, assuming that the Nitrogen applied through fertilizers was already been transformed to its most soluble form (Nitrate-N), process that usually takes a week from the fertilizer application day. On the other hand, denitrification was included in the model through an exponential decay equation but in nature this process depends on the microbiota population and requires anaerobic conditions to be

effected. Mathematical abstractions have limitations to reproduce the complexity that dominate processes in nature.

The conceptualization of physical processes into mathematical expressions comes with the need of finding the parameters that best describe the behavior of the system. Usually, observed datasets for two periods of time are compared with the simulated variables to verify the validity of these parameters. However, it is common that multiple solutions or set of parameters can mimic the behavior of the observed data (i.e., the condition of equifinality) most especially since the inclusion of fate processes in the ADE increased the number of parameters and hence, the degrees of freedom in the calibration process. Equifinality made it challenging to determine the true behavior of the system since it is possible that parameters compensate for errors in the observations or boundary conditions of the model (Beven, 2001). Long periods of continuous water quality data measurements in strategic locations across the watershed are needed to reduce the equifinality of transport models.

The numerical solution of the ADE through finite difference is affected by numerical stability and numerical dispersion. The scheme used in the numerical method imposes a spatial and temporal discretization that introduces a mismatch between the numerical and the exact solution. The numerical solution of the ADE applied by the Mike SHE model for the UZ, SZ and OL is based on the QUICKEST (Quadratic Upstream Interpolation for Convective Kinematics with Estimated Streaming Terms) method (Leonard, 1979; Vested, 1992). This is a fully explicit scheme, with an upstream interpolation method for the advection term and central differencing for the dispersion term and is a third order accurate. It is based on the QUICK (Quadratic Upstream Interpolation for Convective Kinematics) scheme, which uses a control volume formulation for the advection term with the concentration at the wall values computed as quadratic interpolation using the two adjacent nodal values and the next upstream node (E. 26) (Figure 38). Because of this scheme the accuracy is greater than a central differencing. A quadratic interpolation may be interpreted as a corrected linear interpolation by adding a term related to the upstream curvature:

$$c_{i+1/2} = \frac{1}{2}(c_i + c_{i+1}) - \frac{1}{8}(c_{i-1} + c_{i+1} - 2c_i) \qquad \text{Eq. 26}$$

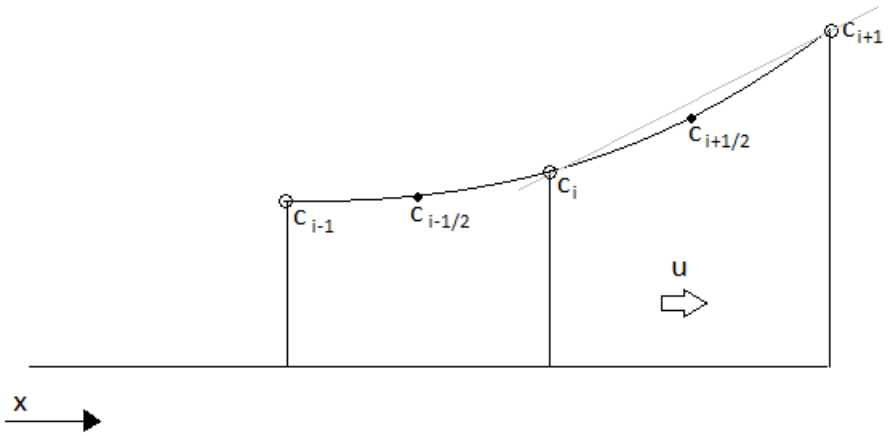

Figure 38. Quadratic upstream interpolation (Adapted from Leonard, 1979).

The gradient can be identical as for the central difference formula and applied in the dispersion term:

$$\left(\frac{\partial c}{\partial x}\right)_i = \frac{c_{i+1/2} - c_{i-1/2}}{\Delta x} \qquad \text{Eq. 27}$$

With this, the one-dimensional conservative ADE with uniform velocity and dispersion coefficient:

$$\frac{\partial c}{\partial t} = -v\frac{\partial c}{\partial x} + D\frac{\partial^2 c}{\partial x^2} \qquad \text{Eq. 28}$$

will be transformed to the QUICK one-dimensional numerical equation, using an explicit forward time-differencing (n), as follows:

$$\frac{c_i^{n+1} - c_i^n}{\Delta t} = -v\frac{c_{i+1/2}^n - c_{i-1/2}^n}{\Delta x} + \frac{D}{\Delta x}\left[\left(\frac{\partial c}{\partial x}\right)_{i+1/2}^n - \left(\frac{\partial c}{\partial x}\right)_{i-1/2}^n\right] \qquad \text{Eq. 29}$$

$$\frac{c_i^{n+1} - c_i^n}{\Delta t} = -v\frac{c_{i+1/2}^n - c_{i-1/2}^n}{\Delta x} + \frac{D}{\Delta x}\left(\frac{c_{i+1}^n - c_i^n}{\Delta x} - \frac{c_i^n - c_{i-1}^n}{\Delta x}\right) \qquad \text{Eq. 30}$$

$$\frac{c_i^{n+1} - c_i^n}{\Delta t} = -v\frac{c_{i+1/2}^n - c_{i-1/2}^n}{\Delta x} + \frac{D}{\Delta x^2}(c_{i+1}^n + c_{i-1}^n - 2c_i^n) \qquad \text{Eq. 31}$$

$$c_i^{n+1} = -\frac{v\Delta t}{\Delta x}c_{i+\frac{1}{2}}^n - c_{i-\frac{1}{2}}^n + \frac{D\Delta t}{\Delta x^2}(c_{i+1}^n + c_{i-1}^n - 2c_i^n) + c_i^n \qquad \text{Eq. 32}$$

Applying the quadratic interpolation of Eq. 26 for the locations *i-1/2* and *i+1/2*:

$$c_i^{n+1} = -\frac{v\Delta t}{\Delta x}\left[\left(\frac{1}{2}(c_i^n + c_{i+1}^n) - \frac{1}{8}(c_{i-1}^n + c_{i+1}^n - 2c_i^n)\right) - \left(\frac{1}{2}(c_{i-1}^n + c_i^n) - \frac{1}{8}(c_{i-2}^n + c_i^n - 2c_{i-1}^n)\right)\right] + \frac{D\Delta t}{\Delta x^2}(c_{i+1}^n + c_{i-1}^n - 2c_i^n) + c_i^n \quad \text{Eq. 33}$$

$$c_i^{n+1} = c_i^n - \frac{v\Delta t}{\Delta x}\left(\frac{1}{8}c_{i-2}^n - \frac{7}{8}c_{i-1}^n + \frac{3}{8}c_i^n + \frac{3}{8}c_{i+1}^n\right) + \frac{D\Delta t}{\Delta x^2}(c_{i+1}^n + c_{i-1}^n - 2c_i^n) \quad \text{Eq. 34}$$

where $\frac{v\Delta t}{\Delta x}$ is the Courant (*T*) number and $\frac{D\Delta t}{\Delta x^2}$ is the diffusion parameter (*F*). The QUICKEST method modifies the QUICK scheme for primarily advective fluxes with non-uniform conditions. It uses the following formula to interpolate the concentration values at the walls (or edges for a 1-dimensional case):

$$c_{i+\frac{1}{2}} = \frac{1}{2}\left[(c_i + c_{i+1}) - T_{i+1/2}(c_{i+1} - c_i)\right] \quad \text{Eq. 35}$$

$$c_{i-\frac{1}{2}} = \frac{1}{2}\left[(c_{i-1} + c_i) - T_{i-1/2}(c_i - c_{i-1})\right] \quad \text{Eq. 36}$$

where $T_{i+1/2}$ and $T_{i-1/2}$ are the Courant numbers at the left and the right side of the wall. Assuming uniform velocity, the advective transport, $\frac{\partial c}{\partial t} = v\frac{\partial c}{\partial x}$, will then be:

$$\frac{c_i^{n+1} - c_i^n}{\Delta t} = -v\frac{c_{i+\frac{1}{2}} - c_{i-\frac{1}{2}}}{\Delta x} \quad \text{Eq. 37}$$

$$\frac{c_i^{n+1} - c_i^n}{\Delta t} = -v\frac{\frac{1}{2}[(c_i^n + c_{i+1}^n) - T(c_{i+1}^n - c_i^n)] - \frac{1}{2}[(c_{i-1}^n + c_i^n) - T(c_i^n - c_{i-1}^n)]}{\Delta x} \quad \text{Eq. 38}$$

$$c_i^{n+1} = c_i^n - T\left\{\frac{1}{2}[(c_i^n + c_{i+1}^n) - T(c_{i+1}^n - c_i^n)] - \frac{1}{2}[(c_{i-1}^n + c_i^n) - T(c_i^n - c_{i-1}^n)]\right\} \quad \text{Eq. 39}$$

$$c_i^{n+1} = c_i^n - \frac{T}{2}c_i^n - \frac{T}{2}c_{i+1}^n + \frac{T^2}{2}c_{i+1}^n - \frac{T^2}{2}c_i^n + \frac{T}{2}c_{i-1}^n + \frac{T}{2}c_i^n - \frac{T^2}{2}c_i^n + \frac{T^2}{2}c_{i-1}^n \quad \text{Eq. 40}$$

$$c_i^{n+1} = c_i^n - \frac{T}{2}(c_{i+1}^n - c_{i-1}^n) + \frac{T^2}{2}(c_{i+1}^n + c_{i-1}^n - 2c_i^n) \quad \text{Eq. 41}$$

For the full advections-dispersion case, the Eq. 41 becomes:

$$c_i^{n+1} = c_i^n - \frac{T}{2}(c_{i+1}^n - c_{i-1}^n) + \left[\frac{T^2}{2} + F\right](c_{i+1}^n + c_{i-1}^n - 2c_i^n) \quad \text{Eq. 42}$$

The stability analysis of this method is evaluated through the Von Neumann method (Leonard, 1979), which applies the Fourier decomposition of the numerical error. A stable scheme maintains the error constant or in decay as the algorithm moves forward. For this, it is

required that the ratio of the error of the current iteration to the error in the previous iteration is less than 1. For the QUICKEST method to be in the stable region it is necessary and sufficient that (Figure 39):

$$0 \leq F \leq \frac{(1-T^2)}{2} \qquad \text{Eq. 43}$$

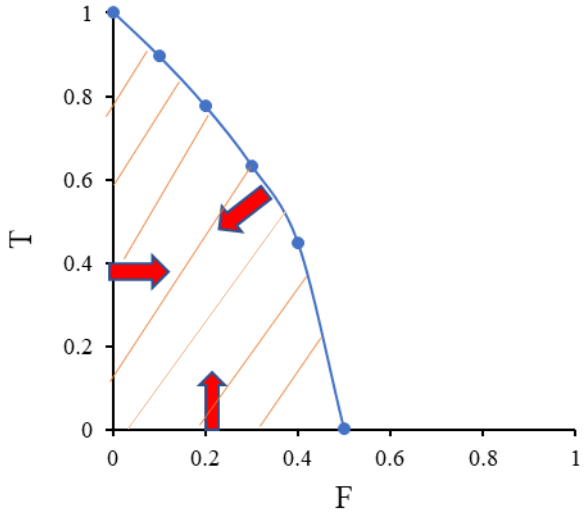

Figure 39. Stability region for the QUICKEST method. Diffusion parameter (*F*) Vs. Courant number (*T*) (Adapted from Leonard, 1979)

Both the Courant number (*T*) and the Diffusion parameter (*F*) depends on the Δt, which is controlled at each iteration to keep the numerical solution in the stability zone. The scheme QUICKEST has been found to circumvent the numerical dispersion, observed in the backward difference classical approach, through the upstream interpolation of the concentration at the walls (or edges for 1-Dimensional case) of a control volume, which gave a third order accuracy to the scheme (Vested, 1992).

4. OVERALL CONCLUSIONS

The study of riparian erosion on Fort Cobb watershed presented in Chapter 1 concluded that land use and soil type were the most influential environmental variables to predict the presence of erosion, followed by the SPI and discharge. Forest was found to be the land use type prone to "very high" erosion based on the difference between two Lidar measurements. This finding was mainly due to the large difference between Lidar scans conducted at different times where one scanned the canopy and the other the ground. The soils from hydrologic groups B and C, with high silt contents, had the highest suitability index to erosion. It was also found that erosion-producing differences in elevation smaller than 0.5 m were randomly located across the Fort Cobb riparian zone. With respect to climate change, no impacts were observed between historic and future scenarios, probably due to the fact that erosion was mainly explained by the soils and land use environmental variables, not modified for the future simulations. The need to provide static maps to the MAXENT model reduced the amount of information provided by dynamic variables (streamflow, OL, lateral flow) to the model.

Aside from climate change, impacts of proposed environmental management schemes over riparian erosion can also be evaluated by applying the methodology proposed in Chapter 1. Scenario-based environmental data, such as projected urbanization or conservation practices, can be used in the hydrologic and habitat models to evaluate the changes in erosion vulnerability to "what-if" scenarios. The framework developed in this study is flexible enough that different types of hydrologic models can be used, depending on available data and suitability to the study area. Although LiDAR elevation datasets were used to identify locations for erosion presence in this study, field identified locations through reconnaissance survey can also be used since the methods do not require actual erosion measurements. If available, unmanned aerial vehicles (UAV), can be used to identify locations where changes in riparian profiles occur during extreme storm events.

Effects of WMPs and climate on the water resources of the USRB were studied in Chapter 2. Wetlands, located in 50% of the total area to simulate the state of the watershed before human settlement, and forested riparian buffer, resulted in a reduction of the average streamflow, regardless the climate scenario. For its part, crop rotation behaved differently, in accordance with the location and the climate case under which it was simulated but did not cause major changes

in the total water balance. Future climate scenarios applied in Chapter 2 (CM3 and ESM2M) were shown to increase the water table depth, regardless of the WMP. The removal of the tile drainage network in the USRB was found to reduce the water table depth by 56%. The lowering of the phreatic level allowed cropland production but also made high magnitude daily streamflow events more frequent, providing a faster flow pathway for contaminants and compromising water quality in Lake Decatur.

Agricultural practices that are predominant in the USRB make this watershed prone to fertilizer leakage and fast transport through the drainage network, as well as soil erosion and sediment transport to main stems through OL runoff. Non-point source pollution in the USRB was studied in Chapter 3. Generally, cover crop was found to be the WMP causing the highest reduction in streamflow and sediment load, while the crop rotation scenario had the highest NO_3-N load reduction, albeit while increasing the sediment load. These performances were similarly observed for the future wettest climate. The future dry climate scenario resulted in a water shortage, reducing the transport of both pollutants regardless of the WMP. Non-structural WMPs were predicted to cause the highest overall reductions of both pollutant loads, while structural WMPs were found to have a greater area-efficient performance.

5. REFERENCES

Abbasi, F.,Simunek, M., van Genuchten, M.Th., Feyen, J., Adamsen, F., Hunsaker, D., Strelkoff, T. and Shouse, P. 2003 Overland water flow and solute transport: Mode development and field-data analysis. Journal of irrigation and drainage engineering, 129: 71-81.

Abbaspour, K., Yang, J., Maximov, I., Siber, R., Bogner, K., Mieleitner, J., Zobrist, J. and Srinivasam, R. 2007. Modelling hydrology and water quality in the pre-alpin/alpine Thur watershed using SWAT. Journal of Hydrology, 333: 413-430.

Abbott, M.B. and Basco, D.R., 1989, Computational fluid dynamics: an introduction for engineers. Longman Scientific & Technical, Harlow.

Adams, E. and Gelhar, L. 1992. Field study of dispersion in a heterogeneous aquifer. Water resources research, 28: 3293-2207.

Aksoy, H. and Kavvas. 2005. A review of hillslope and watershed scale erosion and sediment transport models. *Catena*. 64: 247-271.

Alberts, E., Wendt, R. and Burwell, R. 1985. Division S-6 - soil and water management and conservation. Corn and soybean cropping effects on soil losses and C factor. Soil Science Society of America, 49: 721-728

Anders, A.M., Bettis, E.A. III, Grimley, D.A., Stumpf, A.J. and Kumar P. 2018. Impacts of Quaternary history on critical zone structure and processes: Examples and a conceptual model from the Intensively Managed Landscapes Critical Zone Observatory. Frontiers in Earth Science, 6:24. Retrieved from https://doi.org/10.3389/feart.2018.00024.

Arabi, M., Govindaraju, R., Hantush, M. 2007. A probability approach for analysis of uncertainty in the evaluation of watershed management practices. Journal of Hydrology, 333. 459-471.

ASABE. 2017. Guidelines for calibrating, validating, and evaluating hydrologic and water quality (H/WQ) models. Retrieved from: https://elibrary.asabe.org/abstract.asp?aid=47804

Atkinson, L.A., Ross, M. and Stumpf, A.J. 2014. Three-dimensional hydrofacies assemblage in ice-contact/proximal sediments forming a heterogeneous ‘hybrid’ hydrostratigraphic unit in central Illinois, USA. Hydrogeology Journal, 22, 1605-1624.

Becker, M., 1998. Steady-state Simulation of Ground-water Flow in the Rush Spring Aquifer, Western Oklahoma. Water-resources Investigations Report 98-4082. USGS, Denver, CO.

Bekele, E., Keefer, L., Chandrasekaran, S. 2014. Decision support model for generating optimal alternative scenarios of watershed best management practices. Illinois State Water Survey, Contract Report 2014-02. Retrieved from http://hdl.handle.net/2142/50045

Bentrup, G. 1998. The practical streambank bioengineering guide. USDA. Natural Resources Conservation Service. Retrieved from: http://www.nrcs.usda.gov/Internet/FSE_PLANTMATERIALS/publications/idpmcpu116.pdf

Bermhardt, E. and Palmer, M. 2007. Restoring streams in an urbanizing world. Freshwater Biology. 52: 738-751. doi:10.1111/j.1365-2427.2006.01718.x

Beven, K. 2001. Calibration, validation and equifinality in hydrological modelling: A continuing discussion… Model Validation: Perspectives in Hydrological Science. John Wiley & Sons, Ltd.

Bhaduri, B., Harbor, J., Engel, B. and Grove, M. 2000. Assessing watershed-scale, long-term hydrologic impacts of land-use change using a GIS-NPS model. Environmental Management, 26, 643-658.

Blair, N.E., Leithold, E.L., Papanicolaou, A.N.T, Wilson, C.G., Keefer, L., Kirton, E., Vinson, D., Schnoebelen, D., Rhoads, B., Yu, M. and Lewis, Q. 2018. The C-biogeochemistry of a Midwestern USA agricultural impoundment in context: Lake Decatur in the intensively managed landscape critical zone observatory. Biogeochemistry. Retrieved from http://dx.doi.org/10.1007/s10533-018-0439-9

Blick, S., Kelly, F. and Skupien, J. 2004. New Jersey stormwater best management practices manual. Department of Environmental Protection. State of New Jersey. Retrieved from: http://www.njstormwater.org/bmp_manual/NJ_SWBMP_9.2%20print.pdf

Borsje, B., de Vries, M., Hulscher, S. and Boer, G. 2008. Modeling large-scale cohesive sediment transport affected by small-scale biological activity. Estuarine, Coastal and Shelf Science, 78: 468-480.

Botero-Acosta, A., Chu, M.L, Stumpf, A.J. 2018. Impacts of environmental stressors on the water resources of intensively managed hydrologic systems. Hydrological Processes. 32:2947-2962

Botero-Acosta, A., Chu, M.L., Guzman, J.A., Starks, P.J., Moriasi, D.N. 2017. Riparian erosion vulnerability model based on environmental features. Journal of Environmental Management, 203: 592-602.

Brantley, S.L., Goldhaber, M.B. and Ragnarsdottlr, K.V. 2007. Crossing disciplines and scales to understand the Critical Zone. Elements, 3, 307-314.

Bridges, K., Wilson, S., Perry, R. 2015. Center Pivot Irrigation in Illinois. Illinois State Water Survey, ISWS Map Series 2014-03. Retrieved from http://www.sws.uiuc.edu/iswsdocs/maps/ISWSMS2014-03.pdf.

Calsamiglia, A., García-Comendador, J., Fortesa, J., López-Tarazón, J.A., Crema, M., Cavalli, A., Calvo-Cases, A. and Estrany, J. 2018. Effects of agricultural drainage systems on sediment connectivity in a small Mediterranean lowland catchment. Geomorphology, 318, 162-171.

Carpenter, S.R., Caraco, N.F., Correll, D.L., Howarth, R.W., Sharpley, A.N. and Smith, V. 1998. Nonpoint pollution of surface waters with phosphorus and nitrogen. Ecological Applications, 8(3): 559-568.

Chahor, Y., Casalí, J., Giménez, R., Bingner, R.L., Campo, M.A., Goñi, M. 2014. Evaluation of the AnnAGNPS model for predicting runoff and sediment yield in a small Mediterranean agricultural watershed in Navarre (Spain). Agricultural Water Management, 134:24-37.

Chatterjee, S. and Krishna, A.P. 2014. Geospatial assessment of soil erosion vulnerability at a watershed level in some sections of the Upper Subarnarekha river basin, Jharkhand, India. Enviro. Earth Sci. 71: 357-374.

Chen, Y.D., Li., J., Zhang, Q. and Gu, X. 2018. Projected changes in seasonal temperature extremes across China from 2017 to 2100 based on statistical downscaling. Global and Planetary Change, Article in press.

Cheng, N. 1997. Simplified settling velocity formula for sediment particle. J. Hydraul. Eng., 2: 149 – 152.

Chinnasamy, S., Wang, X., Arnold, J., Williams, J., White, M., Kannan, N. and Diluzo, M. 2013. Documentation on delivery ratio used for CEAP cropland modeling for various river basins in the United States. USDA Agricultural Research Service Grassland Soil and Water

Research Laboratory and Texas AgriLife Research. Retrieved from: https://www.nrcs.usda.gov/Internet/FSE_DOCUMENTS/stelprdb1045451.pdf.

Chorover, J., Troch, P.A., Rasmussen, C., Brooks, P.D., Pelletier, J.D., Breshears, D.D., Huxman, T.E., Kurc, S.A., Lohse, K.A, McIntosh, J.C., Meixner, T., Schaap, M.G., Litvak, M.E., Perdrial, J., Harpold, A. and Durcik, M. 2011. How water, Carbon, and Energy drive critical zone evolution: The Jmez-Santa Catalina Critical Zone Observatory. Vadose Zone Journal, 10, 884-899.

Chow, V.T., 1959, Open-channel hydraulics: New York, McGraw-Hill.

Christensen, M., Graham, M., Vinebrooke, R., Findlay, D., Paterson, M., Turner, M. 2006. Multiple anthropogenic stressors cause ecological surprises in boreal lakes. Global Change Biology, 12, 2316-2322.

Chu-Agor, M., G.A. Fox, and G.V. Wilson. 2009. Empirical sediment transport function predicting seepage erosion undercutting for cohesive bank failure prediction. J. Hydrol. 377(2009), 155-164.

Chu-Agor, M., G.A. Fox, R. Cancienne, and G.V. Wilson. 2008a. Seepage caused tension failures and erosion undercutting of hillslopes. J. Hydrol. 359(2008), 247-259.

Chu-Agor, M., G.V. Wilson, and G.A. Fox. 2008b. Numerical modeling of bank instability by seepage erosion undercutting of layered streambanks. J. Hydrol. Eng. 13(12), 1133-1145

City of Decatur. 2017. Lake Decatur Basin 1 through 4 dredging project fact sheet. Retrieved from: https://www.decaturil.gov/wp-content/uploads/2016/11/Lake-Decatur-Dredging-Fact-Sheet.pdf

Conoscenti, C., Di Maggio, C. and Rotigliano, E. 2008. GIS analysis to assess landslide susceptibility in a fluvial basin of NW Sicily (Italy). Geomorphology. 94: 325 – 339.

Correll, D. 2005. Principles of planning and establishment of buffer zones. Ecological Engineering. 24: 433-439. doi:10.1016/j.ecoleng.2005.01.007.

Coupled Model Intercomparision Project (CMIP5). 2017. Downscaled CMIP5 Climate and Hydrology Projections. Retrieved from: http://gdo-dcp.ucllnl.org/downscaled_cmip_projections/#Welcome.

Coupled Model Intercomparison Project (CMIP5). 2016. Downscaled CMIP5 Climate and Hydrology Projections. Retrieved from: http://gdo-dcp.ucllnl.org/downscaled_cmip_projections/.

Curt, C., AchutaRao, K., Cubasch, U., Jones, P., Lambert, S., Mann, M., Phillips, T. and Taylor, K. 2003. An overview of results from the Coupled Model Intercomparision Project. Global and Planetary Change, 37: 103-133.

Daly, E.R., Miller, R.B., Fox, G.A. 2015. Modeling streambank erosion and failure along protected and unprotected composite streambanks. Advances in Water Resources: 81: 114-127.

Daryanto, S., Wang, L. and Jacinthe, P. 2017. Impacts of no-tillage management on nitrate loss from corn, soybean and wheat cultivation: A meta-analysis. Scientific Reports, 7:1-9.

De Bruin, H.A.R. and Lablans, W.N. 1998. Reference crop evapotranspiration determined with a modified Makkink equation. Hydrol. Process, 12, 1053-1062.

Desmet, P.J.J. and Govers, G. 1996. A GIS procedure for automatically calculating the USLE LS factor on topographically complex landscape units. Journal of Soil and Water Conservation, 51(5) 427-433.

DHI. 2009. MIKE SHE user manual, Volume 1: User guide.

DHI. 2017a. MIKE SHE user manual, Volume 2: Reference Manual.

DHI. 2017b. MIKE 11 user guide. A modelling system for rivers and channels.

Dong, T., Dong, W., Guo, Y., Chou, J., Yang, S., Tian, D., Yan, D. 2018. Future temperature changes over the critical Belt and Roal region based on CMIP5 models. Advances in climate change research, 9: 57-65.

Drake, K. and Hogan, M. 2013. Watershed Management Guidebook. Integrated Environmental Restoration. Retrieved from: http://www.ierstahoe.com/pdf/research/watershed_management_guidebook.pdf

Eckhardt, K. and Ulbrich, U. 2003. Potential impacts of climate change on groundwater recharge and streamflow in a central European low mountain range. Journal of Hydrology, 284, 244-252.

Elith, J., Phillips, J.S., Hastie, T., Dudik, M., Chee, Y.E. and Yates, C.J. 2011. A statistical explanation of MaxEnt for ecologist. Diversity and Distributions. 17: 43-57.

Environmental Protection Agency (EPA). 2017a. Discharge Monitoring Report (DMR) Pollutant Loading Tool. Retrieved from: https://cfpub.epa.gov/dmr/#navigate

Environmental Protection Agency (EPA). 2017b. Watershed ecological risk assessment. Retrieved from: https://cfpub.epa.gov/watertrain/moduleFrame.cfm?parent_object_id=32

Evans, B.M., Lehning, D.W., Corradini, K.J., Petersen, G.W., Nizeyimana, E., Hamlett, J.M., Robillard, P.D. and Day, R.L. 2002, A comprehensive GIS-based modeling approach for predicting nutrient loads in watershed. J. od Spatial Hydrology, 2.

Fischer, R.A. and Fischenich, J.C. 2000. Design recommendations for riparian corridors and vegetated buffer strips. U.S. Army Engineer Research and Development Center, Environmental Laboratory. Vicksburg, MS.

Food and Agriculture Organization of the United Nations (FAO). 2016. CropWat. Retrieved from: http://www.fao.org/land-water/databases-and-software/cropwat/en/

Forrer, I., Kasteel, R., Flury, M. and Fluhler. 1999. Longitudinal and lateral dispersion in an unsaturated field soil. Water Resources Research, 35, NO 10 :3049-3060.

Fox, G.A., Sheshukov, A., Cruse, R., Kolar, R.L., Guertault, L. 2016. Reservoir Sedimentation and Upstream Sediment Sources: Perspectives and Future Research Needs on Streambank and Gully Erosion. Environmental Management. DOI 10.1007/s00267-016-0671-9

Fox, J.F. and Papanicolaou. 2007. The use of carbon and nitrogen isotopes to study watershed erosion processes. Journal of the American Water Resources Association. 43.4: 1047-1064.

Fox, J.F. and Papanicolaou. 2008. An un-mixing model to study watershed erosion processes. Advances in Water Resources. 31: 96-108.

Garbrecht, J. and Starks, P. 2009. Watershed sediment yield reduction through soil conservation in a West-Central Oklahoma watershed. Ecohydrology. 2: 313-320.

Garbrecht, J.D. and Schneider, J.M. 2008. Case of Study of Multiyear Precipitation Variations and the Hydrology of Fort Cobb Reservoir. Journal of Hydrologic Engineering. 13: 64-70.

Garbrecht, J.D., Zhang, X.C. and Steiner, J.L. 2014. Climate change and observed climat trends in the Fort Cobb Experimental Watershed. Journal of Environmental Quality. 43: 1319-1327.

Garcia-Navarro, P., Playan, E., ASCE, and Zapata, N.2000. Solute transport modeling in overland flow applied to fertigation. Journal of irrigation and drainage engineering, 126: 33-40.

Gentile, J.H., Harwell, M.A., Cropper Jr, W., Harwell, C.C., DeAngelis, D., Davis, S., Ogden, J.C. and Lirman, D. 2001. Ecological conceptual models: a framework case study on ecosystem management for South Florida sustainability. The Science of the Total Environment, 274, 231-253.

Geophysical Fluid Dynamics Laboratory (GFDL) from the National Oceanic and Atmospheric Administration (NOAA). 2017. Retrieved from: https://www.gfdl.noaa.gov/cmip/.

Getahun, E., and Keefer, L. 2016. Integrated modeling system for evaluating water quality benefits of agricultural watershed management practices: Case study the Midwest. Sustainability of Water Quality and Ecology, 8, 14-29.

Giere, R. 2004. How models are used to represent reality. Philosophy of Science, 71: 742-752.

Giorgetta, M., Jungclaus, J., Reick, C., Legutke, S., Bader, J., Bottinger, M., Brovkin, V., Crueger, T. Esch, M., Fieg, K., Glushak, K., Gayler, V., Haak, H., Hollweg, H., Ilyina, T., Kinne, S., Kornblueh, L., Matei, D., Mauritsen, T., Mikolajewicz, U., Mueller, W., Notz, D., Pithan, F., Raddatz, T., Rast, S., Redler, R., Roeckner, E., Schmidt, H., Schnur, R., Segschneider, J., Six, K., Stockhause, M., Timmreck,C., Wegner, J., Widmann, H., Wieners, K., Claussen, M., Marotzke, J., and Stevens, B. 2013. Climate and carbon cycle changes from 1850 to 2100 in MPI-ESM simualtions for the Coupled Model Intercomparison Project phase 5. Journal of Advances in Modelling Earth Systems. 5:572-597.

Golden, H., Sander, H., Lane, C., Zhao, C., Price, K., D'Amico, E. and Christensen, J. 2016. Relative effects of geographically isolated wetlands on streamflow: a watershed-scale analysis. Ecohydrology, 9, 21-38.

Grantham, T.E., Merenlender, A.M. and Resh, V.H. 2010. Climatic influences and anthropogenic stressors: an integrated framework for streamflow management in Mediterranean-climate California, U.S.A. Freshwater Biology, 55, 188-204.

Groh, T.A., Gentry, L.E. and David, M.B. 2015. Nitrogen removal and greenhouse gas emissions from constructed wetlands receiving tile drainage water. Journal of Environmental Quality, 44, 1001-1010.

Guzman, J.A., M.L. Chu, P.J. Starks, D.N. Moriasi, J.L. Steiner, C.A. Fiebrich, and A.G. McCombs. 2014. Upper Washita River experimental watersheds: Data screening procedure for data quality assurance. J. Environ. Qual. 43(4): 1250-1261. doi:10.2134/jeq2013.08.0325

Guzman, J.A., Moriasi, D.N., Gowda, P.H., Steiner, J.L., Starks, P.J., Arnold, J.G. 2015. A model integration framework for linking SWAT and MODFLOW. Environmental modeling and software. 73: 103-116.

Haag, I., Luce, A. and Gerlinger K. 2006. Effects of conservation tillage on storm: a model-based assessment for a mesoscale watershed in Germany. Predictions in ungauged basins: Promise and progress. Retrieved from: https://iahs.info/uploads/dms/13446.43-342-350-S7-38-Haag-Gerlinger-Luce.pdf

Hamdi, W., Gamaoun, F., Pelster, D. and Seffen, M. 2013. Nitrate sorption in and agricultural soil profile. Applied and Environmental Soil Science, 2013, 1-7.

Hawes, E. and Smith M. 2005. Riparian buffer zones: Functions and recommended widths. Eightmile River Wild and Scenic Study Committee. Yale School of Forestry and Environmental Studies.

Henderson, J.E. 1986. Environmental designs for streambank protection projects. Water Resources Bulletin. 22: 549-558.

Hensel, B. and Miller, M. 1991. Effects of wetlands creation on groundwater flow. Journal of Hydrology, 126, 293-314.

Heumann, B.W., Walsh, S.J., Verdery, A.M., McDaniel, P.M. and Rindfuss, R.R. 2013. Land suitability modeling using a geographic socio-environmental niche-based approach: A case study from Northeastern Thailand. Annals of the Association of America Geographers. 103: 764-784.

Huffer, R. 2016. Sediment traps in Lake Decatur reduce need for dredging. Retrieved from: http://www.nowdecatur.com/2016/10/06/sediment-traps-in-lake-decatur-reduce-need-for-dredging/

Hundecha, Y. and Bárdossy, A. 2004. Modeling of the effect of land use changes on the runoff generation of a river basin through parameter regionalization of a watershed model. Journal of Hydrology, 292, 281-295.

Illinois Environmental Protection Agency (IEPA). 2007. Sangamon River/Lake Decatur watershed TMDL report. Springfield, IL.

Illinois Environmental Protection Agency (IEPA). 2017. Illinois Nutrient Loss Reduction Strategy. Retrieved from: http://www.epa.illinois.gov/Assets/iepa/water-quality/watershed-management/nlrs/nlrs-final-revised-083115.pdf

Illinois State Water Survey (ISWS). 1987. Sedimentation and hydrologic processes in Lake Decatur and its watershed. Champaign, IL.

Illinois State Water Survey (ISWS). 1994. Watershed monitoring and land use evaluation for the Lake Decatur Watershed. Retrieved from: http://www.isws.uiuc.edu/pubdoc/MP/ISWSMP-159.pdf.

Illinois State Water Survey (ISWS). 1996. Watershed Monitoring and Land Use Evaluation for the Lake Decatur Watershed. Retrieved from: http://www.isws.illinois.edu/pubdoc/MP/ISWSMP-169.pdf

Illinois State Water Survey (ISWS). 2000. Watershed monitoring for the Lake DecaturWatershed, 1998-1999. Retrieved from: https://www.ideals.illinois.edu/bitstream/handle/2142/94327/ISWSCR2000-06.pdf?sequence=1

Illinois State Water Survey (ISWS). 2001. Sedimentation survey of Lake Decatur's basin 6, Macon County, Illinois. Champaign, IL.

International Plant Nutrition Institute (IPNI). 2015a. Nutrient source specifics, Nitrification Inhibitors. Retrieved from: https://www.ipni.net/specifics-en

International Plant Nutrition Institute (IPNI). 2015b. Nitrogen notes, denitrification. Retrieved from: http://www.ipni.net/NitrogenNotes

Islam, Z. 2011. Physically based hydrologic modelling. Department of Civil and Environmental Engineering. University of Alberta.

Jacoby, B.S., Peterson, E.W., Dogwiler, T. 2011. Identifying the stream erosion potential of cave levels in Carter Cave tate resort park, Kentucky, U.S.A. Journal of Geographic Information System. 3: 323-333.

Jetten, V, Govers, G. and Hessel, R. 2003. Erosion models: quality of spatial predictions. Hydrological Processes. 17: 887-900

Jiang, J., Li, S., Hu, J. and Huang, J. 2014. A modeling approach to evaluating the impacts of policy-induced land management practices on non-point source pollution: A case study of the Liiuxi River watershed, China. Agricultural Water Management, 131: 1-16.

Kirchner J. 2006. Getting the right answers for the right reasons: Linking measurements, analyses, and models to advance the science of hydrology. Water Resources Research, 42, 1-5.

Kumar, P., Le, P.V.V., Papanicolaou, A.N.T., Rhoads, B.L., Anders, A.M., Stumpf, A.J., Wilson, C.G., Bettis, E.A. III, Blair, N., Ward, A.S., Filley, T., Lin, H., Keefer, L., Keefer, D.A.,

Lin, Y-F., Muste, M., Royer, T.V., Foufoula-Georgiou, E., Belmont, P. (in press). Critical transition in critical zone of intensively managed landscapes. Anthropocene.

Leonard, B.P. 1979: A stable and accurate convective modelling procedure based on quadratic upstream interpolation. Comput. Methods Appl. Mech. Engrg., 19: 59-98.

Li, H., Sivapalan, M., Tian, F. and Liu, D. 2010. Water and nutrient balances in a large tile-drained agricultural catchment: a distributed modeling study. Hydrol. Earth Syst. Sci, 14: 2259-2275.

Linhoss, A.C., Underwood, W.V. 2015. Modeling salt panne land-cover suitability under sea-level rise. Journal of Coastal Research.

Lumborg, U. and Vested, H. 2008. Modelling of cohesive sediment dynamics (chapter 6). Retrieved from: https://www.mikepoweredbydhi.com/~/media/Microsite_MIKEbyDHI/Publications/PDF/Lumborg_Vested.ashx

Luna, M.F. 2016. Determinación de la erosion hídrica y la producción de sedimentos en la cuenca del río Pixcayá aplicando herramientas SIG. Revista de la Universidad de Guatemala, 32, 105-117.

Marta-Almeida, M., Teixeira, C., Carvalho, M. Melo-Goncalves, P. and Rocha, A. 2016. High resolution WRF climatic simulations for the Iberian Peninsula: Model validation. Physics and chemistry of the Earth, 94: 94-105.

Mausbach, M.J., and Dedrick, A.R. 2004. The length we go – measuring environmental benefits of conservation practices. Journal of Soil and Water Conservation 59(5):96A-103A.

Maxwell, R.M. and Kollet, S.J. 2008. Interdependence of groundwater dynamics and land-energy feedbacks under climate change. Nature Geoscience, 1, 665-669.

McCool, D.K., Brown, L.C., Foster, G.R., Mutchler, C.K., and Meyer, L.D. 1987. Revised slope steepness factor for the Universal Soil Loss Equation. Trans ASAE, 30, 1387-1396.

Merow, C., Smith, M.J., and Silander, J. A. 2013. A practical guide to MaxEnt for modeling species' distributions: what it does, and why inputs and settings matter. Ecography. 36: 1058-1069.

Merritt, W.S., Letcher, R.A. and Jakeman, A.J. 2003. A review of erosion and sediment transport models. Environmental Modelling & Software. 18: 761-799.

Minnesota Department of Agriculture. 2010. Workshop Exercises for Digital Terrain Analysis with LiDAR for clean water implementation. Retrieved from: https://www.mda.state.mn.us/protecting/cleanwaterfund/toolstechnology/~/media/Files/protecting/waterprotection/lidarworkshopmanual.ashx.

Mohamoud, Y.M. 1992. Evaluating Manning's roughness coefficients for tilled soils. Journal of Hydrology, 135: 143-156.

Moore, I.D., Grayson, R.B., Ladson, A.R. 1991. Digital terrain modelling: a review of hydrological, geomorphological and biological applications. Hydrological Processes. 5: 3 – 30.

Morgan, R., Quinton, J., Smith, R., Govers, G., Poesen, J., Auerswald, K., Chisci, G., Torri, D., Styczen, M. and Folly, A. 1998. The European Soil Erosion Model (EUROSEM) documentation and user guide. Retrieved from: https://core.ac.uk/download/pdf/70066.pdf

Moriasi, D. N., Guzman, J. A., Steiner, J. L., Starks, P. J., & Garbrecht, J. D. 2014. Seasonal sediment and nutrient transport patterns. J. Environ. Qual., 43: 1334-1344.National Cooperative Soil Survey (NCSS). 2012. Soil Characterization Database. Retrieved from: http://ncsslabdatamart.sc.egov.usda.gov.

Moriasi, D., Zeckoski, R. Arnold, J., Baffaut, C., Malone, R., Daggupati, P., Guzman, J., Saraswat, D., Yuan, Y., Wilson, B., Shirmohammadi, A. and Douglas-Mankin, K. 2015. Hydrologic and water quality models: Key calibration and validations topics. Transactions of ASABE, 58: 1609-1618

National Atmospheric Deposition Program. 2018. NTN site information. Retrieved from: http://nadp.slh.wisc.edu/data/sites/map/?net=NTN

Natural Resources Conservation Service (NRCS). 2016. Web soil survey. Retrieved from: https://websoilsurvey.sc.egov.usda.gov/App/WebSoilSurvey.aspx

Natural Resources Conservation Service (NRCS). 2017. United States Department of Agriculture. Soil Survey Geographic (SSURGO) Database. Retrieved from: https://sdmdataaccess.sc.egov.usda.gov.

Neuman, S. 1990. Universal scaling of hydraulic conductivities and dispersivities in geologic media, Water resources research,8: 1749-1758.

New Jersey Stormwater Best Management Practices Manual. 2004. Chapter 9.2: Standard for Constructed Stormwater Wetlands. Retrieved from: http://www.njstormwater.org/bmp_manual/NJ_SWBMP_9.2%20print.pdf

Niehoff, D., Fritsch, U. and Bronstert, A. 2002. Land-use impacts on storm-runoff generation: scenarios of land-use change and simulation of hydrological response in a meso-scale catchment in SW-Germany. Journal of Hydrology, 267: 80-93.

NOAA. 2016. Climate date service. Retrieved from: https://gis.ncdc.noaa.gov/maps/clim/

Oklahoma Conservation Commission. 2009. Fort Cobb Watershed Implementation Project. Oklahoma: Oklahoma Conservation Commission. Retrieved from: https://www.ok.gov/conservation/documents/Ft_Cobb_Project_final_report_2009.pdf.

Oklahoma Water Resources Board (OWRB). 2012. Rush Springs Aquifer of Oklahoma. Hydrologic study newsletter. Retrieved from: https://www.owrb.ok.gov/studies/groundwater/RushSprings/RSfactsheet.pdf.

Panagos, P., Borrelli, P. and Meusburger, K. 2015a. A new European slope length and steepness factor (LS-Factor) for modeling soil erosion by water. Geosciences, 5, 117-126.

Panagos, P., Borrelli, P., Poesen, J., Ballabio, C., Lugato, E., Meusburger, K., Montanarella, L. and Alewell, C. 2015b. The new assessment of soil loss by water erosion in Europe. Environmental Science and Policy,54: 438-447.

Panno, S., Kelly, W., Hackley, K., Hwang, H. and Martinsek, A. 2008. Sources and fate of nitrate in the Illinois River Basin, Illinois. Journal of Hydrology, 359: 174-188.

Parkyn, S. 2004. Review of riparian buffer zone effectiveness. Ministry of Agriculture and Forestry, New Zealand. Retrieved from: http://citeseerx.ist.psu.edu/viewdoc/download?doi=10.1.1.74.742&rep=rep1&type=pdf.

Penderson, R.L., 1999. Steady-state Simulation of Ground-water Flow in the Rush Spring Aquifer, Cobb Creek Basin, Caddo County, Oklahoma. Master thesis. Oklahoma State University.

Phillips, S., Anderson, R., Schapire, R. 2006. Maximum entropy modeling of species geographic distributions. MaxEnt. Ecological Modelling.190: 231-259.

Purvis, R.A. and Fox G.A. 2016. Streambank sediment loading rates at the watershed scale and the benefit of riparian protection. Earth Surface Processes and Landforms. DOI: 10.1002/esp.3901.

Randall, G.W. and Mulla, D.J. 2001. Nitrate nitrogen in surface waters as influenced by climatic conditions and agricultural practices. J. Eviron. Qual, 30: 337-344.

RCP Database. 2008. Information on Individual RCPs. RCP database, version 2.0. Retrieved from: http://tntcat.iiasa.ac.at:8787/RcpDb/dsd?Action=htmlpage&page=welcome#rcpinfo.

Refsgaard, J. C. & Storm, B. 1995. MIKE SHE. In: Singh, V. P. (ed.) Computer Models of Watershed Hydrology. Water Resources Publications, Highlands Ranch, Colorado, pp. 809–846.

Rejesus, R., Hornbaker, R. 1999. Economic and environmental evaluation of alternative pollution-reducing nitrogen management practices in central Illinois. Agriculture, ecosystems and environment, 75, 41-53.

Renard, K., Foster, G., Weesies, G. and Porter, J. 1991. Revised universal soil loss equation. Soil and Water Conservation. 46: 30-33.

Renard, K.G., Foster, G.R., Weesies, G.A., McCool, D.K. and Yoder, D.C. 1997. Predicting soil erosion by water: A guide to conservation planning with the Revised Universal Soil Loss Equation (RUSLE). Agricultural Handbook 703; U.S. Government Printing Office: Washington, DC, USA.

Rhoads, B.L., Lewis, Q.W. and Andresen, W. 2016. Historical changes in channel network extent and channel planform in an intensively managed landscape: Natural versus human-induced effects. Geomorphology, 252: 17-31.

Riahi, K., Rao, S., Krey, V., Cho, C., Chirkov, V., Fischer, G., Kindermann, G., Nakicenovic, N. and Rafaj, P. 2011. RCP 8.5 – A scenario of comparatively high greenhouse gas emissions. Climatic Change, 109, 33-57.

Sadeghi, S.H. 2004, Application of MUSLE in prediction of sediment yield in Iranian conditions. Conserving Soil and Water for Society: Sharing Solutions, July: 1-4.

Schaefer, D. 2018. Director of Nutrient Stewardship at Illinois Fertilizer & Chemical Association. Personal communication.

Serveiss, V., Bowen, J., Dow, D., Valiela, I. 2004. Using ecological risk assessment to identify the major anthropogenic stressor in the Waquoit Bay Watershed, Cape Cod, Massachusetts. Environmental Management, 33, 730-740.

Shen, Z., Qiu, J., Hong, Q. and Chen, L. 2014. Simulation of spatial and temporal distributions of non-point source pollution load in the Three Gorges Reservoir Region. Science of the Total Environment, 493: 138-146.

Shields, F.D., Bowie, A.J. and Cooper, C. M. 1995. Control of Streambank Erosion Due to Bed Degradation with Vegetation and Structure. Water Resources Bulletin. 31: 475-489.

Simon, A. and Klimetz, L. 2008. Relative magnitudes and sources of sediment in benchmark watersheds of the Conservation Effects Assessment Project. Journal of Soil and Water Conservation. 63: 504-522.

Simon, A., Pollen-Bankhead, N. and Thomas, R. 2011. Development and application of a deterministic bank stability and toe erosion model for stream restoration. Geophysical Monographs. 10.1029/2010GM001006.

Smith, R.E., Goodrich, D.C. and Quinton, J.N. 1995. Dynamic, distributed simulation of watershed erosion: The KINEROS2 and EUROSEM models. Journal of Soil and Water Conservation. 50.5: 517

Smith, R., Goodrich, D., Woolhiser, D. and Unkrich, C. 1990. KINEROS – a kinematic runoff and erosion model. Computer models of Watershed Hydrology. Water Resources Publications. Chapter 20.

Soil Survey Staff-Natural Resources Conservation Service (SSS-NRCS). 2016. United States Department of Agriculture. Soil Survey Area (SSURGO) Retrieved from: http://websoilsurvey.sc.egov.usda.gov/App/WebSoilSurvey.aspx.

Soil Survey Staff-Natural Resources Conservation Service (SSS-NRCS). 2012. United States Department of Agriculture. U.S. General soil map (STATSGO) Retrieved from: http://websoilsurvey.sc.egov.usda.gov/App/WebSoilSurvey.aspx.

Spieles, D. and Mitsch, W. 2000. The effects of season and hydrologic and chemical loading on nitrate retention in constructed wetlands: a comparison of low – and high-nutrient riverine system. Ecological Engineering, 14: 77-91.

Starks, P.J., Fiebrich, C.A., Grimsley, D.L., Garbrecht, J.D, Steiner, J.L., Guzman, J.A. and Moriasi, D.N. 2014. Upper Washita River Experimental Watersheds: Meteorologic and Soil Climate Measurement Networks. Journal of Environmental Quality. 43: 1239-1249.

Steiner, J.L., Starks, P.J., Daniel, J.A., Garbrecht, J.D., Moriasi, D., McIntyre, S., and Chen, J-S. 2008. Environmental effects of agricultural conservation: a framework for research in two watersheds in Oklahoma's Upper Washita River basin. Journal of Soil and Water Conservation 63(6):443-452.

Storm, D. E., Busteed, P. R., & White, M. J. 2006. Fort-Cobb Basin. Modeling and land cover classification. Retrieved from Draft reported to the Oklahoma Department of Environmental Quality. Retrieved from: http://www.deq.state.ok.us/WQDnew/tmdl/fort_cobb/osu_fort_cobb_modeling_jan_2006.pdf.

Storm, D. E., White, M.J. and Stoodley, S. 2003. Fort Cobb Basin – Modeling and land cover classification. Retrieved from: http://www.deq.state.ok.us/WQDnew/tmdl/fort_cobb/model.pdf.

Strauch, M., Lima, J., Volk, M., Lorz, C and Makeschin, F. 2013. The impact of best management practices on simulated streamflow and sediment load in a Central Brazilian catchment. Journal of Environmental Management, 127: S24-S36

Stumpf, A. and Atkinson, L.A. 2015. Geologic cross sections across the Mahomet Bedrock Valley, Champaign, Ford, McLean, Piatt and Vermilion Counties, Illinois. Illinois State Geological Survey. IMap 19, scale 1:48,000.. Retrieved from http://hdl.handle.net/2142/89865

Stumpf, A.J., and W.S. Dey, eds. 2012. Understanding the Mahomet aquifer: Geological, geophysical, and hydrogeological studies in Champaign County and adjacent areas. Illinois State Geological Survey, draft report to Illinois American Water, contract no. 2007-02899. Retrieved from http://hdl.handle.net/2142/89865.

Sugg, Z., 2007. Assessing U.S. farm drainage: Can GIS lead to better estimates of subsurface drainage extent? World Resources Institute.

Sustainable Agriculture Research & Education (SARE). 2012. Managing cover crops profitably. Third Edition. Retrieved from: https://www.sare.org/Learning-Center/Books/Managing-Cover-Crops-Profitably-3rd-Edition/Text-Version

Suthernland, B., Barrett, K. and Gingras, M. 2013. Clay settling in fresh and saltwater. Department of Physics, University of Alberta, Canada.

Talebizadeh, M., Morid, S., Ayyoubzadeh,S. and Ghasemzadeh, M. 2010. Uncerainty analysis in sediment load modeling using ANN and SWAT model. Water Resources Management, 24: 1747-1761.

Tang, Z., Engel, B.A., Pijanowski, B.C. and Lim, K.J. 2005. Forecasting land use change and its environmental impact at a watershed scale. Journal of Environmental Management, 76, 35-45.

Taylor, K.E. 2001. Summarizing multiple aspects of model performance in a single diagram, J. Geophys. Res. 106, 7183-7192.

Taylor, K.E., Stouffer, R. J., Meehl, G.A. 2012. An overview of CMIP5 and the experiment design. American Meteorological Society, 485-798.

Taylor, R., Scanlon, B., Döll, P., Rodell, M., van Beek, R., Wada, Y., Longuevergne, L., Leblanc, M., Famiglietti, J., Edmunds, M., Konikow, L., Green, T., Chen, J., Taniguchi, M., Bierkens, M., MacDonald, A., Fan, Y., Maxwell, R., Yechieli, Y., Gurdak, J., Allen, D., Shamsudduha, M., Hiscock, K., Yeh, P., Holman, I. and Treidel, H. 2012. Ground water and climate change. Nature Climate Change, 3, 322-329.

The Nature Conservancy. 2017. Working to catalyze change in the Upper Sangamon. Meeting held on October 26, 2017 at Decatur, IL.

The Nature Conservancy. 2018. Heart of the Sangamon River Ecosystem Partnership meeting. Meeting held on May 9, 2018 at Decatur, IL

Tim, U.S. and Jolly, R. 1994. Evaluating agricultural nonpoint-source pollution using integrated geographic information system and hydrologic/water quality model. J. Environ. Qual, 23: 25-35.

Trenberth, K. 2011. Changes in precipitation with climate change. Climate Research. 47: 123-138.

Tsihrintzis, V.A. and Madiedo, E.E. 2000. Hydraulic resistance determination in Marsh Wetlands. Water Resources Management, 14:285-309.

United States Geological Survey (USGS). 2016a. LiDAR 2012. Retrieved from: http://viewer.nationalmap.gov/basic/.

United States Geological Survey (USGS). 2016b. National land cover database 2006. Retrieved from: http://landcover.usgs.gov/landcoverdata.php#regional.

United States Geological Survey (USGS). 2016c. Ground water atlas of the United States. Oklahoma, Texas. Retrieved from: https://pubs.usgs.gov/ha/ha730/ch_e/E-text9.html#rshspr.

USCB. 2016. United States Census Bureau.

USDA. 2007. Riparian buffer design and species consideration. Technical note. Retrieved from:

https://www.nrcs.usda.gov/Internet/FSE_PLANTMATERIALS/publications/idpmstn7248.pdf

USDA. 2016. USDA-NASS Cropland data layer. United States Department of Agriculture. Retrieved from: https://nassgeodata.gmu.edu/CropScape/

USGS. 2016. National Elevation Dataset (NED). Retrieved from: https://earthexplorer.usgs.gov/

USGS. 2017. Surface water daily data for the nation. Retrieved from: https://waterdata.usgs.gov/nwis/dv/?referred_module=sw

Van der Kamp, G. and Hayashi, M. 1998. The groundwater recharge function of small wetlands in the semi-arid northern prairies. Great Plains Research, 8, 39-56.

Vested, H.J., Justesen, P. and Ekebjærg, L. (1992): Advection-dispersion modelling in three dimensions. Appl. Math. Modelling,16,: 506-519

Wall, D. 2013. Nitrogen in Waters: Forms and Concerns, Nitrogen in Minnesota Surface Waters. Minnesota Pollution Control Agency. Retrieved from: https://www.pca.state.mn.us/sites/default/files/wq-s6-26a2.pdf

Ward, A.D., Trimble, S.W., Burckhard, S.R. & Lyon, J.G. 2016. Environmental Hydrology. Third Edition. CRC Press, Taylor and Francis Group.

Wenger, S. 1999. A review of the scientific literature on riprian buffer width, extent and vegetation. Office of Public Service & Outreach, University of Georgia. Retrieved from: http://wolfrunwater.org/Stream-Restoration/riparianbuffer%201%20.pdf.

Wesstrom, I., Messing, I., Linnér, H. and Lindstrom, J. 2000. Controlled drainage – effects on drain outflow and water quality. Agricultural Water Management, 47, 85-100.

Williams, J.R. and Berndt, H.D. 1977. Sediment yield prediction based on the watershed hydrology. Transactions of the ASAE, August: 1100-1104.

Wilson, C.G., Kuhnle, R.A., Bosch, D.D., Steiner, J.L., Starks, P.J., Tomer, M.D., and Wilson, G.V. 2008. Quantifying relative contributions from sediment sources in Conservation Effects Assessment Project watersheds. Journal of Soil and Water Conservation 63(6):523-532.

Wilson, P.J. and Gallant, J.2000. Terrain Analysis: Principles and Applications. John Wiley & Sons. U.S.A.

Wiskow, E. and van der Ploeg, R. 2003. Calculation of drain spacings for optimal rainstorm flood control. Journal of Hydrology, 272, 163-174.

World Meteorological Organization, n.d. Emission Scenarios. Retrieved from: https://www.wmo.int/pages/themes/climate/emission_scenarios.php.

Wynn, T. and Mostaghimi S. 2006. The effect of vegetation and soil type on streambank erosion, southwestern Virginia, USA. Journal of the American Water Resources Association: 69-82

Yan, Q., Lei, T., Yuan, C., Lei, Q., Yang, X., Zhang, M., Su, G., An, L. 2015. Effects of watershed management practices in the relationships among rainfall, runoff, and sediment delivery in the hilly-gully region of the Loess Plateau in China. Geomorphology, 228, 735-745.

Young, R.A., Onstad, C.A., Bosch, D.D. and Anderson, W.P. 1989. Journal of soil and water conservation, 44 (2): 168-173.

Zaimes, G.N., Schultz, R.C., Isenhart, T.M. 2004. Stream bank erosion adjacent to riparian forest buffers, row-crop fields, and continuously-grazed pastures along Bear Creek in central Iowa. Soil and Water Conservation Society. 59: 19-27.

Zhai. X, Zhang, Y., Wang, X., Xia, J. and Liang, T. 2014. Non-point source pollution modelling using Soil and Water Assessment Tool and its parameter sensitivity analysis in Xin'anjiang catchment, China. Hydrological Processes, 28: 1627-1640.

Zhang, X. and Zhang, M. 2011. Modeling effectiveness of agricultural BMPs to reduce sediment load and organophosphate pesticides in surface runoff. Science of the Total Environment, 409: 1949-1958.

Zhenyao, S., Qiu, Q. and Chen, L. 2014. Simulation of spatial and temporal distribution of non-point source pollution load in the three Gorges Reservoir Region. Science of the Total Environemt, 493: 138-146.

Zhou, X., Helmers, M. and Qi, Z. 2013. Modeling of subsurface tile drainage using MIKE SHE. Applied Engineering in Agriculture, 29, 865-873.